SPATIALLY RESOLVED GALAXY STAR FORMATION AND ITS ENVIRONMENTAL DEPENDENCE

by

Niraj D. Welikala

Master of Physics, University of Oxford, 2002

Diploma in Computer Science, University of Cambridge, 2003

Submitted to the Graduate Faculty of

the Department of Physics & Astronomy in partial fulfillment

of the requirements for the degree of

Doctor of Philosophy

University of Pittsburgh

2008

UNIVERSITY OF PITTSBURGH

DEPARTMENT OF PHYSICS & ASTRONOMY

This dissertation was presented

by

Niraj D. Welikala

It was defended on

September 25th 2008

and approved by

Dr. Andrew Connolly, University of Pittsburgh & University of Washington

Dr. Arthur Kosowsky, University of Pittsburgh

Dr. David Turnshek, University of Pittsburgh

Dr. Vladimir Savinov, University of Pittsburgh

Dr. Rupert Croft, Carnegie Mellon University

Dissertation Director: Dr. Andrew Connolly, University of Pittsburgh & University of Washington

SPATIALLY RESOLVED GALAXY STAR FORMATION AND ITS ENVIRONMENTAL DEPENDENCE

Niraj D. Welikala, PhD

University of Pittsburgh, 2008

The role of star formation in galaxies is clearly a fundamental component of their evolution, although it is becoming clear that galaxy environments may also play a significant role. To explore the relationship between environment and star formation in galaxies, I use the photometric information contained in individual pixels of 44 964 galaxies (volume-limited) from the Fourth Data Release of the Sloan Digital Sky Survey. I use the pixel-z technique, which combines stellar population synthesis models with photometric redshift template fitting on the scale of individual pixels in galaxy images. Spectral energy distributions are constructed, sampling a wide range of properties such as age, star formation rate (SFR), dust obscuration and metallicity. By summing the SFRs in the pixels, I show that, as found in other studies, the distribution of total galaxy SFR shifts to lower values as the local density of surrounding galaxies increases. The effect is most prominent in the galaxies with the highest SFR. Since the method enables an estimate to be made of the spatial distribution of star formation *within* galaxies, the mean SFR of each galaxy is then calculated as a function of radius. I find that, on average, the mean SFR is dominated by star formation in the central regions of galaxies and it is this central star formation that is suppressed in high density environments. The mean SFR in the outskirts of galaxies is found to be largely independent of environmental effects. These trends are shared by galaxies which are highly star forming. I also investigate the impact of the density-morphology relation of galaxies on the observed trends. Early-type and late-type galaxies exhibit distinct radial SFR distributions. A suppression of star formation in the highest density environments is still found in the highest

star forming galaxies within each type. I show that the density-morphology relation alone cannot account for this observed suppression. This points to a mechanism by which the environment governs the evolution of galaxies, affecting the star formation in the innermost regions in both early and late-type galaxies. I suggest that this is a natural consequence of "downsizing" in galaxies.

keywords: galaxies: structure — galaxies: statistics — galaxies: distances and redshifts — galaxies: evolution — galaxies: formation.

TABLE OF CONTENTS

LIST OF FIGURES

PREFACE

Many people helped me throughout my research and my time in graduate school. I would first like to say a big thank-you to my adviser, Andy Connolly, for his help, advice and support throughout my research and graduate career, for introducing me to this new and exciting way to study galaxies and galaxy evolution, and for his thought-provoking questions and discussions throughout. I am very grateful to Andrew Hopkins for his help, suggestions and advice throughout my research and in my papers. I thank Ryan Scranton for his many valuable suggestions, and for making the density measurements from the SDSS available. I thank my co-adviser Arthur Kosowsky for his advice and encouragement throughout. I would especially like to mention Andrew Zentner for his advice and comments, for supporting me as a graduate student researcher during August, September and October 2008 and for the great Astro-coffees and discussions! I acknowledge and thank Tamás Budavári and Alberto Conti for their help and for useful discussions. I thank Jeffrey Newman for useful discussions and feedback. Ching-Wa Yip provided the MCMC quantities and also gave other useful suggestions. Many thanks also to Jeff Gardner for his help with using the NCSA supercomputing cluster for this work. I would also like to thank my committee members, David Turnshek, Rupert Croft and Vladimir Savinov for their suggestions and advice. I would like to thank Simon Krughoff for his help and would also like to mention my fellow graduate students – Cameron McBride, Suman Bhattacharya, Sam Schmidt, Jeremy Brewer and Vikas Bansal – for discussions, help and banter.

I thank Lance Miller for his advice and encouragement at Oxford. I also thank the many friends I made in Pittsburgh including those in the tennis and climbing worlds and in the "Coffee Tree". And finally, I thank my parents, my sister Sohanya, Uncle Alun and Aunty Patsy for all their support and encouragement – and I hope they enjoyed listening to me talk

about galaxies and galaxy formation as much as I did telling them about it! The dissertation is dedicated to my parents and to the memory of Dr. Mike Leask, my physics tutor at St. Catherine's College, Oxford.

This material is based upon work supported by the National Science Foundation under Grant Nos. 0851007 and AST 0806367.

1.0 INTRODUCTION

1.1 BACKGROUND AND MOTIVATION

The formation and evolution of galaxies is one of the most challenging problems in astrophysics today. Throughout the 20th century, our understanding of the way we think galaxies form has changed dramatically. Some of the early models of galaxy formation favored "Monolithic Collapse", whereby galaxies form through the collapse of a protogalactic cloud. The most famous example of this model was one by Eggen et al. (1962) who studied the motions of a sample of high-velocity stars in the Milky Way. They found that the metal-poor halo stars in the Milky Way have highly elliptical orbits which are characteristic of a system in free fall. They inferred that the Galaxy formed quickly through the collapse of a uniform, isolated protogalactic cloud. In 1978, this model was challenged by Searle and Zinn (1978) who analyzed globular clusters in the Milky Way (low metallicity and old Population II stars which form a halo around the Galactic disk) and concluded from the low metallicity gradient and large age spread of these stars that the halo was built instead on a timescale of several Gigayears (Gyrs) from separate, low mass fragments.

Today, a basic framework exists to describe the formation of galaxies from primordial fluctuations in the density field (White and Rees, 1978; Blumenthal et al., 1986; White and Frenk, 1991). The standard picture of structure formation is that we live in a Cold Dark Matter (CDM) Universe with hierarchical clustering: the smallest objects in the Universe collapse first and merge to form larger ones. In a CDM Universe, the initial small density fluctuations grow due to gravitational instability and eventually form virialized objects called "dark matter halos". Halos grow as a result of a series of mergers, assembling mass in a hierarchical fashion, with less massive halos in the past merging to form more massive ones.

The spectrum of fluctuations is roughly flat on scales greater than 100 Megaparsecs (Mpc)[1] and on these scales the density fluctuations are small in size (rms fluctuations of the order ~ 0.1 at 1 Gpc). However, on scales of the order of 10 Mpc, the density fluctuations are large (~ 1). The most apparent overdensities are therefore on small scales, less than 10 Mpc which are the typical scale of galaxy clusters. It is the environments around galaxies on those scales that are of interest to those who study galaxy evolution. Galaxies are thought to reside in dark matter halos and just like the dark matter halos, undergo hierarchical merging, with smaller galaxies merging to become larger ones. In this picture, the clusters of galaxies we see today, such as the Coma cluster, shown in the top left panel of Figure 1.2 must have been assembled from this mass buildup through the hierarchical merging of smaller galaxies in the past. Despite this framework for the way galaxies form, many of the processes that accompany galaxy formation are not well understood.

What is known about the physical processes, both internal and external to galaxies? The first indicator of the internal structure within a galaxy is the galaxy morphology. Edwin Hubble first classified galaxies according to their morphology along the so-called "Tuning-fork diagram" (Hubble, 1936; Sandage, 1961). Some of the more common classifications are based on visually determining the galaxy morphologies, (de Vaucouleurs et al., 1991; Lintott et al., 2008). Other studies over the past decade have attempted to quantify morphology using measurements of concentration, color, surface brightness profiles or features in the galaxy spectrum (e.g., Abraham et al. (2003); Conselice (2006); Goto et al. (2003b); Strateva et al. (2001)). Broadly speaking, galaxies classified as "early-type" have morphologies that are typically elliptical and lenticular while "late-type" morphologies are either spiral or irregular. Early-types also tend to be redder, more luminous, gas-poor and have older stellar populations than do late-types. Figure 1.1 shows an example of a "late-type" and an "early-type" galaxy both of which have been imaged by the Hubble Space Telescope (HST).

How are these stellar populations distributed throughout a galaxy? Although there is a strong empirical connection between the ages of stellar populations and the galaxy morphology, it still does not give a complete picture of the properties of these stellar populations.

There are strong correlations among the measurable physical properties of galaxies. As

[1] $1pc = 3.26$ light years (ly)

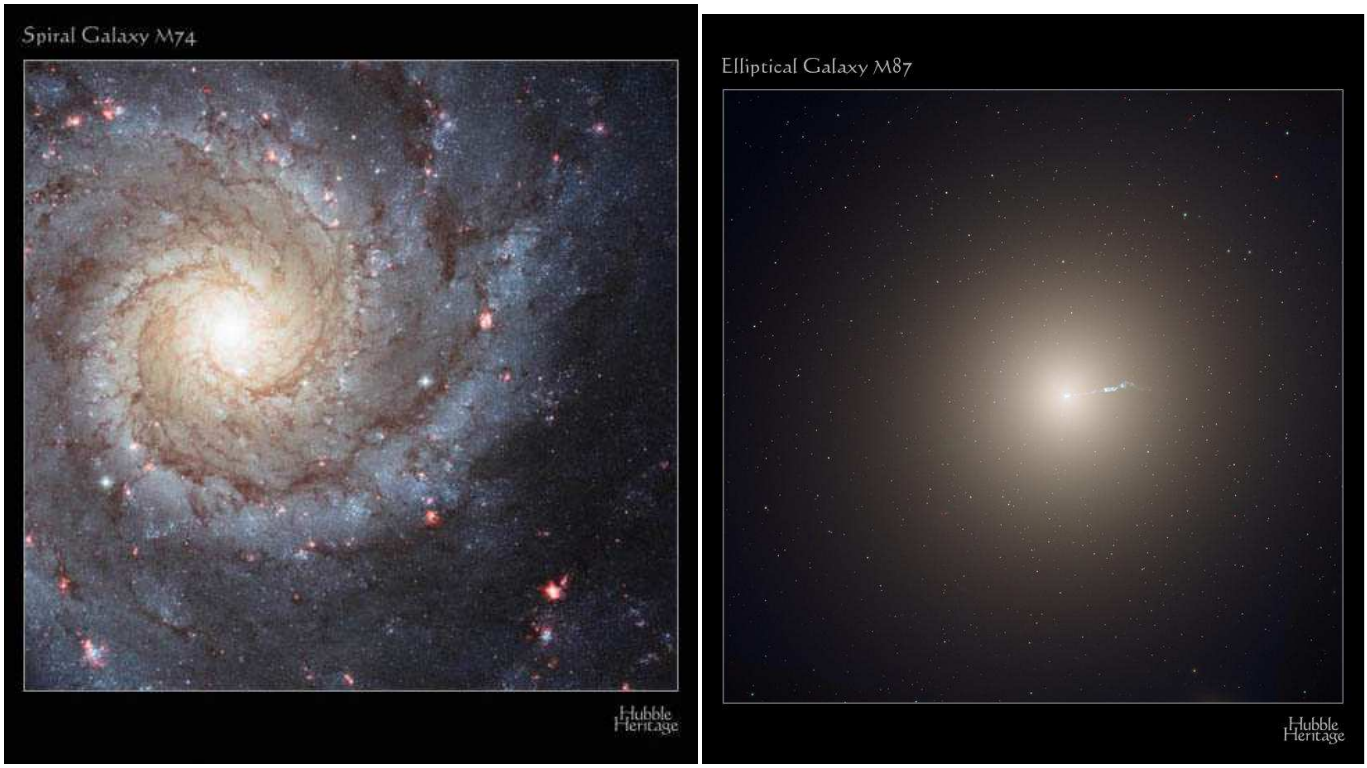

Figure 1.1: Left panel: An example of a late-type galaxy: the spiral galaxy M74 seen face-on. The galaxy is at a distance of around 30 million light years. The spiral arms, which consist of gas and dust, are about 1000 light years across. They contain many young and blue stars with high rates of star formation. The pink, colored regions correspond to diffuse gaseous nebulae (HII regions). The galaxy also consists of a bulge containing older, redder stellar populations. Right panel: An example of an early-type galaxy: the elliptical galaxy M87. This is a bulge-dominated galaxy containing old stellar populations, giving the galaxy a red color. There is very little gas or dust and little star formation. Images are taken from the Hubble Space Telescope (HST). Source: Hubble Heritage Project (NASA and STScI, http://heritage.stsci.edu/).

noted by Blanton et al. (2003b), the visual morphologies of the galaxies, classified according to the "Tuning Fork Diagram" (Hubble, 1936) correlate well with other properties such as surface brightness, color, star formation rate (SFR), luminosity, the winding angle of spiral arms in disk galaxies and the extent to which the bulge of the galaxy dominates (Roberts and Haynes, 1994). The mass of a galaxy is known to be closely related to its luminosity, while the surface brightnesses of giant elliptical galaxies are known to be strongly correlated with their sizes (Kormendy, 1977). These relations express themselves in the Tully-Fisher relation for spiral galaxies (Tully and Fisher, 1977), which relates luminosity with rotation velocity of the disk, and the Fundamental Plane for elliptical galaxies (Faber and Jackson, 1976), which relates luminosity, surface brightness and effective radius. Many physical properties of galaxies are also correlated with the galaxy environment. The most noted correlation is that between the environment of the galaxy and its type. Early-type galaxies are found in denser regions than late-type galaxies, as was first observed by Hubble (1936) and confirmed by many subsequent studies (Oemler, 1974; Dressler, 1980; Hashimoto and Oemler, 1999).

How do galaxies acquire their current properties? To answer this within a theoretical framework, it is necessary to characterize the observed distribution of galaxy properties in a systematic manner (Blanton et al., 2005). There have been a number of studies that describe the joint distribution of galaxy properties, including studies of the number density and luminosity density distributions of galaxy colors, luminosities, stellar masses, SFRs, surface brightnesses, sizes and galaxy concentrations. These galaxy properties are particularly of interest because they can be predicted in cosmological hydro-dynamical simulations (Nagamine et al., 2001; Steinmetz and Navarro, 2002); or in semi-analytic models (Somerville et al., 2001; Mathis et al., 2002). While galaxy formation theory has had some success in predicting some of the spatial clustering of galaxies, it does not yet successfully predict the detailed joint distribution of the above properties. Progress in the field is hampered by the lack of a complete understanding of the gas dynamics and feedback mechanisms in galaxies which in turn affects the evolution of their stellar populations and hence the properties of the galaxies. Thus, as yet, we do not have a complete understanding of the physical processes associated with galaxy formation.

The fact that the most overdense fluctuations preferentially reside within overdensities

on larger scales implies that there should be a connection between halo mass and environment (Mo and White, 1996; Lemson and Kauffmann, 1999). The relationships between the properties of a halo and the properties of the galaxy or galaxies it hosts are not understood, so conventional theories do not currently make predictions for how the observed galaxy properties depend on environment. Studies to date (Kauffmann et al., 1997, 1999; Benson et al., 2000) suggest that observables such as SFR, luminosity, color and morphology will all be related to the galaxy environment. A more detailed understanding of the relationship between those properties and the galaxy environment is an important ingredient in galaxy formation. In what follows we examine the observational and theoretical evidence for a correlation between these galaxy properties and the environment of the galaxies.

The star formation rate, luminosity, color and morphology in these studies of "environment" are calculated for each galaxy as a whole rather than for individual components within the galaxy. They are therefore integrated over the stellar populations in the galaxy so we have no sense of how the stellar populations, and processes such as star formation (SF) that occur on the scales of molecular clouds, are distributed within the galaxies. Integral field spectroscopy (e.g., Reunanen et al. (2007)) provides evidence for this for small numbers of galaxies but it is not possible to do this for large samples of galaxies. *The main motivation of this work is to provide a means to study the internal spatial distribution of galaxy properties, particularly those related to the underlying stellar populations, and to study how this spatial distribution changes as a function of the galaxy environment.* The aims of this are two-fold:

- Studying the spatial distribution of these galaxy properties should provide a new tool with which to study galaxy formation. Current models of formation, as we shall see, make predictions about how the integrated galaxy properties vary with their environment. Given our current understanding of the physical processes that influence the way a galaxy interacts with its environment, we can use those models to make predictions about how the spatial distribution of galaxy properties vary with environment. By comparing the spatial distributions (and their dependence on environment) with theoretical predictions, we may be able to determine which models of galaxy formation are favored.
- Having a large sample of galaxies with resolved SFR will lead to a better understanding of the physical processes that are currently modelled in hydro-dynamic simulations. These

processes include gas infall, disk dynamics, galaxy mergers, star formation, and feedback in the Interstellar Medium (ISM), including feedback from supernovae and central black holes.

Our focus in this work will be on what can be inferred about stellar populations of galaxies. In §1.2 we describe the stellar populations that underlie the majority of these galaxy properties. In §1.3, we describe the observed correlations between various galaxy properties (including star formation) and their environment. Theoretical predictions from current semi-analytic models of hierarchical structure formation and numerical simulations are presented in §1.4, as well as details of the physical mechanisms that underlie many galaxy interactions and which characterize the "environment" of the galaxies. We must also address another issue: there has long been speculation regarding whether galaxies evolve primarily because of their environment (we shall call this "Nurture") or because of their intrinsic properties such as mass (we shall call this "Nature"). §1.5 presents evidence for the fact that galaxy properties may not be shaped primarily by these physical mechanisms but may have already been in place at early epochs, with the environment perhaps shaping the subsequent evolution. §1.6 discusses how studying the spatial distribution of galaxy properties can provide insight into the relative importance of these two different ideas of galaxy formation.

1.2 STELLAR POPULATIONS AND STAR FORMATION

The discovery by Lindblad and Oort that spiral galaxies could be decomposed into separate spheroidal and disk components ties in closely with galaxies having distinct stellar populations. Baade (1944) used the 100-inch Mount Wilson telescope to resolve individual stars in the inner regions of several spiral galaxies where the spheroidal component dominates. He also obtained resolved stellar images in a few nearby elliptical galaxies. By analyzing the colors and luminosities of the stellar images, he realized that the brightest stars in both elliptical galaxies and in the spheroidal components of the spiral galaxies are red giants, distinct from the blue supergiants which dominate the spiral arms in the disks. These ob-

servations implied that there were two characteristic stellar populations: "Population I", containing luminous, blue stars, accompanied by gas and dust; and "Population II", which is dominated by luminous red stars in a dust-free and gas-free environment. Open clusters and stellar disks comprise Population I stars, while globular clusters, galactic spheroids and elliptical galaxies are made of Population II stars. Hertzsprung and Russell analyzed the distribution of stars in the so-called 'HR' or Color-Magnitude Diagrams of stellar clusters [2], and found that stars are not randomly scattered but are concentrated within tightly defined bands. The bands which are populated by the stars in open clusters were found to differ from those which are populated by globular-cluster stars. It followed that the stellar populations of these two types of clusters contain very different types of stars.

Star formation shapes the observable galaxy properties. But star formation involves many complicated dynamical, thermal, radiative and chemical processes on a wide range of scales (see McKee and Ostriker (2007) for a review). A key ingredient in the understanding and modelling of galaxy evolution is the relationship between the SFR and the physical conditions in the interstellar medium (ISM). Most current galaxy formation and evolution models (e.g., Navarro and Steinmetz (1997)) treat star formation using simple, ad hoc parameterizations, and our limited understanding of the actual form and nature of the SFR-ISM interaction remains one of the greatest limitations in these models. Measurements of the star formation law in nearby galaxies (Kennicutt, 1998b) can address the problem, by providing empirical recipes that can be incorporated into analytical models and numerical simulations, and by providing clues to the physical mechanisms that underlie the observed correlations (Robertson and Kravtsov, 2008).

Observed galaxies exhibit large-scale correlations between their global star formation rate surface density and their average gas surface density (Kennicutt, 1989, 1998b). These correlations can be used in many galaxy formation models to characterize star formation. However, the global SFR density-gas density correlation is now known to be not universally valid (Wong and Blitz, 2002; Boissier et al., 2003). We know now that the efficiency of converting gas into stars depends strongly on the mass of the galaxy. For example, as

[2]the "magnitude" refers to the absolute magnitude of the stars which is a measure of their luminosity and the color is a measure of the relative fluxes at two different wavelengths

observed by Robertson and Kravtsov (2008), the faint-end of the galaxy luminosity function has a shallower slope (Blanton et al., 2001, 2003c) compared to the steeper mass function of dark matter halos (Press and Schechter, 1974; Sheth and Tormen, 1999) which suggests a decrease in SF efficiency in low-mass systems. While feedback processes from supernovae and AGN (e.g., Brooks et al. (2007); Sijacki et al. (2007)), or the efficiency of gas cooling and accretion (Dekel and Birnboim, 2008) may account for star formation efficiency being a function of galaxy mass, it may also be due to processes intrinsic to the ISM (Tassis et al., 2008). There is, therefore, a need for an intrinsic model for the conversion of gas into stars in galaxies.

The most widely applied relation between star formation and gas density in galaxies is the empirical Schmidt-Kennicutt relation (Schmidt, 1959; Kennicutt, 1998b) in which the star formation rate Σ_{SFR} is a universal power-law function of the total disk-averaged or global gas surface density Σ_{gas}.

$$\Sigma_{SFR} = (2.5 \pm 0.7) \times 10^{-4} \left(\frac{\Sigma_{gas}}{1\ M_{\odot}\ \mathrm{pc}^{-2}}\right)^{n}\ \mathrm{M}_{\odot}\ \mathrm{yr}^{-1}\ \mathrm{kpc}^{-2}. \tag{1.1}$$

$n_{tot} \approx 1.4$ describes the correlation for the entire population of normal and starburst galaxies. There is now, however, evidence of deviations from this relation as a function of spatial trends in the H_2 molecular fraction which traces the total gas distribution in disk galaxies (Robertson and Kravtsov, 2008). In low-mass systems, the distribution of H_2 is patchy throughout the galaxy, and this is shown to cause a break in the above relation.

1.3 OBSERVED RELATIONS BETWEEN GALAXY PROPERTIES AND THEIR ENVIRONMENT

1.3.1 The Dependence of Star Formation Rate on Environment

1.3.1.1 Estimating Star Formation There are many methods of determining SFRs in galaxies. One of them relies on the fact that the SFR is correlated with measurements of the far-infrared luminosity (Kennicutt, 1998a). This arises because of dust heated by star

formation. Other measurements include the radio luminosity (resulting from synchrotron emission associated with supernovae, Condon (1992)). There are also indicators that are sensitive to the ionizing flux from massive stars. These includes measurement of the UV continuum and the fluxes of nebular emission lines. Each of these techniques is subject to different biases and calibration uncertainties as detailed in Hopkins et al. (2003), but they give consistent estimates for "normal" galaxies when these are accounted for (Hopkins et al., 2001, 2003).

The equivalent widths (EW) of the H_α emission lines in particular is often used as a measure of recent star formation activity in young, massive stars. UV radiation is absorbed by Hydrogen and will ionize any neutral Hydrogen gas in the vicinity of O and B stars. The de-excitation of the resulting ionized gas will result in H_α emission. It traces unobscured star formation since the H_α photons are efficiently absorbed by dust. The H_α line has been used in many studies of SFR and environment in the SDSS (e.g., Gómez et al. (2003)). The $[OII]$ emission line is also used frequently in these studies as it is correlated with H_α and remains in the optical window to higher redshifts (H_α can typically be measured out to $z \approx 0.3$ at optical wavelengths while $[OII]$ can be measured to $z \approx 1$). This makes it an important tracer of SF in galaxies to higher redshift. Both lines are sensitive to the metallicity and ionizing levels of the gas, although the problem is more significant for $[O_{II}]$. Dust extinction is the largest source of uncertainty - both the effective optical depth and dust geometry must be considered (Calzetti, 2001).

In their measurements of galaxy SFRs, Hopkins et al. (2003) used the calibration of the SFR to the H_α luminosity, which was formulated by Kennicutt (1998a):

$$\mathrm{SFR}_{\mathrm{H}\alpha}\,(M_\odot\,\mathrm{yr}^{-1}) = \frac{L_{\mathrm{H}\alpha}}{1.27 \times 10^{34}\,\mathrm{W}}. \tag{1.2}$$

The SFR is obtained by applying a scaling factor to the star formation sensitive luminosity measurement for the galaxy, which is derived from a flux measurement from a fiber-based spectrum. The calibration assumes a form for the initial mass function (IMF) - the distribution of initial stellar mass - that was proposed by Salpeter (1955) and a stellar mass range from 0.1 to $100 M_\odot$.

There are two steps that have to be taken before applying this calibration. The flux has to be obscuration-corrected to account for the intrinsic dust content of the galaxy. Second, the flux needs to be aperture-corrected to account for the emission that is missed due to the finite size of the SDSS fiber ($3''$) which can be smaller than the size of the target galaxy. Both the obscuration and aperture corrections are described in detail in Hopkins et al. (2003).

1.3.1.2 The Environmental Dependence It has been known for over 40 years that cluster regions lack emission-line galaxies (Dressler et al., 1985). Recent studies have shown that the star formation in cores of clusters is much lower than in the surrounding field (Balogh et al., 1999; Poggianti et al., 1999; Couch et al., 2001; Balogh et al., 2002).

Lewis et al. (2002) measured the equivalent width (EW) of the Hα emission line for 11 006 galaxies brighter than $M_b = -19$ at $0.05 < z < 0.1$ in the 2degree Field Galaxy Redshift Survey (2dFGRS), in the fields of 17 known galaxy clusters. They used this measurement to trace the distribution of $\mu_\star$, the specific SFR (normalized to $L_\star$) as a function of distance from the cluster center and the local projected galaxy density. They found that the distribution of $\mu_\star$ steadily shifts towards lower values with decreasing distance to the cluster center. Away from the cluster center, the distribution of $\mu_\star$ eventually converges to the field distribution at distances greater than ≈ 3 times the virial radius. A correlation between SFR and local projected gas density is also observed, which is independent of cluster velocity dispersion and disappears at projected densities below $\sim 1\,(h^{-1}\,Mpc)^{-2}$. This characteristic scale was shown to correspond to the mean density at the virial radius of the cluster. The same correlation between SFR and galaxy density is seen to hold true for galaxies more than two virial radii from the cluster center. This suggests that the influence of the environment is not simply confined to cluster cores, but extends to all groups where the density exceeds $\approx 1\,(h^{-1}\,Mpc)^{-2}$.

Gómez et al. (2003), using Hα equivalent widths (EW) as an indicator of SFR in the Early Data Release (EDR) of the SDSS, confirmed this result and established a SFR-density relation for the SDSS galaxies. They found that the overall distribution of SFRs is shifted toward lower values in more dense environments. The effect is most noticeable for the strongly star-forming galaxies (EW(Hα)$>$ 5 Å) in the 75th percentile of the SFR distribution. They

also found a characteristic "break" (or characteristic density) in the density-SFR relation at a local galaxy density of $\approx 1\,(h^{-1}\,Mpc)^{-2}$. They explored whether the density-morphology relation (Dressler (1980), see §1.3.3) alone could explain the density-SFR relation and concluded that it could not. Using the concentration index of SDSS galaxies as a morphology indicator, they showed that SFRs for galaxies of the same type were suppressed in dense regions. Samples at $z > 0.2$ have also been used to suggest a suppression in the SFR of galaxies in the cores of distant clusters compared to those in the field (Balogh et al., 1997; Hashimoto et al., 1998; Couch et al., 2001; Postman et al., 2001). Together this provides strong evidence for a decrease in SFR of galaxies in dense environments, spanning a wide range of densities ($0.08 - 10\,(h^{-1}\,Mpc)^{-2}$) and redshift (out to $z \approx 0.5$). In addition, Balogh et al. (1997) and Hashimoto et al. (1998) found that cluster galaxies have a reduced SFR compared with the field, independent of morphology.

Not all studies agree with the general SFR-density trend though. Balogh et al. (2004) analyzed Hα emission strength as a function of galaxy environment using galaxies selected from the SDSS and 2dFGRS. They found that the distribution of Hα EWs is bimodal, consisting of actively star-forming populations with EW(Hα)$>$ 4 Å and a quiescent population with little current SF. They showed that the distribution of EW(Hα) for the star forming population does not itself depend on environment, and concluded that it was unlikely that SFRs are gradually decreasing in a substantial number of star-forming galaxies in or near dense regions today. They did find, however, that the fraction of galaxies with EW(Hα)$>$ 4 Å decreases steadily with increasing local density.

At higher redshifts, we are beginning to see evidence that the SFR-density relation may be inverted. Cooper et al. (2008), using galaxies from the SDSS and DEEP2, studied the relationship between star formation and environment at $z \approx 0.1$ and at $z \approx 1$. The SFR is estimated using the [OII]$\lambda 3727\,\AA$ nebular line luminosity. The SFR-density relation at $z \approx 1$ is found to be inverted relative to the local relation, with the average SFR in galaxies being higher in more dense regions as we go to higher redshifts. This observed evolution in the relation is thought to be driven by a population of bright, blue galaxies in dense environments at $z \approx 1$. This population, which lacks a counterpart at $z \approx 0$, is thought to evolve into members of the red sequence of galaxies from $z \approx 1$ to $z \approx 0$. The trend in

the SFR-density relation at high redshift was also confirmed by Elbaz et al. (2007) using galaxies in the Great Observatories Origins Deep Survey (GOODS) at $z \approx 1$. We discuss the inversion of the SFR-density relation in §1.5.

1.3.2 The Dependence of Luminosity and Color on Environment

Blanton et al. (2003b) observed that the distribution of *(g-r)* color of galaxies is bimodal for galaxies in the SDSS, there being a strong correlation between the very reddest galaxies and their exponential light profile. They found that the most luminous galaxies consist of a homogeneous red, highly-concentrated, high-surface brightness population which resides in dense environments in the Universe. Underluminous galaxies are less homogeneous, but are generally bluer, less concentrated, with lower surface brightness, and reside in less dense environments. The relationships between galaxy luminosities, surface brightness profiles and colors were found to separate clearly for concentrated versus unconcentrated galaxies. Some of these relationships, like the color-magnitude relation of concentrated galaxies (Baum, 1959) have already been well established.

Blanton et al. (2003b) showed that galaxy luminosity is a strong function of the local galaxy density. The most luminous galaxies exist preferentially in the densest regions of the Universe. Density is found to increase with luminosity for all absolute magnitudes above $M_i = -18$. At lower luminosities, the local density increases again – this is related to the existence of dwarf spheroidal galaxies in clusters. This result agrees with results from the Center for Astrophysics (CfA) redshift survey (Hamilton, 1988), the Optical Redshift Survey (Hermit et al., 1996), as well as with the results of Zehavi et al. (2002) in the SDSS. It turns out that the dependence on luminosity is not independent of galaxy color; in fact, there is a complex interrelationship between galaxy density, color and luminosity as was shown by Hogg et al. (2003).

Hogg et al. (2003) studied the mean environment of 115 000 galaxies in the Sloan Digital Sky Survey (SDSS) as a function of their rest-frame luminosity and color. Galaxy overdensities were estimated in 8 and 1 $h^{-1}\,Mpc$ spheres centered on each galaxy. They observed that blue galaxies i.e., those bluer than the red sequence of old stellar populations, show no corre-

lations between their luminosities and their overdensities, at fixed color. These galaxies are "late-type" and include most spiral and irregular galaxies. This suggests that at fixed star formation history, the late-type mass is only a weak function of environment. For galaxies with the red colors of early-types, the environment does seem to depend on their luminosity. Both low-luminosity and high-luminosity red galaxies were found to be in highly overdense regions.

Hogg et al. (2004) also studied the distribution of color and absolute magnitude for 55 158 galaxies in the redshift range $0.08 < z < 0.12$ as a function of galaxy overdensity. The latter was measured in a cylinder of transverse radius $1\,h^{-1}\,Mpc$ and line-of-sight half-length $8\,h^{-1}\,Mpc$. In all environments, they showed that the color-magnitude diagrams of bulge-dominated galaxies were dominated by red galaxies and the mode of the color distribution at fixed absolute magnitude varied linearly as a function of the absolute magnitude. They concluded that although the most luminous galaxies reside preferentially in high-density regions and blue galaxies reside preferentially in low-density regions, there was only a very small variation with overdensity in the color (zero-point) or slope of that linear relation between color and luminosity (< 0.02 mag in $g - r$.). They used these results to constrain variations with environment in the ages and metallicities of typical bulge-dominated galaxies to be under 20 percent.

The relationship between color and environment observed locally has been shown to occur at higher redshifts as well. Cooper et al. (2006) studied the relationship between color and environment in a sample of 19 464 galaxies drawn from the DEEP2 Galaxy Redshift Survey, with redshifts in the range $0.4 < z < 1.35$. They found that the fraction of galaxies on the red sequence depends strongly on the local environment out to $z > 1$, being larger at higher galaxy densities. They also observed a small population of red, early-type galaxies in low density environments over the entire redshift range. They showed that the color-density relation in galaxies evolves continuously over the redshift range studied, and became weaker at higher redshifts. Red galaxies are seen to favor more dense environments at low redshifts compared to their red-sequence counterparts at high redshifts. At $z > 1.3$ there is no detectable dependence of galaxy color with environment in the DEEP2 sample. The results support a picture whereby the red sequence grew preferentially in dense environments

(i.e. galaxy groups) at $z < 1.5$. It suggests that the environment does play an important role in establishing the existence of the color-density and morphology-density relation in galaxies over cosmic time. Their findings also suggest that there should be little color dependence in the clustering of $\sim L^{\star}$ galaxies at $z > 1.3$.

Cucciati et al. (2006) also studied the color-density relation up to $z \approx 1.5$ using 6582 galaxies from the First Epoch VIMOS-VLT Deep Survey (VVDS) and observed similar results. They show that the color-density relation undergoes a large change as a function of cosmic time. At lower redshift, they found a steep color-density relation, with the fraction of the reddest galaxies of the same luminosity increasing as a function of density, while this trend progressively disappears at higher redshifts. The results suggest the existence of an epoch characterized by the absence of the color-density relation. The rest frame $u - g$ color-magnitude diagram shows a bimodal distribution in both low and high density environments up to $z \approx 1.5$. The bimodal distribution is not universal but is found to depend strongly on the galaxy environment: at lower redshifts the color-magnitude diagrams in low and high density regions are quite different. At high redshifts the two distributions almost mirror each other, reflecting the progressive weakening of the color-density relation.

1.3.3 The Dependence of Galaxy Morphology on Environment

In dense environments the galaxy population is dominated by early-types. This was first established by Dressler (1980) who studied 55 nearby, rich clusters and found that the S0 fraction increases steadily and the elliptical galaxy fraction increases sharply at the highest densities while the fraction of spiral galaxies decreases steadily with increasing local galaxy density. This density-morphology relation implies that the morphology of the galaxy is shaped by the physical mechanisms that are prevalent in its particular environment. The density-morphology relation was also observed in groups of galaxies. Postman and Geller (1984), looking at the same dataset found that the relation extended to galaxy group environments identified in the CfA Redshift Survey. The relation was also observed in X-ray selected poor groups (Tran et al., 2001). However Whitmore (1995) found that the relation is very weak or non-existent in groups.

Goto et al. (2003b) studied the density-morphology relation and the morphology-cluster-centric-radius relation in galaxies in the SDSS and found that the elliptical fraction increases and the disk fraction decreases with increasing galaxy density. They also found that there are two characteristic changes in both relations, suggesting that two different mechanisms are responsible for the relations. In the sparsest regions (below 1 $(h^{-1}\,Mpc)^{-2}$ or outside of 1 virial radius), they found that both relations became less noticeable, but in the intermediate-density regions (density between 1 and 6 $(\mathrm{h}^{-1}\,Mpc)^{-2}$ or between 0.3 and 1 virial radii), they found that the fraction of S0s increases in higher density environments, whereas the disk fraction decreases. In the densest regions (above 6 $(h^{-1}\,Mpc)^{-2}$ or inside 1 virial radius), the S0 fraction decreases rapidly and the elliptical fraction increases, suggesting that a second mechanism is responsible for any morphological transformation of galaxies in the cluster cores.

The density-morphology relation has also been detected at higher redshifts. Dressler et al. (1997) found a strong relation for centrally concentrated clusters at $z \approx 0.5$ but not for less concentrated ones. Fasano et al. (2000) studied nine clusters in the redshift range $0.1 \leq z \leq 0.25$ and found a density-morphology relation in high elliptical concentration clusters though not in low elliptical concentration clusters, consistent with Dressler et al. (1997). They also traced the morphological fraction as a function of cosmic time and found that the S0 fraction in clusters decreases with increasing redshift while the spiral fraction increases, a phenomenon known as the "Butcher-Oemler effect" (Butcher and Oemler, 1978). However, Holden et al. (2007), using galaxies in five massive X-ray clusters from $z = 0.023$ to $z = 0.83$ found that the evolution of the morphology-density relation differs considerably between galaxies selected by stellar mass and those selected by luminosity, the early-type fraction changing much less in mass-selected samples. The result is echoed by van der Wel et al. (2007) who used galaxies in the SDSS and the GOODS-South field and found little change in the morphology-density relation since $z \approx 0.8$ for galaxies more massive than $0.5\,M_{\star}$.

We now examine the theoretical predictions from numerical simulation and semi-analytic models of galaxy formation that attempt to account for the above trends between galaxy properties and their environment. While a majority of the observed trends can be replicated

by these predictions, some of them, especially the evolution of these trends with redshift, cannot. We attempt to understand the source of this disagreement.

1.4 THEORETICAL PREDICTIONS: HIERARCHICAL STRUCTURE FORMATION

According to models of hierarchical formation (Kauffmann et al., 1993; Somerville and Primack, 1999; Cole et al., 2000), galaxies form in less dense environments and are then accreted into larger halos (e.g., falling into clusters or groups), having their hot gas reservoir removed as this occurs. Galaxies therefore experience different environments during their lifetimes. Recent N-body simulations and semi-analytical models have addressed a number of the important issues with the hierarchical formation scenario. The models predict that "integrated" galaxy properties such as color, luminosity and SFR, are correlated with their environment. However, it is difficult to make model predictions about how properties *within* galaxies depend on their environment. The reason for this is that processes such as star formation which occur on the scales of molecular clouds, are an order of magnitude smaller in scale than those of galaxies themselves.

In the semi-analytic models by Kauffmann et al. (1993), for example, a morphology-density relation is, in some sense, built into the model: early-type galaxies form by mergers within galaxy groups and are then incorporated into larger systems such as clusters. Their colors are predicted to redden as a result of accretion into the high density region and this environment is also expected to host the most massive and luminous bulge-dominated systems. This prediction is in agreement with the the observed dependence of the mean galaxy environment on the color and luminosity of galaxies in the SDSS (Hogg et al., 2003; Blanton et al., 2003b) and also the dependence of the color-magnitude relation of bulge-dominated galaxies on their environment (Hogg et al., 2004) as was discussed in the previous section. The models also predict a gradual decrease in SF activity in more dense regions as the remaining cold gas in the accreting galaxies is used up. As was discussed earlier, this effect is observed by Lewis et al. (2002) with the 2dFGRS and Gómez et al. (2003) with the

SDSS.

Which galaxy interactions are incorporated in the environment of galaxies? Figure 1.2 shows a sample of different environments that galaxies can reside in, as well as the interactions they undergo in these environments. We first examine the numerous physical mechanisms that have been proposed for how the SFR and other physical properties in galaxies are affected by their environments. Not all mechanisms have been included in the latest models, but it is important to characterize the different mechanisms that are at play and also their relative importance in different environments.

1.4.1 Physical Mechanisms That Affect Galaxies

1.4.1.1 Mergers Galaxy mergers, such as the one shown in the top right of Figure 1.2, are thought to be quite rare in massive clusters because of the large velocity dispersion in clusters, but they are much more common in the infalling group environment (De Lucia, 2006). According to De Lucia (2006), mergers are an integral "preprocessing" step in the evolution of galaxy clusters. They are important at early times in the life of a cluster, when it is first collapsing, and at later times in the outskirts of the cluster, as it accretes groups from the field. Numerical simulations (e.g., Mihos (2004)) have shown that close encounters can result in the formation of spiral arms and in some cases, bars. The axisymmetry of these structures leads to the funnelling and compression of the gas and this in turn can fuel starburst or AGN activity. A direct merger, however, can completely destroy the disk. The hot remnant then has the photometric and structural properties of elliptical galaxies (as in the right of Figure 1.1) which explains why mergers are thought to be the main mechanism by which bulges are formed.

Given their importance in the evolution of clusters, mergers are included in standard semi-analytic models. As discussed previously, in the hierarchical formation scenario, smaller galaxies merge to form larger systems. In their model, De Lucia et al. (2006) defined every galaxy as an effective number of stellar progenitors. They found that in contrast to the formation history of stars themselves, the assembly history of ellipticals mirrors the hierarchical growth of dark matter halos. Their work suggested that a significant fraction of

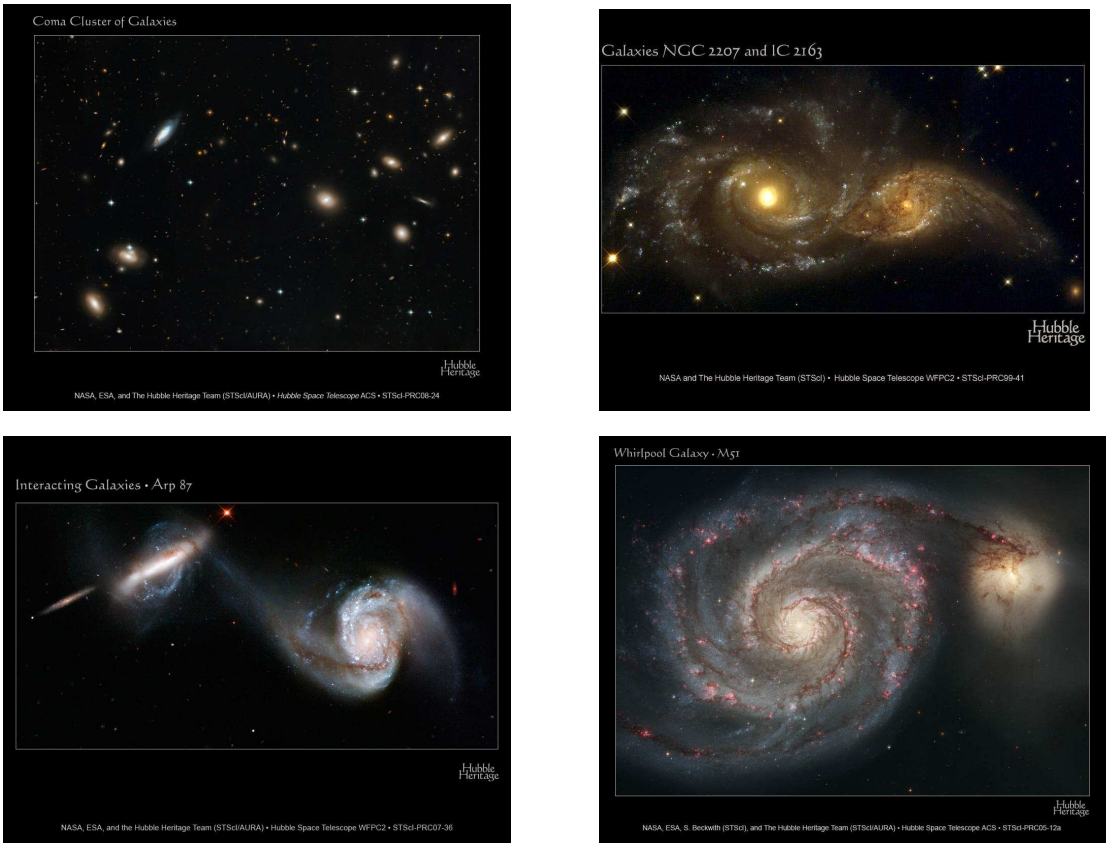

Figure 1.2: Different galaxy environments. Top left: A galaxy cluster – this is the Coma Cluster of Galaxies, which is more than 350 Mly away and 1 Mpc in diameter. It is one of the densest clusters known, containing over 1000 galaxies. It consists mainly of elliptical galaxies although a blue spiral galaxy can be seen in the upper left. Top right: A merger of two spiral galaxies – NGC 2207 and its smaller companion, IC 2163. The merger disrupts the morphologies of the two objects, creating sheets of shocked gas, dust lanes and starbursts. The merger remnant is likely to be an elliptical. Bottom left: An interacting galaxy pair, Arp 87 before a merger. The bridge of stars, gas and dust, which stretches for over 75 000 ly, and joins the two galaxies, is evidence that a close encounter took place. Both galaxies experience strong tides due to mutual gravity which distorts their shapes. Repeated close encounters over several Gyr should result in an eventual merger. Bottom right: Evidence of Cannibalism (see §1.4.1.5). The larger galaxy is M51, the "Whirlpool Galaxy" which is about 37 Mly away and the smaller companion is NGC 5195. Due to the interaction, the gas in the larger galaxy is disturbed and compressed in some regions, triggering new star formation. Source: Hubble Heritage Project (http://heritage.stsci.edu/).

present ellipticals have assembled relatively recently through mergers alone, and this is also in agreement with recent observations (van Dokkum, 2005; De Lucia et al., 2006).

1.4.1.2 Galaxy Harassment "Galaxy harassment" refers to repeated, high-velocity interactions between galaxies. It is a high density phenomenon and has been studied by Richstone (1976) in their work on the dynamical evolution of cluster galaxies. It has also been explored in numerical simulations by Farouki and Shapiro (1981). Harassment is distinct from galaxy mergers. Moore et al. (1996) observed that spiral galaxies that have disturbed morphologies and show bursts of star formation pervaded clusters at $z \approx 0.4$ while nearby clusters strongly favor ellipticals over spirals. Harassment is believed to drive the morphological transformation of galaxies in clusters and it also provides fuel for quasars in subluminous hosts and leaves detectable debris arcs, as observed with Hubble Space Telescope (HST) imaging. While merging of spirals in groups creates bright ellipticals, in a cluster, dwarf ellipticals are created by harassment of low luminosity spirals. Harassment thus can change any internal property of a galaxy within a cluster, including the gas distribution, the orbital distribution of stars and the overall morphology by destroying low surface brightness galaxies in clusters. Moore et al. (1999) showed, through more detailed simulations, that the efficiency of this process is indeed limited to low-luminosity hosts, due to their slowly rising rotation curves and their low density cores, as was noted by De Lucia et al. (2006). Harassment is less able to explain the evolution of massive, luminous cluster galaxies.

Harassment is not currently included in semi-analytic models of galaxy formation. Moore et al. (1998) showed that both harassment and the interaction with the global tidal field of the cluster (discussed below) can drive a strong response in cluster galaxies and lead to a similar effect on the star formation and morphology of the galaxies.

1.4.1.3 Ram-pressure stripping Ram-pressure stripping requires dense, hot intracluster gas and takes place in the cores of clusters or in dense sub-clumps. If a cluster galaxy moves through the hot, dense intracluster medium (ICM), it undergoes a pressure front from the ICM which depends on the density of the ICM and the relative velocity between the galaxy and the ICM (Gunn and Gott, 1972; Fujita, 2001). A schematic figure of

this effect is shown in Figure 1.3. Depending on the binding energy of the gas in the galaxy, the ICM will either be forced to flow around the galaxy or will just blow through it, removing some of the diffuse interstellar medium (ISM) in the disk, according to De Lucia et al. (2006). High-resolution three-dimensional numerical simulations show that the ram-pressure can remove almost all of the atomic hydrogen of luminous galaxies within 10 Gyr (Quilis et al., 2000). Even if ram-pressure stripping is not effective, similar mechanisms can take its place, including thermal evaporation (Cowie and Songaila, 1977) and viscous stripping of galaxy disks (Nulsen, 1982). In the latter case, turbulence in the gas flowing around the galaxy causes the depletion of the ISM.

Unlike mergers which result in bulge formation, gas stripping can only change the galaxy morphology indirectly. It can halt star formation in the disk resulting in the disk becoming fainter and in a higher bulge-to-disk luminosity, seeming to make the galaxy more "early-type" (De Lucia et al., 2006). The effects of ram-pressure stripping have only been discussed in a handful of studies that employed semi-analytic models (Lanzoni et al., 2005). These studies conclude that the inclusion of gas stripping causes only mild variations in galaxy colors and SFR. Driver et al. (2008) has also proposed that stripping the dust (instead of the gas) can also make galaxies brighter and also redder, as the red bulge light which was previously concealed behind optically-thick dust screens, becomes visible.

Sometimes the pressure front can be so strong as to strip the hot gas from the halo of the infalling galaxy, not just the cold gas in the disk. This is referred to as "strangulation" and has been shown to suppress star formation in the infalling galaxy very efficiently.

1.4.1.4 Interaction with the Cluster Tidal Field

It was observed by Gavazzi (1987) that some very active spiral galaxies exist in nearby rich clusters, such as the Coma Cluster shown in Figure 1.2, in which a blue disk galaxy can be observed. Byrd and Valtonen (1990) demonstrated, using computer simulations, that the tidal field of a cluster as a whole should have major effects on gas-rich spiral galaxies. They found that spirals within several core radii of the center of the cluster (roughly 800 kpc) should experience nuclear inflow and disk star formation, and thus be triggered into activity. Mutual collisions of gas clouds within the disk can be induced by tidal perturbations and this will trigger cloud collapse and star

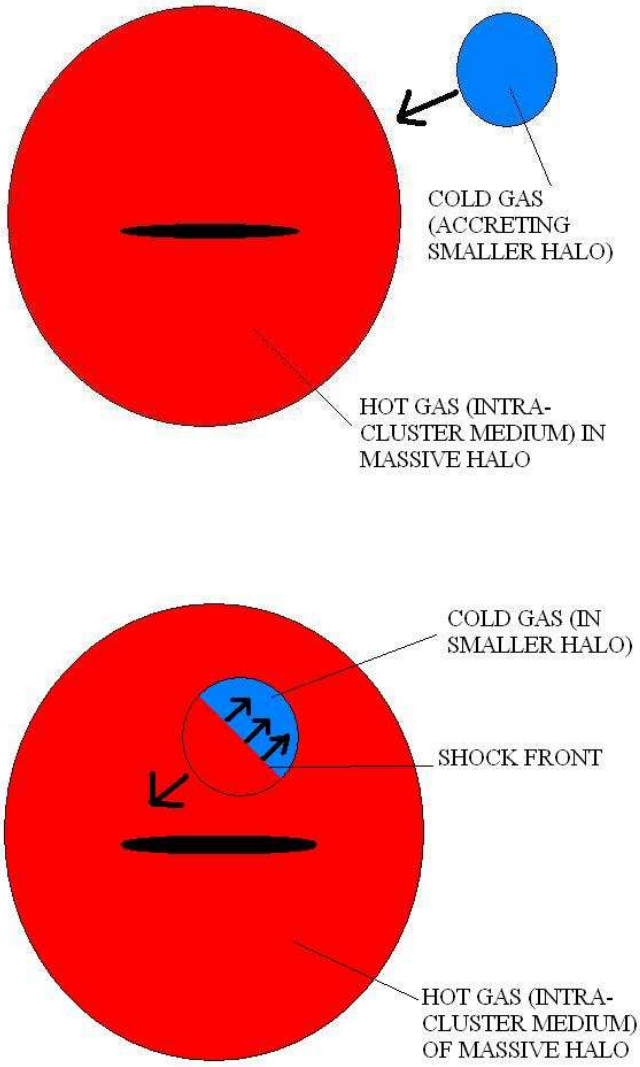

Figure 1.3: A schematic representation of ram-pressure stripping. Top panel: A low mass galaxy containing cold gas, before accretion into a more more massive halo (a cluster of galaxies) containing the dense, hot intra-cluster medium (ICM). Only the central galaxy in the cluster is shown. The arrow shows the velocity of the infalling satellite galaxy. Bottom panel: After the smaller satellite galaxy is accreted into the larger halo, it experiences a pressure front due to the ICM (indicated by the boundary between the cold and hot gas in the smaller halo) – the direction of the front is shown by the three arrows. The hot ICM will either be forced to flow around the smaller satellite galaxy or will blow through it, removing the cold gas in the smaller galaxy in the process.

formation because of the thinness of the cluster medium compared to the high density of the molecular clouds (Byrd and Valtonen, 1990). The presence of active spiral galaxies in rich clusters suggests that mergers and harassment are not the only mechanisms to generate starburst spirals in clusters. In the long-term, such activity will remove the disk gas from spirals, truncating their star formation and changing them into S0s. This would suggest that gas rich spirals would be rare in such clusters. Byrd and Valtonen (1990) showed that ram-pressure stripping by the ICM is unlikely to produce these gas-poor S0s.

The blue but H-I poor disk galaxies identified in the central part of the Coma Cluster (Bothun and Dressler, 1986) are probably galaxies which initially underwent a tidally induced burst of star formation followed by "disk cleaning", as was pointed out by Byrd and Valtonen (1990). Red gas-poor disk galaxies in the same cluster regions were probably cleaned at an earlier time. Byrd and Valtonen (1990) also showed from simulations that a strong tidal field could transform a normal spiral into a barred spiral, which would explain the overabundance of barred spirals in the central regions of the Coma Cluster.

1.4.1.5 Cannibalism: Dynamical Friction Cannibalism refers to a slow encounter between a large and small galaxy. An example of cannibalism is shown in the bottom right panel of Figure 1.2. While the smaller galaxy is tidally disrupted by the larger companion, gas and stars are incorporated into the larger galaxy. Isolated galaxies can grow in this way by accreting their dwarf companions, and those in clusters can grow by accreting their satellite galaxies, via dynamical friction. This is responsible for forming the brightest cluster galaxies (Ostriker and Tremaine, 1975; White, 1976) and is in agreement with the hierarchical growth of structure. Like galaxy-galaxy mergers, this phenomenon is most efficient within small halos with low velocity dispersion. According to De Lucia et al. (2006), it is the accretion rate of the galaxies into the proto-cluster, along with the cluster growth itself, that controls and sets the conditions for cannibalism as well as galaxy merging.

1.4.1.6 AGN heating It was realized that there must be some mechanism which stops the cooling flows that would otherwise produce too many massive and luminous galaxies compared to the observed number (De Lucia et al., 2006). Early semi-analytic models

included an ad-hoc prescription to suppress cooling flows in halos above a critical mass. More recent models have included more physically motivated prescriptions and have confirmed that AGN heating is indeed important to reduce the exponential cut-off at the bright end of the galaxy luminosity function (Croton et al., 2006). Recently, Somerville et al. (2008) presented a new semi-analytic model that self-consistently traces the growth of supermassive black holes and their host galaxies within the context of the LCDM cosmological framework. In this model, the energy emitted by accreting black holes regulates the growth of the black holes themselves, and produces powerful jets that heat the hot gas atmospheres that surround groups and clusters. The model predicts that star formation should be largely quenched in massive galaxies at $z \approx 0$. These prescriptions are still not well grounded in observations, and much more work needs to be done to understand the role of AGN in galaxy evolution.

Unfortunately, there exists little empirical evidence that any one of the above processes is actually responsible for driving trends in galaxy evolution. These processes act over a long period of time, and observations at a specific redshift cannot provide the detail that is necessary to understand what is happening in each of these complex interactions (De Lucia et al., 2006). One way of making progress is to specify the environment in which the properties of galaxies change, from say blue star-forming systems to red, quiescent systems.

1.4.2 Comparing Theoretical Predictions to Observations

The results of Gómez et al. (2003) with the SDSS, and Lewis et al. (2002) with the 2dFGRS, show that suppressed star formation is not limited to the cores of rich clusters, but is found in any environment in which the local projected galaxy density exceeds one galaxy (brighter than $M_b = -19$) per Mpc^{-2}. This is in approximate agreement with the results of Kodama et al. (2001), though a direct comparison is not possible because that survey probes much deeper down the luminosity function, so the local projected galaxy densities are higher in the same environments. Whatever mechanism is responsible for terminating star formation in galaxies is therefore not specific to the cores of rich clusters, but is also associated with dense groups in the cluster infall regions as well. The low SFRs even well beyond the virialized cluster seem to rule out the physical processes that are predominant in the cores of rich

clusters. Mechanisms such as ram-pressure stripping of galaxy disks appear not to be solely responsible for the correlation of star formation with local density.

The observations are in qualitative agreement with the predictions of present-day hierarchical models of galaxy formation. Unfortunately, these are somewhat limited in that they do not directly model all the above processes – instead there are some assumptions about them that are built-in. In particular, most do not include a calculation of ram-pressure stripping of the cold, disk gas, nor of other physical processes like galaxy harassment which might play a role in dense environments. The only environmental effect on star formation rate in these models, apart from a possible difference in merging history, is related to the hot, halo gas which is thought to surround every isolated galaxy (Diaferio et al., 2001). According to Diaferio et al. (2001), it is assumed that galaxies maintain the supply of cold gas (to fuel star formation) via continuous cooling from a hot, diffuse gas halo associated with the dark matter potential (Somerville and Primack, 1999; Kauffmann et al., 1999; Cole et al., 2000). In halos with more than one galaxy, this hot gas is only associated with the central galaxy; satellite galaxies are assumed to lose their supply of fresh fuel through ram pressure stripping and tidal effects (though these are not directly modelled). In these models, therefore, star formation rates begin to decline for any satellite galaxy, whether in a poor group or a rich cluster.

These models are able to reproduce radial gradients in star formation within the virial radius of clusters to a very high accuracy. Diaferio et al. (2001) predict that the mean star formation rate should be equivalent to the field value beyond $\sim 2R_v$, in physical (i.e. not projected) space. Balogh et al. (2000) also investigated the origin of cluster-centric gradients in SFRs and colors of rich cluster galaxies in the CNOC1 data set of intermediate-redshift clusters. They used a more simplified version of the Diaferio et al. (2001) model, where clusters are built through the ongoing accretion of field galaxies. These models assume that after galaxies enter the cluster their SFRs decline on a timescale of a few Gyr (comparable to the typical gas consumption timescale for disk galaxies in the field). They combined these timescales with mass accretion histories from N-body simulations of cluster formation in a ΛCDM universe to show that there is an expected strong suppression of SF in cluster galaxies. The simulations also show that a significant fraction of galaxies beyond the virial

radius of the cluster may have been within the main body of the cluster in the past. This would explain why star formation in the outskirts of clusters (and as far out as two virial radii) is systematically suppressed relative to the field. The agreement with data beyond the cluster virial radius is further improved by assuming that gas-stripping happens within lower mass systems, before the galaxy is actually accreted into the cluster. The suggestion is that the SFRs of cluster galaxies depend primarily on the the time since their accretion onto massive virialized systems, and that the SFR suppression happens gradually over a few Gyr.

In their work, Balogh et al. (2000) do not model the properties of the field galaxy population directly, but they take them empirically from observations of the $z \sim 0.3$ field. The advantage of this is that the effects of halo-stripping can be seen directly, since that is the only physical process (apart from gravity) which is accounted for. They traced the mean star formation rate relative to the field, as a function of the local projected density of galaxies. Local density is defined as the projected surface mass density, computed by finding the radius encompassing the ten nearest (in projection) particles in the simulations. According to Balogh et al. (2000), galaxies are assumed to lose their reservoir of hot gas when they are associated with a group with circular velocity $V_c > 600$ km s^{-1}. While a direct comparison with the data is not possible since the simulations only provide the dark matter density, they argued that a comparison relative to the mean surface density within R_v should be fair if the mass distribution traces the light distribution. They found that the mean star formation rate decreases by a factor of ~ 3 for every factor 10 increase in surface density and that the correlation plateaus at surface densities $\sim 1/7$ that of the mean projected density within R_v. This threshold is a factor ~ 2 lower than seen in the data, but the agreement was considered quite promising given the crudity of the model. The simulations used in the model do not include a large enough volume to probe beyond a few R_v.

However, we now know that current models in which halo-stripping of the satellite galaxies is the only direct effect of the "environment" (simply assuming that every satellite galaxy has no reservoir of hot gas immediately after it merges with a larger halo) do not agree with the observations. Coil et al. (2008), compared measurements of the color and luminosity

dependence of galaxy clustering at $z \approx 1$ in DEEP2, with the predictions of a semi-analytic galaxy formation model that was applied to the Millennium Run simulation. Differences between the data and the model suggest that in the model, star formation is shut down too efficiently in these infalling satellite galaxies. Much work therefore needs to be done to improve the success of the models in the lower density regions, far from the cluster core.

1.5 EVIDENCE FOR "NATURE": DOWNSIZING

The most massive galaxies known today are giant ellipticals that reside in the most dense galaxy environments (Dressler, 1980), which are also known to have formed their stars rapidly at an early stage in cosmic history. Recent studies of the evolution in the global space density of galaxy SFRs find that the majority of the observed SF occurs in the highest mass galaxies at high redshift, moving to lower mass galaxies at lower redshifts (Panter et al., 2004; Juneau et al., 2005; Panter, 2006; Seymour et al., 2008; Feulner et al., 2005). This is referred to as "downsizing" (Cowie et al., 1996). It is characterized by a decline in the mass of the galaxies that dominate the star-formation rate density with decreasing redshift ("downsizing of star formation"). The term "downsizing" was coined by Cowie et al. (1996) to describe the decline with time of the K-band rest-frame luminosity of galaxies with the highest specific SFR as observed in the redshift interval $0.2 < z < 1.7$. This "downsizing" has been confirmed by other studies.

"Downsizing" is clearly evident in the stellar populations of galaxies. Thomas et al. (2005) used star formation histories derived from observed line indices and abundance ratios in combination with the predictions of stellar evolution models and showed that there is a strong correlation between mean stellar age and galactic stellar mass both in elliptical galaxies and in the general population of galaxies from the SDSS. Heavens et al. (2004), using 96 545 nearby galaxies in the SDSS, found that the larger the stellar mass of the galaxy, the earlier its stars were formed. This points to a very different formation history for high- and low-mass galaxies. Juneau et al. (2005) studied the cosmic SFR and its dependence on galaxy stellar mass over the redshift range $0.8 < z < 2$ using data from the Gemini

Deep Deep Survey (GDDS). They discovered that the SFR in the most massive galaxies ($M_\star > 10^{10.8}\,M_\odot$) is higher at $z = 2$ than it is today. It was shown to drop steeply from $z = 2$, reaching its present value by $z \approx 1$. In contrast, the SFR density of intermediate-mass galaxies ($10^{10.2}\,M_\odot < M_\star < 10^{10.8}\,M_\odot$) declines more slowly and may peak or plateau at $z \approx 1.5$. They use the characteristic growth time (given by the ratio of stellar mass density to SFR density), $t_{SFR} = \rho_{M\star}/\,\rho_{SFR}$, to provide evidence of an associated transition in massive galaxies from a bursty star formation mode to a quiescent one at $z \approx 2$. Intermediate-mass systems transit from burst to quiescent mode later, at $z \approx 1$, while the lowest mass objects are found to undergo bursts throughout their evolution. Their results showed that the formation era for galaxies was extended and proceeded from high- to low-mass systems. The most massive galaxies formed most of their stars in the first ~ 3 Gyr of cosmic history. Intermediate-mass objects continued to form their dominant stellar mass for an additional ~ 2 Gyr. But the lowest mass systems were shown to have been forming over the whole cosmic epoch spanned by GDDS. These observations clearly support the "downsizing" in the SFR whereby galaxy formation proceeds from larger to smaller mass scales.

It is possible that downsizing and galaxy bimodality are connected through the same underlying physics. Recent models of galaxy formation (Cattaneo et al., 2006; Bower et al., 2006) have been driven by the fact that there are two distinct galaxy types: blue star-forming late-type galaxies tend to reside in low-density environments while red quiescent early-type galaxies reside in groups and clusters. Blue galaxies fall below a critical stellar mass of $M_\star \approx 3 \times 10^{10} M_\odot$ while red galaxies have higher stellar masses. The color bimodality itself is therefore evidence for downsizing: the most massive galaxies which happen to be the red ones have converted their gas into stars several billion years ago, while less massive galaxies which are generally blue, are still making stars. In fact, downsizing can be viewed as part of a more general phenomenon which takes place across the Hubble sequence of galaxy types. Even with the same spectral type, less massive galaxies contain younger stars.

Our primary focus in this work is on star formation. What does this imply for the environmental dependence of star formation in galaxies that formed in different epochs? Together with the trend for massive systems to occur predominantly in dense environments, downsizing should result in a scenario where the SFRs in dense environments at low redshifts

are lower than in less dense regions, and this is consistent with the observations. The implication is that at sufficiently high redshifts, ($z \geq 2$) where the SFR is dominated by the most massive galaxies, the SFR-density relation should invert, with the most dense environments hosting elevated SFRs compared to the field.

This trend is beginning to be observed. Elbaz et al. (2007) observe this reversal in the SFR-density relation at higher redshifts for galaxies in the redshift range $0.8 < z < 1.2$. Poggianti et al. (2006) show that at $0.4 < z < 0.8$ the suppression of SFR in dense environments is weaker than that observed locally. Ilbert et al. (2006) show environmental dependent evolution in the galaxy luminosity function from $0.4 < z < 1.2$, suggesting an increase in the density of faint red galaxies in overdense regions as cosmic time increases. More confirmation is clearly needed but these examples are consistent with the scenario that galaxies in dense environments form stars rapidly at early times, quickly building up mass and becoming quiescent, while galaxies in less dense environments form stars at a more sedate pace but over longer timescales.

There is another type of downsizing that has an important distinction from that described above. This is "downsizing with quenching" and it follows a different timescale - spheroidal galaxies have been known to have a second star-formation timescale, namely that of "quenching": it becomes easier to keep galaxies gas-free with time. In fact, recent studies of the galaxy luminosity function at $z \approx 1$ (Bell et al., 2004; Faber et al., 2007) conclude that massive red galaxies observed at $z \approx 0$ migrated to the bright end of the red sequence by a combination of two process: the quenching of star formation in blue galaxies and the merging of less-luminous, previously quenched red galaxies. Faber et al. (2007) conclude that the typical mass at which a blue, star-forming galaxy is quenched (and therefore enters the red sequence) decreases with time. Our work will focus on the "downsizing of star formation" as opposed to this "downsizing with quenching".

1.6 DISTINGUISHING BETWEEN NATURE AND NURTURE USING THE SPATIAL VARIATION OF STAR FORMATION IN GALAXIES

In this work, we aim to determine whether it is indeed the strong physical "infall and quench" processes described in §1.4 that shape the properties of galaxies or whether there exists some other mechanism by which galaxy properties are determined. This alternate mechanism is independent of the strong physical interactions that galaxies undergo but may still be indirectly dependent on the galaxy environment. Indeed, we have outlined one such scenario in §1.5 whereby galaxies evolve primarily because of their intrinsic properties such as mass. These intrinsic properties could still be shaped by the environment in which the galaxy resides (for example, more massive galaxies reside preferentially in more dense regions). We can thus refer to this latter scenario as "environmentally-governed evolution". It is possible that both of these scenarios play a role in the evolution of galaxies. Perhaps one may be significantly or even marginally dominant over the other.

Can we then distinguish between these two scenarios of galaxy evolution? In fact, the "environmentally-governed evolution" scenario makes a distinct prediction compared to the "infall and quench" one. The latter incorporates strong physical interactions such as ram-pressure stripping and galaxy harassment and these processes should affect the outskirts of galaxies before they affect the interiors. This suggests that galaxies in dense environments should show an SFR distribution that is progressively suppressed from the outside in, as the outer regions are those which will be affected first by their rapidly changing environment. The "environmentally-governed evolution" scenario, on the other hand, makes quite a different prediction. It suggests that the suppression should either happen uniformly as a galaxy ages or that the inner regions should be suppressed first, since nuclear star formation seems to occur more rapidly than star formation in the disk given the elevated gas densities present. Thus by studying the spatial distribution of SFR in star-forming galaxies as a function of environment, we should be able to distinguish clearly between these two scenarios. The spatial distributions of SFR in galaxies should be obtained in a statistical way in order to make this distinction. The very large sample of galaxies available in present multicolor imaging surveys such as the SDSS will provide an excellent data set with which to explore

this. The SDSS is the largest imaging and spectroscopic survey of galaxies that has been undertaken to date, having mapped more than one quarter of the sky using a dedicated wide-angle $2.5\,m$ optical telescope.

Previous studies on the radial dependence of SF have focused on individual galaxies. Pérez-González et al. (2006) studied the recent SF in the early-type galaxy M81 using imaging observations from the far-ultraviolet (UV) to the far-infrared (IR). The data was then compared to models of stellar, gas and dust emission, with results from different sub-galactic regions, including individual HII regions (around $0.1\,kpc$). They were able to confirm the existence of a diffuse dust emission not directly linked to the SF. Using the Hα emission that probes the unobscured SF, and the IR luminosity (especially the $24\,\mu$m emission) that probes the obscured SF in the galaxy, they found a decrease in the ratio of obscured SF to total SF with radius. This fraction varies from an obscured SF of 60% in the inner regions of the galaxy to 30% in the outer regions. Johnston et al. (2005) used pixel-based spectral energy distribution (SED) fitting to a merging system hosting a compact steep spectrum radio source, in order to explore the connection between the nuclear radio emission and the distribution of star formation. Kassin et al. (2003) used pixel-based colors to explore stellar populations and obscuration in the Antennae, and de Grijs et al. (2003) used the same technique to explore the Mice and the Tadpole interacting galaxy systems. Boissier et al. (2007) showed, using GALEX and Spitzer data, that for disk galaxies the attenuation varies radially, being highest in the nuclear regions, and is correlated with metallicity. They also found that the Schmidt law connecting the SF and gas surface densities continues beyond the traditional "threshold" radius. Lanyon-Foster et al. (2007) used a study of pixel Color-Magnitude Diagrams for a sample of 69 nearby galaxies to study stellar populations and structure of galaxies. They found that these Color-Magnitude Diagrams of each galaxy type have distinct trends. In addition, they performed a pixel-by-pixel analysis to show that there is a steady progression in the average pixel color along the Hubble sequence. Finally they compared pixel colors to the Bruzual and Charlot (2003) stellar population models and used these to map the stellar mass distribution and M/L ratio in galaxies.

The current analysis has the advantage of a very large sample, accessible as a result of the SDSS, which enables a study of the environmental dependence of spatially distributed star

formation within galaxies. Also, since the inferred SFRs come from fitting SEDs, derived from stellar population synthesis models, to broadband photometry, there is no aperture effect such as that affecting fiber-based spectroscopy. By fitting SEDs to individual pixels within resolved galaxy images, we can spatially resolve the star formation and explore how this distribution varies for galaxies as a function of local galaxy density.

We will first detail the technique (known as "pixel-z") that will be used to study the spatially resolved star formation in galaxies. This is described in Chapter 2. We will use the "pixel-z" technique to analyze a large sample (more than 40 000) of galaxies in the SDSS. The technique is applied to galaxies in the imaging survey which enables us to determine the SFR (as well as metallicities, age and dust obscuration) of the stellar populations contained in individual pixels of galaxy images. We then use these calculated quantities to explore the radial dependence of SFR *within* galaxies as a function of the galaxy environment and morphological type. This is described in Chapter 3. In Chapter 4, we attempt to determine to what extent the known morphology-density relation of galaxies affects the radial dependence of SFR in them. As we shall see by the end of the analysis, the environment of galaxies plays a significant role in governing their properties.

1.7 PUBLICATIONS AND CONTRIBUTIONS

The following is a list of my papers and publications whose content is described in this thesis:

- Welikala et al. (2008b)
- Welikala et al. (2008a)

This thesis is my own work but I received much help and advice throughout from my advisor, Dr. Andrew Connolly, and also from Dr. Andrew Hopkins and Dr. Ryan Scranton. In addition, Dr. Scranton provided the estimates of local density for galaxies in SDSS DR4, which are described in §3.2.3.

2.0 THE PIXEL-Z: SPATIALLY RESOLVED PROPERTIES OF GALAXY STELLAR POPULATIONS FROM PHOTOMETRY

2.1 INTRODUCTION

The spatially resolved properties of stellar populations in galaxies, such as the rate of star formation, can be a key probe in studying galaxy evolution. In the previous chapter, we proposed that studying these properties as a function of the galaxy environment could put constraints on different galaxy formation scenarios. In this chapter, we describe a method to determine how the parameters that characterize the stellar populations, such as their ages, the rate of star formation (SFR), metallicities and obscuration, are spatially distributed within galaxies. The principle is based on an extension of a technique to obtain photometric redshift ("photo-z") estimates of galaxies. We call it "pixel-z" because the method can be applied to individual pixels in galaxies and makes use of the photometry in these pixels. First however, we describe the motivation for developing the method and the proof-of-concept idea that gave rise to the "pixel-z" technique. We illustrate the method here and before applying the technique to galaxies in the Sloan Digital Sky Survey (SDSS), we test it on galaxies in one multicolor imaging survey: the Hubble Deep Field (HDF). We also discuss the uncertainties in the estimates of the various stellar population parameters that are obtained from the photometric fluxes in the pixels of galaxies.

2.2 SPATIALLY RESOLVED COLORS AND GALAXY EVOLUTION

Deep surveys such as the Hubble Deep Fields[1] (Williams et al., 1996, 2000) have stimulated the growth of new ideas for studying galaxy evolution. One of these papers (Abraham et al., 1999), focused on "*exploring the resolved multicolor data for galaxies of known redshift using spectral-synthesis models*". They studied the star formation history of the Hubble sequence using spatially resolved color distributions of intermediate-redshift galaxies in the Hubble Deep Field (HDF). They used a technique based on matching resolved four-band colors to the predictions of evolutionary synthesis models (the methodology will be discussed in more detail in §2.3.2). The technique enabled them to quantify the relative age, dispersion in age, on-going SFR and star formation history *in distinct subcomponents* of each galaxy. For spiral galaxies, for example, the properties of the underlying stellar populations in the bulge and the disk could be studied separately. In this way, the technique was used to determine the evolutionary history of high-redshift galaxies. They studied spiral and elliptical systems in a near-complete sample of 32 $I_{814} < 21.9$ mag galaxies with $z \approx 0.5$ studied by (Bouwens et al., 1998).

How can multi-color data in subcomponents of a galaxy, perhaps pixels in the galaxy image, be used to place constraints on its past star formation history? To answer this, Abraham et al. (1999) considered the following example: take a late-type spiral galaxy whose star formation history can be approximated by a constant SFR. In reality the constant SFR is effectively a time-average of spatially distinct star forming regions, each of which can be considered as a simple stellar population with a lifetime which is short compared to the dynamical timescale of the galaxy. Over time these young populations would mix with older stars and become part of older components of the galaxy. Abraham et al. (1999) showed that this qualitative picture can be described quantitatively by spectral synthesis modelling, and we will turn to this in §2.4.2.

Abraham et al. (1999) recognized that galaxies are not homogeneous systems with a single age and star-formation history. They argued that this meant that when they are

[1]Based on observations with the NASA/ESA *Hubble Space Telescope* obtained at the Space Telescope Science Institute

spatially resolved, one can expect a dispersion of points on the color-color diagrams, since colors are sensitive to the star formation histories in galaxies. The distribution of pixel-by-pixel colors within a galaxy image is therefore a fossil record, storing the manner in which the stellar population was assembled in a galaxy (e.g., through many small bursts, or by a few larger bursts). The distribution of pixel colors should directly trace the shape of the flux from stars with a range of ages (and metallicities) – such a stellar population is known as a Composite Stellar Population (CSP) (a Single Stellar Population (SSP) refers to a collection of single stars all with the same age and metallicity). This is where the stellar population synthesis codes becomes relevant – in generating the spectra of these stellar populations.

The technique thus makes an explicit connection between evolutionary history and stellar populations. Abraham et al. (1999) used the dispersion around the color-color tracks to distinguish between models that are degenerate in their integrated color. This allows the dust content to be explicitly parameterized and the star-formation histories of spatially distinct galactic subcomponents to be derived. Most importantly, they argued that these spatially resolved color analyses could enable robust studies of the relative ages of stellar populations within galaxies. This can be used to determine whether or not the stellar populations are homogeneous and also to study the order in which the components of the galaxy were assembled.

The findings of Abraham et al. (1999) are now briefly discussed. For elliptical systems, they found that the dispersion of the internal colors of a sample of $0.4< z <1$ field galaxies in the HDF are consistent with them being old and coeval, with $\sim$ 40% showing evidence of younger stellar populations with star formation which must have occurred more recently. The field sample is much too small for robust conclusions to be drawn regarding the star-formation history of early type systems as a whole, but the current fraction ($\sim$ 40%) of young early-type systems is quite consistent with the predictions from hierarchical models.

For the spiral systems, they similarly exploit the dispersion in color to analyze the relative histories of bulge and disk stars, in order to estimate the ages of galactic bulges, which are currently under dispute. Hierarchical galaxy formation scenarios require old bulges formed by mergers (e.g., Kauffmann et al. (1993)). However, N-body simulations indicate that bulges form instead from bulge instabilities in disks (Norman et al., 1996) and this has been

supported by observations of boxy or "peanut" shaped bulges (Kuijken and Merrifield, 1995). The median ages of the stellar populations in the bulge are found to be significantly older than those in galactic disks, and exhibit very different star-formation histories, suggesting that the bulges have a short initial period of star formation followed by relative quiescence. They concluded that unless bulges are heavily enriched relative to disks, this result is inconsistent with the secular growth of bulges from disk instabilities, but consistent with gradual disk formation by accretion of gas onto bulges, as predicted by hierarchical models.

The star-formation histories they inferred for the spiral galaxies in the field agree with those derived from deep galaxy surveys. If significant morphological transformations have not occurred within the spiral sample, then the declining star-formation histories are consistent with typical fading in disk light by $M_B \sim 0.4$ mag between $z = 1$ and $z = 0.5$. This agrees with observations from the CFRS survey (Brinchmann et al., 1997).

Abraham et al. (1999) did not state it explicitly at the time but their methodology is an offshoot of a broader idea, that of obtaining photometric redshifts of galaxies by utilizing their colors or magnitudes in different passbands. When the redshifts of the galaxies in question are known, the concept can be modified in order to probe the internal structure of the galaxy in terms of the quantities that describe the stellar content. As we shall see, this information can be derived, not from a galaxy spectrum but from its internal colors and broad-band fluxes.

2.3 TOWARDS A BILLION REDSHIFTS: THE ERA OF PHOTO-ZS

Photometric redshifts or "photo-z"s (Koo, 1985; Connolly et al., 1995; Gwyn and Hartwick, 1996; Sawicki et al., 1997; Wang et al., 1998; Fernández-Soto et al., 1999; Benítez, 2000; Csabai et al., 2000; Budavári et al., 2000; Csabai et al., 2003) are a means to obtain redshifts for large samples of galaxies, including faint objects whose spectra cannot be measured. They can be measured much faster and in larger quantities than their spectroscopic counterparts. In spectroscopy, the light from the galaxy is separated into narrow wavelength bins of a few Angstroms in width. Each bin then receives only a small fraction of the total light from the

galaxy. So to achieve a sufficiently high signal-to-noise ratio in each bin, long integration times are required. For photometry, the bins are much larger: typically 1000 Å wide. This requires a relatively short exposure time to reach the same signal-to-noise ratio. In addition, imaging detectors generally cover a greater area of the sky than multi-object spectrographs. Thus the redshifts of more objects can be measured simultaneously by using photometry than by spectroscopy. Due to this, they have been seen as an efficient and effective means of studying the statistical properties of galaxies and their evolution.

The goal of photometric redshifts is to derive estimates of the physical properties of galaxies (e.g., redshift, type and luminosity) from a set of observed properties (e.g., colors) (Csabai et al., 2003). With past and ongoing large multicolor observational programs such as the SDSS and 2MASS and future photometric surveys such as the Large Synoptic Survey Telescope (LSST), the photometric redshift technique will prove to be an even more powerful tool in interpreting these very large and detailed data sets. Photometric redshifts have enabled the galaxy luminosity function to be studied (Subbarao et al., 1996) and large distributions of redshifts of any galaxy population can now be created. In addition, obtaining accurate estimates of photometric redshifts (and characterizing the uncertainties in those redshifts) is crucial to weak lensing studies that aim to map out the mass distribution in the Universe. The LSST in particular will obtain thousands of images of each patch of sky covering 20 000 square degrees, integrating to 26.5 mag in 6 bands: u,g,r,i,z,y, covering the ultra-violet (UV) to the infrared (IR). Photometric redshifts will be available for $\sim 3\,billion$ detected galaxies.

The SDSS provides a very large sample of galaxies whose "photo-z"s can be measured. Purger et al. (2006) applied photometric redshift estimation techniques to Data Release Five (DR5) of the SDSS, which contained more than 215 million unique objects and spectroscopy for 675 000 galaxies. This is an order of magnitude increase in sample size compared to the HDF and the wide angle camera of the SDSS allows a much larger cosmological volume to be probed, compared to the previous narrow pencil beam surveys. In the Sixth Data Release (DR6) (Stoughton et al., 2002), there were over 287 million objects imaged. Out of these, there are approximately 791 000 galaxies with published spectroscopic redshifts from which to calibrate the photo-zs and determine both their statistical and systematic uncertainties.

2.3.1 Techniques for Photometric Redshift Estimation

Both empirical and template-fitting techniques have been applied extensively to estimate redshifts of galaxies using broadband colors, although there are many others (see Csabai et al. (2003) for a review).

Empirical approaches use the data itself to obtain a relation between color and redshift for the galaxies and is relatively free from systematic effects within the photometric calibration (Csabai et al., 2003). They can be used when one has a sufficiently large (∼100–1000, depending on the redshift range) and representative subsample with spectroscopic redshifts. They are based on fitting a functional form (typically a 2nd or 3rd order polynomial) to obtain the spectroscopic redshifts from the colors (or magnitudes). The mapping between color and spectroscopic redshift is then used to estimate redshifts for the remainder of the sample with unknown redshifts (Connolly et al., 1995; Wang et al., 1998; Brunner et al., 1999). Errors in the estimated redshifts are estimated analytically or through Monte Carlo simulations. Another empirical approach is the nearest neighbor method (Csabai et al., 2003). For a test galaxy, this finds the galaxy in a training set which has the smallest distance in the color (or magnitude) space (weighted by the errors). The test galaxy is then given the redshift of this closest match. Ideally, the training set has so many galaxies that for each unknown object there is a close neighbor. The disadvantage of this method is that these relations can only be applied to galaxies with colors that lie within the range of colors and redshifts found within the training set.

The second approach is that of template-fitting (Koo, 1985; Gwyn and Hartwick, 1996; Sawicki et al., 1997; Connolly et al., 1999; Fernández-Soto et al., 1999; Benítez, 2000; Budavári et al., 1999, 2000; Csabai et al., 2000, 2003). This involves compiling a library of template spectra - either theoretical SEDs from stellar population synthesis models (e.g., Bruzual and Charlot (2003)) or empirical SEDs (e.g., Coleman et al. (1980)). The expected flux through each passband is calculated for each template SED on a grid of redshifts. By comparing these fluxes to the observed ones, a redshift and spectral type can be estimated. The usual method is to minimize χ^2 with respect to redshift, z, and spectral type, where

$$\chi^2(z, \text{type}) = \sum_i \left(\frac{F_i - b(z, \text{type}) T_i(z, \text{type})}{\sigma_i} \right)^2 , \tag{2.1}$$

F_i is the observed flux in filter i, σ_i is the error in F_i, $T_i(z, \mathrm{SED})$ is the flux in filter i for the template SED at redshift z and $b(z, \mathrm{SED})$ (the scaling factor that normalizes the template to the observed flux) is determined by minimizing equation 2.1 with respect to b, giving

$$b(z, \mathrm{type}) = \left(\sum_i \frac{F_i T_i(z, \mathrm{type})}{\sigma_i^2} \right) / \left(\sum_i \frac{T_i(z, \mathrm{type})^2}{\sigma_i^2} \right). \tag{2.2}$$

As mentioned by Csabai et al. (2003), the standard procedure for template fitting is to chose a small number of SEDs corresponding to different galaxy types (e.g., E, Sa, Sb and Irr galaxies) and then choose the best fit.

Template-fitting photometric redshift estimation techniques do not have the limitation of a training set and can be applied over a wide range of redshifts and intrinsic colors. It makes use of a relatively detailed knowledge of galaxy SEDs that exists today and in principle it may be used to estimate redshifts reliably even for populations of galaxies for which there are few or no spectroscopically confirmed redshifts (Csabai et al., 2003). However, in order to do this, it is critical to have a library of accurate and representative template SEDs (see e.g., Hogg et al. (1998); Firth et al. (2002)). Empirical templates are typically derived from nearby bright galaxies which may not be truly representative of high redshift galaxies. Theoretical SEDs, generated from stellar population synthesis models, on the other hand, can cover a large range of star formation histories, metallicities, dust extinction models etc. A pitfall of this is that not all all combinations of these parameters (at any particular redshift) are realistic, and it could result in including superfluous templates. This can be particularly problematic when using observations with noisy photometry (Csabai et al., 2003).

According to Csabai et al. (2003), it is difficult to obtain an optimal set of galaxy spectral templates, especially spectrophotometrically calibrated spectral templates. The first difficulty with empirical spectra lies in calibrating them spectrophotometrically over the full spectral range. The situation has improved with the SDSS which has measured spectrophotometrically calibrated spectra for approximately a million objects in the 3800–9200Å range. A second caveat with spectral templates is that, because the galaxy spectrum is redshifted, there is a need to have spectra over a wavelength range that is wider than the range of the optical passbands (3000–12 000Å). Finally, multi-fiber spectrographs, such as those used in

the SDSS, usually sample only the central region of the galaxy while photometric measurements integrate over the entire galaxy. On the theoretical front, the accuracy of spectra generated from stellar population synthesis models is now improving (Bruzual and Charlot, 2003) but deriving redshifts using them is still not as accurate as directly measuring the galaxy spectra.

2.3.2 A Byproduct of "Photo-z"s: Spatially Resolved Properties of Stellar Populations with SED Fits

The use of sophisticated training algorithms highlighted above allows for a better interpretation of the intrinsic photometric properties of a galaxy sample. Here we focus on an offshoot of the template-based photometric redshift technique, namely the best fitting spectral energy distribution (SED) template. We can extend the work of Abraham et al. (1999) by applying the template-fitting photometric redshift technique to individual pixels of resolved galaxy images which have measured fluxes and flux errors (in place of colors and their associated errors). Given a library of SED templates constructed from population synthesis codes, for which the underlying physical parameters are defined, the spatial distribution of those parameters *within* the galaxy can be determined. The SED templates are functions of galaxy type: early-types which are typically S0s, ellipticals and lenticulars and late-types which are typically spirals. We can thus shift the focus from the inferred photometric redshifts themselves, to what the best fitting SEDs can say about the properties of the galaxy sample whose redshifts are known. The presence of multiband imaging surveys also provide ideal testing beds for this technique.

Abraham et al. (1999) first applied the technique to galaxies in the Hubble Deep Field (HDF). Their methodology is as follows: They generated model tracks in color-color space i.e. in the V-I versus U-B plane for stellar populations using the GISSEL96 spectral synthesis code of Charlot and Bruzual (1991). They assumed a Salpter IMF and that the colors of individual pixels can be modeled using an exponential star formation history with a characteristic time-scale τ, i.e. $\psi(t) = \psi_0 e^{-t/\tau}$ which is often used to model the integrated colors of galaxies (Caldwell et al., 1991). This allows a general parameterization of the star

formation history of the galaxies. The color-color tracks were generated for model galaxies at fixed redshift values and for stellar populations with four free parameters: age t, e-folding time for star formation τ, dust extinction $E(B-V)$ and metallicity Z. For each pixel in the galaxy image, they computed the optimum evolutionary track in color-color space using a maximum likelihood estimator $\mathcal{L}$ that is effectively least-squares (Abraham et al., 1999):

$$\mathcal{L}(t,\tau,Z,E(B-V)) = \prod_{n=1}^{4} \frac{1}{\sqrt{2\pi}\Delta C_n} \exp\left(-\frac{(c_n - C_n)^2}{2\Delta C_n{}^2}\right) \tag{2.3}$$

where the product is over the four colors, and $[C_n, \Delta C_n]$ are the data colors and errors in the pixel (determined using the formulae in Williams et al. (1996)). Thus, each pixel could now be assigned a value of t, τ, Z and $E(B-V)$, so that each galaxy considered now had a pixelized map showing the distribution of t, τ and so on.

In fact, Conti et al. (2003) extended this work and applied a similar SED fitting procedure, a technique referred to as "pixel-z," to individual pixels in $\sim$ 150 galaxies with measured spectroscopic redshifts, and $\sim$ 1500 galaxies with measured photometric redshifts, in the Hubble Deep Field-North (HDFN). The aim was to decompose the internal photometric structure of galaxies into intrinsic properties of the stellar populations like stellar ages and metallicities. The study made several enhancements on the technique used by Abraham et al. (1999). The first was that it was able to use all available redshifts, photometric as well as spectroscopic. They extended the Abraham et al. (1999) sample by including not only the $\sim$ 190 object in the HDFN with measured spectroscopic redshifts, but all of the $\sim$ 1500 galaxies detected in the HDFN for which only photometric redshifts were measured. While this approach propagates the larger redshift uncertainties associated with photometric redshifts onto the measured properties of galaxies, the use of the original HDFN passbands extended by the NICMOS data (J, F and K bands) was found to reduce the redshift uncertainty to more than acceptable levels with $\sigma_z \sim 0.05$ (Conti et al., 1999). Each pixel was regarded as the smallest "multicolor unit" available in the HDFN. Thus they made use of the multicolor information for each of the pixels in a galaxy to constrain the relative ages for physically distinct sub-components of the galaxy and determine their dust and metallicity content as well as the timescale τ for their star formation histories. They used the pixels to calculate the comoving density of star formation and metallicity enrichment in galaxies, as a

function of redshift. With the sample of galaxies available, they were able to directly assess the drivers behind the current understanding of the global star formation history.

We aim to extend this work by applying the pixel-z technique to galaxies in the SDSS, to study the dependence on environment of both the total "integrated" galaxy SFR and the spatial distribution of SFR within those galaxies. First, however, we describe the "pixel-z" methodology.

2.4 PIXEL-Z

2.4.1 Method

By making use of strong spectral features such as the 4000 Å break, the Balmer break and the Lyman decrement, the standard photometric redshift techniques can be used to quickly provide an estimate of a galaxy's redshift. Each SED is systematically redshifted through the photometric filters as shown in Figure 2.1. The SED F_λ is then convolved with each of the photometric filter response functions S_λ according to:

$$F_T(\lambda) = \frac{\int_{\lambda_i}^{\lambda_f} d\lambda\, \lambda\, F_\lambda(\lambda)\, S_\lambda(\lambda)}{\int_{\lambda_i}^{\lambda_f} d\lambda S_\lambda(\lambda)} \tag{2.4}$$

λ_i and λ_f are the wavelength limits of each filter. The convolved SED fluxes F_T are then compared with the observed fluxes through each filter.

In the pixel-z method, we assume a redshift and fit for the SED type. In fact, for the SDSS Main Galaxy Sample, all galaxies have measured spectroscopic redshifts, so z can therefore be fixed in the fitting function. The best-fitting template is then established for each pixel at that particular redshift. The fitting function, which is a modification of equation (2.1), has the form:

$$\chi^2(T) = \sum_{i=1}^{N_\mathrm{f}} \frac{[F_{\mathrm{obs},i} - b_j \times F_{i,j}(T)]^2}{\sigma_i^2} \tag{2.5}$$

$F_{\mathrm{obs},i}$ is the flux through the ith filter, b_j is a scaling factor, $F_{i,j}$ is the flux through the ith filter of the jth SED template (calculated at redshift z) and σ_i is the uncertainty in the observed flux. The sum is carried out over all available filters N_f. The resulting χ^2 is

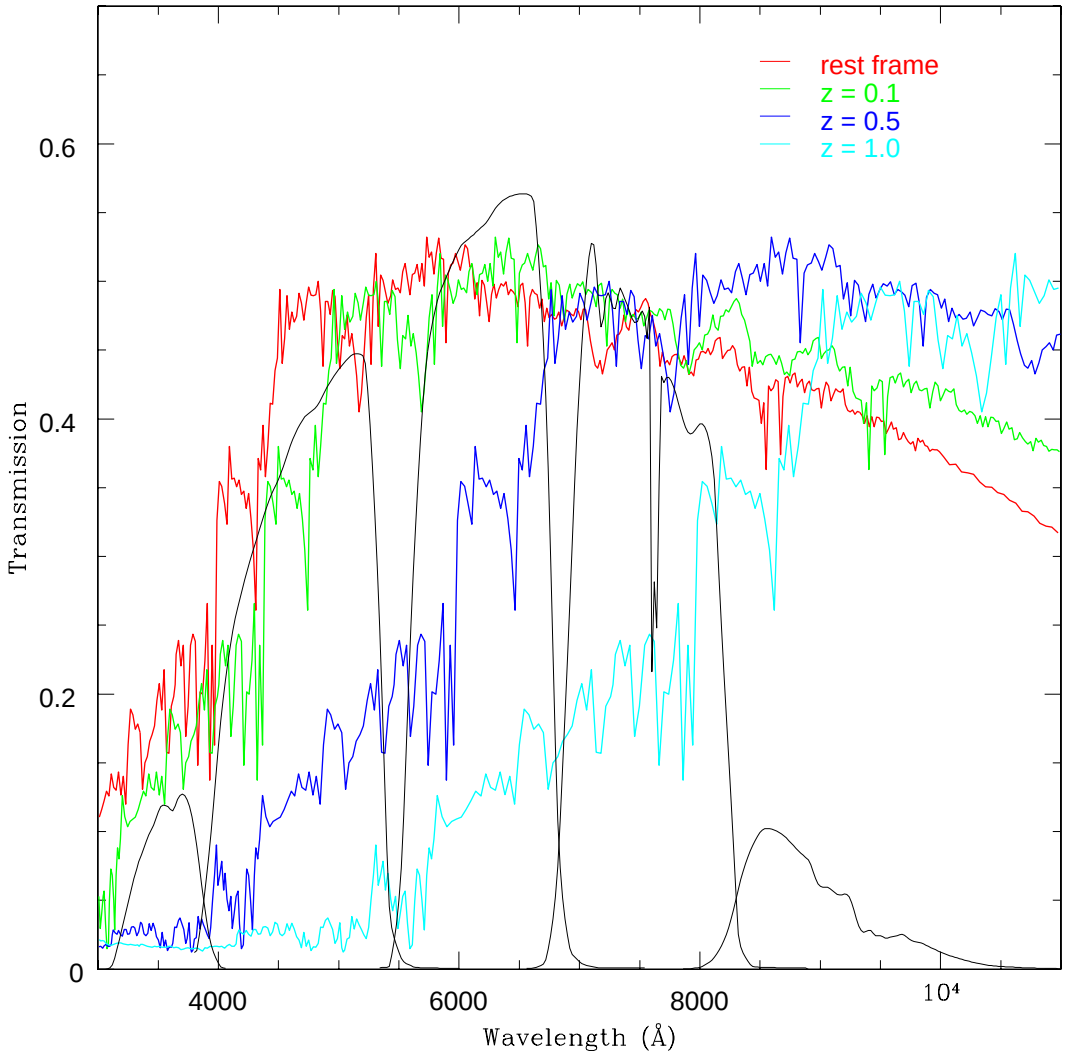

Figure 2.1: Redshifting a model SED through the SDSS u,g,r,i,z passbands. The filter response functions are shown in black. The original spectrum (in red) is redshifted through three redshifts: $z = 0.1$ (green), $z = 0.5$ (blue), $z = 1.0$ (cyan). The 4000 Å break in the spectrum now moves through the g,r and i filters as a result. In the pixel-z method, since the redshift of the pixel is known, the model SED can be redshifted and then convolved with each passband to obtain a theoretical filter-convolved flux in each passband. These fluxes can then be compared to the observed fluxes in the pixel.

minimized as a function of template T providing an estimate of its spectral type (together with the variance on this measure). Minimizing χ^2 in equation 2.5 with respect to b_j gives

$$b_j(T) = \frac{\sum_{i=1}^{N_\mathrm{f}} \frac{F_{\mathrm{obs},i} F_{i,j}(T)}{\sigma_i^2}}{\sum_{i=1}^{N_\mathrm{f}} \frac{F_{i,j}(T)^2}{\sigma_i^2}}, \tag{2.6}$$

which determines the normalization of the SFR obtained from the best fitting SED template.

Rather than applying this technique to the integrated fluxes of galaxies, we instead apply it to the fluxes of pixels within resolved galaxy images. The individual pixels typically have larger photometric uncertainties than integrated fluxes measured in apertures, and careful account needs to be made of the uncertainties and error-propagation. The optimum solution would be to keep the spatial information present in the resolved image together with the improved signal-to-noise ratio offered by combining pixels. A step in this direction is indicated by Budavári (2003) (private communication), where spatially connected pixels of similar colors are joined into *superpixels* in order to improve on the statistical errors without mixing the different galaxy components, such as a red bulge or bluer SF regions in spiral arms. Incorporating this technique into the current pixel-z implementation is beyond the scope of this investigation, but holds promise for future work.

By careful choice of the SED template library, the pixel-z technique enables a decomposition of the internal photometric structure of galaxies into basic constituents such as the ages of the stellar population, their metallicities and their dust content. It can therefore be used to determine the SFR for each pixel inside a galaxy and the contribution of each pixel to the SFR of either the whole galaxy or a projected radial shell of that galaxy.

We have thus shifted the attention of the technique from the photometric redshift itself to the SED templates. In fact, the SED of a galaxy should reflect the distribution of stellar masses, ages and metallicities and hence provide clues to the past history of star formation. By fitting SEDs to individual pixels in a galaxy, we can recover the morphological characteristics of the galaxy and separate out the individual contributions of age, metallicity, dust and star formation history.

Next, we describe the SED templates used in our analysis.

2.4.2 The SED Templates

We use a large number of SEDs generated by the Bruzual and Charlot (2003) stellar population synthesis models. The main input parameters are the form of the SFR, the stellar initial mass function (we assume a Salpeter function with $M_l = 0.1\,M_\odot$ and $M_u = 100\,M_\odot$), and the rate of metal enrichment. Using assumptions about the time evolution of these parameters, they compute the age-dependent distribution of stars in the Hertzsprung-Russell (HR) diagram from which they obtain the integrated spectral evolution of the stellar population. These models have become standard tools in the interpretation of galaxy colors and spectra.

The model computes the spectral evolution of stellar populations of different metallicities at ages between 1×10^5 yr and 2×10^{10} yr at a resolution of 3 Å FWHM across the whole wavelength range from 3200 Å to 9500 Å (corresponding to a median resolving power $\lambda/\Delta\lambda \approx 2000$). These predictions are based on a new library of observed stellar spectra assembled by Le Borgne et al. (2003). It also computes the spectral evolution across a larger wavelength range, from 91 Å to 160 μm, at lower spectral resolution.

2.4.2.1 Isochrone Synthesis and Simple Stellar Populations (SSPs) 'Isochrone synthesis' is used to compute the spectral evolution of stellar populations (Charlot and Bruzual, 1991; Bruzual A. and Charlot, 1993). This technique is based on the property that stellar populations with any star formation history can be expanded in a series of instantaneous starbursts - the simple stellar populations (SSPs). The spectral energy distribution at time t of a stellar population characterized by a star formation rate $\psi(t)$ and a metal-enrichment law $\zeta(t)$ can be written (Bruzual and Charlot, 2003; Tinsley, 1980)

$$F_\lambda(t) = \int_0^t \psi(t-t')\, S_\lambda\left[t', \zeta(t-t')\right]\, dt'\,, \tag{2.7}$$

where $S_\lambda\left[t', \zeta(t-t')\right]$ is the power radiated per unit wavelength per unit initial mass by an SSP of age t' and metallicity $\zeta(t-t')$. The above expression assumes that the initial mass function (IMF) is independent of time.

The function $S_\lambda\left[t', \zeta(t-t')\right]$ is the sum of the spectra of stars defining the isochrone of an SSP of metallicity $\zeta(t-t')$ at age t'. To compute $S_\lambda(t', Z_i)$ at a given metallicity Z_i of the

stellar evolutionary tracks, the isochrone at age t' must be interpolated from the tracks in the HR diagram, as is described by Bruzual and Charlot (2003). The different evolutionary stages along the isochrone are populated by stars of different initial masses in proportions given by the IMF weight $\phi(m)$ [defined such that $\phi(m)dm$ is the number of stars born with masses between m and $m + dm$]. Spectral libraries are then used to assign spectra to stars in the different evolutionary stages. In the model by Bruzual and Charlot (2003), the SED of the SSP is obtained by summing the spectra of the individual stars along the isochrone.

The IMF is an adjustable parameter of the model. In this work, the Salpter IMF is employed, which corresponds to $\phi(\log m) \propto m^{-1.35}$, or equivalently $\phi(m) \propto m^{-2.35}$. We adopt lower and upper IMF mass cutoffs $m_L = 0.1\ M_\odot$ and $m_U = 100\ M_\odot$. The spectral energy distribution of a model SSP is normalized to a total mass of 1 $M_\odot$ in stars at age $t' = 0$, and the spectra are computed at 221 unequally spaced time steps from 0 to 20 Gyr. Each spectrum covers the wavelength range from 91 Å to 160 μ.

2.4.2.2 The Generated Spectra and the Underlying Properties of the Stellar Populations The input parameters for our SED templates are chosen to maximize our ability to solve for the above quantities. The SEDs have the following properties:

1. We allow the underlying stellar population within each pixel to vary over a wide age range. The age in the synthesis model is defined as the time since the most recent burst of star formation. We sample extremely young $(0.001, 0.01, 0.1, 0.5$ Gyr), to middle age $(1, 3, 5$ Gyr), to old and very old $(9, 12, 15$ Gyr), for a total of ten ages.
2. We restrict our parameterization of the star formation history of the underlying stellar population within each pixel to an exponential function and reject other parameterizations that are available in the model. We assume that the fluxes of individual pixels can be modeled using an exponentially declining SFR with an e-folding timescale τ, i.e. $\Psi(t) = \Psi_0 e^{(-t/\tau)}$. This parameterization is convenient for its simplicity in describing the SFR of an instantaneous burst when $\tau \to 0$ and a constant SFR when $\tau \to \infty$. The e-folding times we use for τ range from 0.1 Gyr for a short burst, to $1, 3, 5, 9$ and 12 Gyr for subsequently longer bursts. It is worth noting at this point that an exponential SFR for individual pixels does not inevitably lead to an exponentially decaying SFR for the

galaxy as a whole, other than in the special case in which every pixel in the galaxy is coeval and all have the same SFR (Conti et al., 2003).

3. Since pixels with any SF history can be expanded in a series of instantaneous bursts, each having fixed metallicity, the spectral evolution of individual pixels (or whole galaxies) can be investigated without prior knowledge of the chemical evolution. We assume the SEDs to be characterized by six possible metallicities spanning $\frac{1}{50}$ to 2.5 solar.
4. The general spectral characteristics of the SEDs of galaxies will be modified by the presence of dust. We parameterize dust obscuration in terms of the relative optical extinction in the rest frame $E(B-V)$ using the reddening curve $k(\lambda) = A(\lambda)/E(B-V)$, for star-forming systems formulated by Calzetti et al. (2000). For each of the SEDs we allow for six independent values of extinction ranging from no extinction to $E(B-V) =$ 0.9 magnitudes of extinction.

In Figure 2.2, we show some examples of the generated galaxy SEDs and how these change as the underlying properties of their stellar populations are allowed to vary. Panels (a) and (b) show the spectral evolution of stellar populations with two different time scales for star formation: $\tau = 3$ Gyr and $\tau = 9$ Gyr. In each case, we show the evolution of the spectrum from $t = 0.001$ Gyr to $t = 9$ Gyr where t is the age of the stellar population. The UV-to-optical spectrum remains approximately constant during the main episode of star formation because of the continuous input of young massive stars, but the near-infrared light rises as more and more evolved stars accumulate. When star formation decreases, the properties of the spectrum are now determined by stars which are in the advanced stages of stellar evolution. Panel (c) shows the effect of dust extinction for stellar populations with fixed age ($t = 1$ Gyr, $\tau = 3$ Gyr and for $Z = Z_{\odot}$). The spectrum is reddened according to the Calzetti (2000) extinction curve. Panel (d) shows the effect of varying metallicity for a population with $t = 1$ Gyr, $\tau = 3$ Gyr and $E(B-V) = 0.1$ mag. It is seen that increasing metallicity decreases the UV part of the spectrum while not affecting the infra-red part significantly.

The *pixel-z* technique therefore allows us to probe not only the underlying morphological details of the galaxy, but also the relation between a galaxy's morphology and its stellar constituents which characterize the fitted SEDs. To verify our implementation of pixel-z and

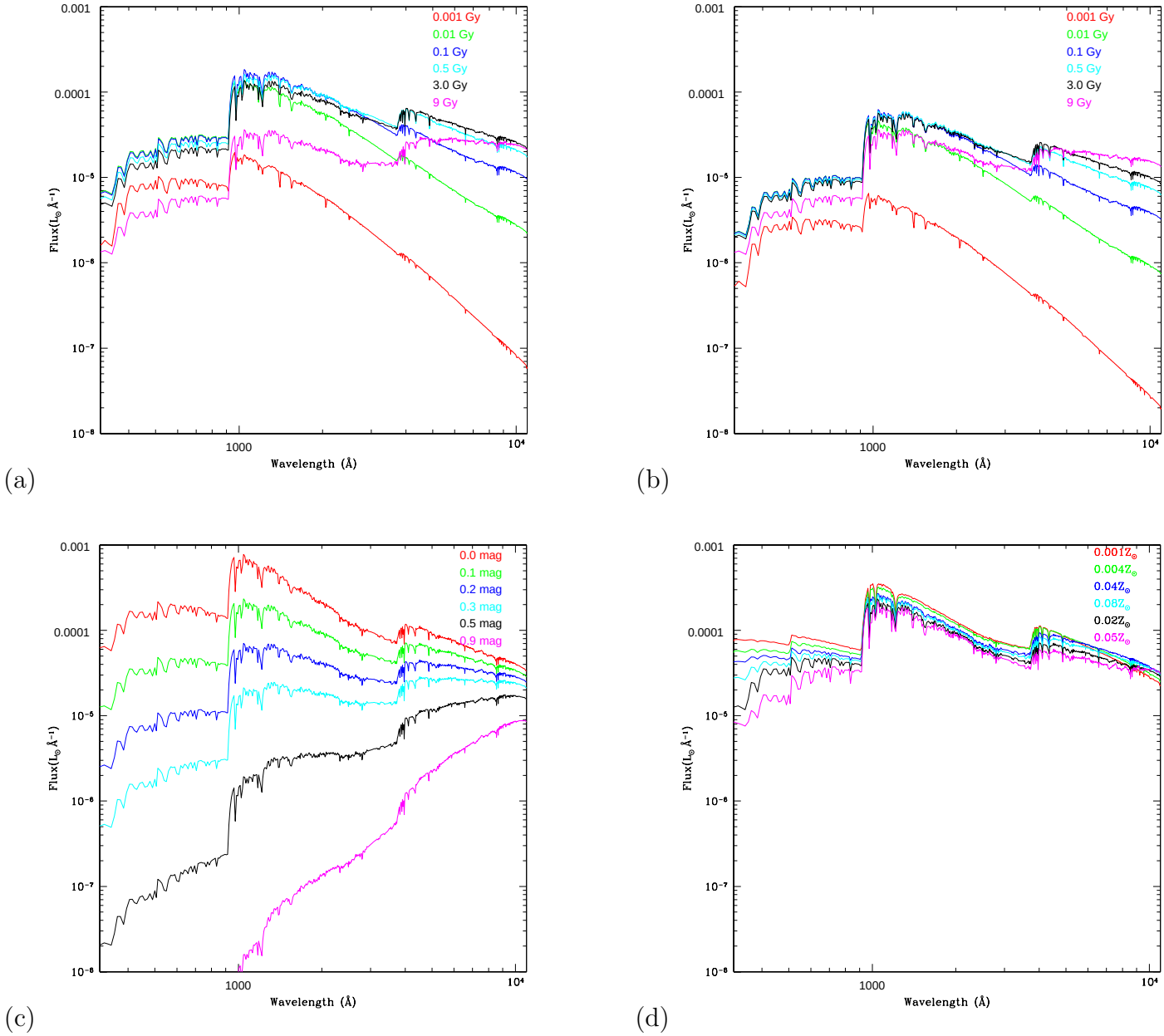

Figure 2.2: Model spectra of stellar populations as predicted by the stellar population synthesis model (Bruzual and Charlot, 2003). Both panels (a) and (b) shows the evolution of the spectrum from $t = 0.001$ Gyr to $t = 9$ Gyr where t is the age of the stellar population. In (a), $\tau = 3$ Gyr; (b) $\tau = 9$ Gyr. $E(B-V) = 0.1$ mag and the metallicity is fixed to $Z = Z_{\odot}$; (c) The effect of varying the dust obscuration $E(B-V)$ (in magnitudes) using the Calzetti et al. (2000) extinction curve, for stellar populations with $t = 1$ Gyr, $\tau = 3$ Gyr and $Z = Z_{\odot}$; (d) The effect of varying metallicity for stellar populations with $t = 1$ Gyr, $\tau = 3$ Gyr and $E(B-V) = 0.1$ mag.

for comparison with the initial application to the HDFN by Conti et al. (2003), we test our method first on HDFN galaxies before moving to our SDSS sample.

2.5 PIXEL-Z IMPLEMENTATION: AN INITIAL APPLICATION TO THE HUBBLE DEEP FIELD NORTH

2.5.1 The Hubble Deep Field North

The Hubble Deep Field (HDF) is a Director's Discretionary program on the Hubble Space Telescope (HST) to image an undistinguished field at high Galactic latitude in four passbands as deeply as possible (Williams et al., 1996, 2000). These images provide one of the most detailed views to date of distant field galaxies and have been central to a wide range of studies in galaxy evolution and cosmology. In order to optimize observing in the time available, a field in the northern continuous viewing zone was selected and images were taken for ten consecutive days, or approximately 150 orbits. Shorter 1-2 orbit images were obtained of the fields immediately adjacent to the primary HDF in order to facilitate spectroscopic follow-up by ground-based telescopes. The observations were made from 18 to 30 December 1995, and both raw and reduced data were put in the public domain. Imaging was done using four filters (U, V, B, I), centered on 300 nm, 450 nm, 606 nm and 814 nm respectively.

The rich dataset has many of the characteristics that make it an ideal testbed for our purpose. First and foremost, it is among the best studied areas of the sky and, as such, can be regarded an ideal benchmark for our technique. The HDFN also provides morphological and size information for high redshift galaxies. For our analysis we will make use of the 2500×2500 pixel versions of the HDFN and NICMOS data together with the corresponding relative weight maps. The latter are needed to correctly estimate the photometric errors on individual pixels. We use version 1.04 of the renormalized rms maps. These maps give the "true" noise level in the data, corrected for inter-pixel correlations. With the rms images, one can sum (in quadrature) the noise values for pixels over any aperture and determine the effective flux uncertainty within that aperture or use the measure on a pixel-by-pixel basis.

The rms maps quantify the uncertainty due to noise in the background. These maps are used to determine the detection significance of an object or a pixel. As we shall see, the error in the photometric flux in the pixels of an object will be used to assess the significance of our photometric decomposition performed with the pixel-z method.

2.5.2 Galaxy Maps: The Hubble Deep Field

We first test our code on the same galaxies in the HDFN as used by Conti et al. (2003). As in their analysis, we are able to connect features in the parameter maps (of age, SFR, obscuration, metallicity) of galaxies to individual morphological features such as knots of star formation that appear in the original images. Figure 2.3 shows the result of fitting 2160 SED templates to a spiral galaxy in the HDFN at $z = 1.2$. The top left image shows a face-on spiral galaxy in the $F606W$ (V-band) filter. The other images show the decomposition of the best-fitting SED template according to the values of the SFR e-folding time τ, $E(B-V)$, and metallicity relative to solar $[Fe/H]$. The redshift of all pixels have been fixed to that of the galaxy. As the assumption of a common age for all the pixels was used by Conti et al. (2003), we have implemented it only for this comparison. All future results will have this assumption relaxed. The results can be seen to be highly consistent with those from Conti et al. (2003), clearly identifying the same structures and regions, such as the dark "knots" in the spiral arms, elevated metallicity and obscuration in the nucleus, and strong contrast between the arm and inter-arm regions.

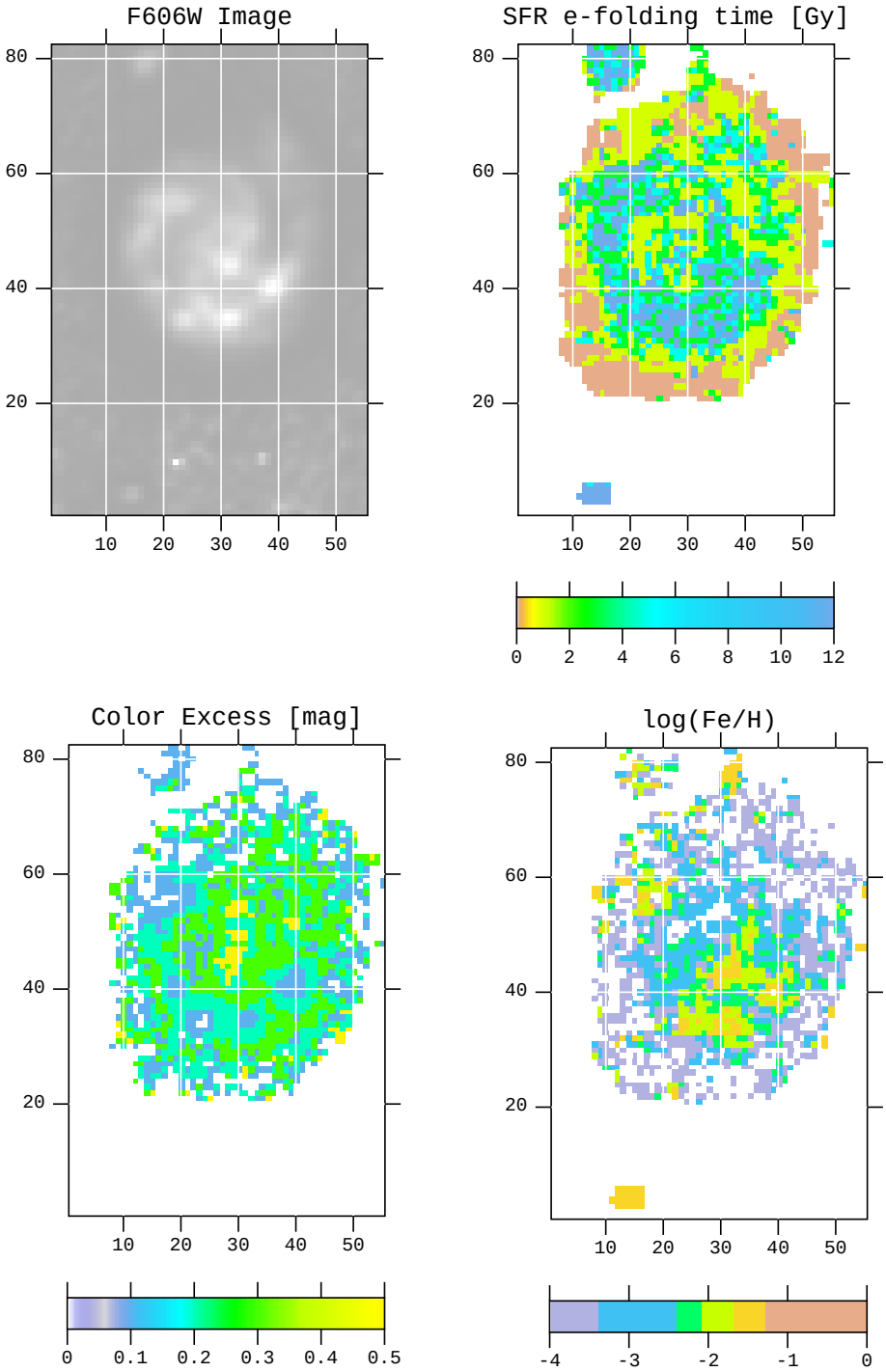

Figure 2.3: Result of fitting 2160 SED templates to a large spiral galaxy in the Hubble Deep Field-North as was done by Conti et al. (2003). The top left map shows the galaxy in the F606W WFPC2 (V) filter. The other three maps display the breakdown of the best-fitting template in each pixel according to the values of star formation rate e-folding time τ in Gyr, color excess $E(B-V)$ in magnitudes, and metallicity relative to solar.

2.5.3 Error Maps: The Hubble Deep Field

The pixel-z method also involves calculating the intrinsic error arising from the SED fitting, for each property that characterizes the best-fitting SED. This is detailed by Conti et al. (2003). We provide a brief summary of the process here. Each pixel has a 4-dimensional likelihood function $L(t, \tau, E(B-V), [Fe/H])$ that results from fitting each of the 2160 templates to the multi-band fluxes in that pixel. In order to calculate the uncertainty associated with each of the four axes of variability (t, τ, $E(B-V)$ and $[Fe/H]$), we marginalize the likelihood over the three remaining parameters, essentially collapsing the four dimensional function along each of its axes. These probabilities are sampled at the allowed values of each parameter (based on the grid of parameters defined in §2.4.2.2). For example, the age likelihood is sampled at 10 different points corresponding to the 10 different ages.

The errors are then the $1\,\sigma$ uncertainties (corresponding to $\Delta\chi^2 = 1$) found by measuring the width of the $1\,\sigma$ line that intersects the curve that is fitted to the points. This provides a conservative estimate of the errors. Each pixel thus has uncertainties associated with each of the four parameters.

The results are shown in Figure 2.4 for the galaxy in Figure 2.3, where the age dependence has been suppressed as we compute the "best fitting age" for the galaxy using the method described in Conti et al. (2003). As expected, those pixels with the highest signal-to-noise ratio in all passbands, usually the pixels towards the center of the object, have relatively small errors in contrast with "sky pixels". Direct comparison with the V band image of Figure 2.4 underlines how the uncertainty in τ, for example, is indeed reliable only within the source and then degrades in the outskirts. The distribution of the uncertainty in the obscuration is even more marked. Although the central pixel itself has a relatively high error in $E(B-V)$, the dark knots of star formation seen in the original image have very low uncertainties in $E(B-V)$ (less than 0.05 magnitudes) as evident in the dark blue regions of the $E(B-V)$ map. Elsewhere in the galaxy, the light blue regions represent pixels where the $E(B-V)$ estimate is reliable to less than 0.1 magnitudes. As we move outward our estimate of $E(B-V)$ degrades rapidly, with uncertainties greater than 0.2 magnitudes. A similar trend is seen in the metallicity error map although the knots of star formation are

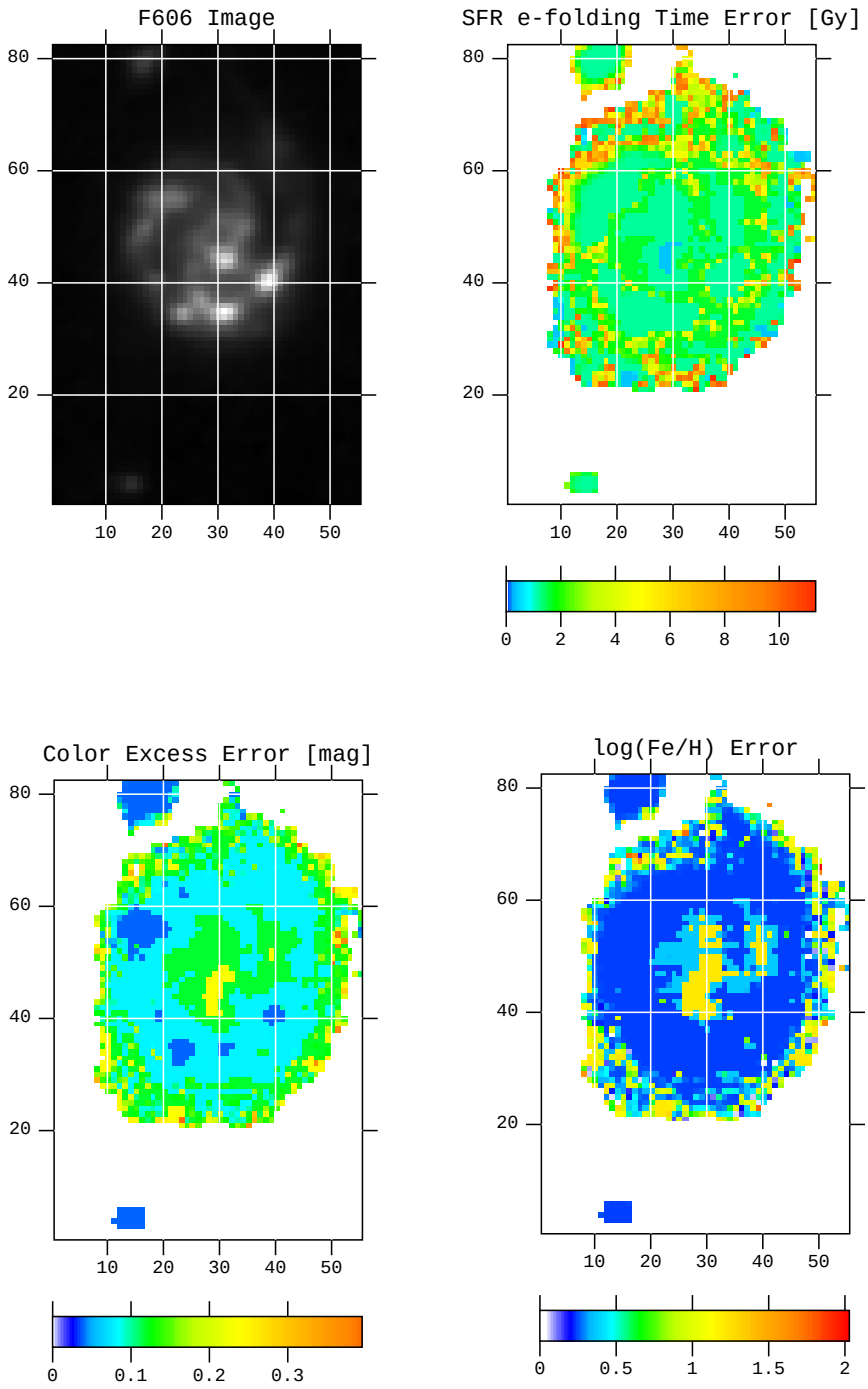

Figure 2.4: Error maps for the galaxy shown in Figure 2.3. The top left map shows the galaxy in the F606W filter. The other three maps show the errors (in every pixel) in the star formation rate e-folding time τ, color excess $E(B-V)$ and metallicity relative to solar $[Fe/H]$, respectively. These error maps are obtained by computing the marginalized likelihood in a particular parameter for each pixel in the galaxy, as described in §2.5.3.

not as apparent here.

Having shown that our results are consistent with the findings of Conti et al. (2003), we now turn our attention to galaxies in the SDSS. Before doing so, we address the issue of degeneracies between the fitted parameters that characterize the SED templates.

2.5.4 SED Degeneracies

Another source of uncertainty in the pixel-z method is introduced by the degeneracies between the different parameters that characterize the model SEDs which are fitted to the photometric fluxes of every pixel in the galaxy. This is particularly relevant when the number of templates that are used in the fitting is large. Population synthesis models showed that age, metallicity and dust all tend to affect spectra in similar ways (Bruzual and Charlot, 2003). This was found to be particularly true at the low resolving power of the earlier models, typically ~ 250 at optical wavelengths. The most well known degeneracy is that between age and metallicity: it is known that luminosity-weighted ages and metallicities which are derived from galaxy spectra tend to be strongly degenerate (Bruzual and Charlot, 2003). Worthey (1994) explored this phenomenon while constructing detailed models for intermediate and old stellar populations in galaxies. The parameters that were input to the model were the metallicities ($-2 < [Fe/H] < 0.5$), single-burst ages (between 1.5 and 17 Gyr) and the exponent of the IMF. Broadband magnitudes, SEDs, surface brightness fluctuation magnitudes, and 21 different absorption feature indices in the spectra were output from the model and compared with a wide range of available observations.

It was concluded that if the percentage change $\delta\,(age)/\delta\,Z \approx 3/2$ for two populations, they would appear almost identical in most of the absorption indices. This rule holds to within 50% for almost every color and index. Worthey (1994) found that a few indices can break this degeneracy, for example, those that are more sensitive to the abundance (Fe4668, Fe5015, Fe5709 and Fe5782) and those that are more age sensitive (G4300, H_β and higher Balmer lines) than usual. They were able to use the H_β index to crudely date recent merger events in galaxies. He pointed out that the reason for this is that a difference between populations of say, 5 and 15 Gyr in age is easily measurable using H_β. It was also noted

that due to the similar effects of age and metallicity, changes in the abundance ratios are most noticeably apparent in the spectra of old stellar populations. Other studies found that in old populations, the age-metallicity degeneracy can be broken by studying surface brightness fluctuations which are more sensitive to details of the stellar luminosity function than ordinary integrated light (Liu et al., 2000; Blakeslee et al., 2001). However, it was found that using surface brightness fluctuations was mostly only applicable to studies of nearby ellipticals and spiral bulges.

The age-metallicity degeneracy is therefore inherent in the SSP model that we use. While the degeneracy affects the spectral evolution of an SSP, Bruzual and Charlot (2003) show that the models can also trace how it affects the photometric evolution. From this, the origins of this degeneracy can be understood. Optical and near-infrared colors reflect the relative contribution of hot and cool stars to the integrated light. Bruzual and Charlot (2003) followed the evolution of B-V and V-K colors and the stellar mass-to-light ratio M/L_V for different metallicities. At fixed age, they found that increasing metallicity tends to redden the colors and increase the M/L ratio. They explained this as follows: at fixed initial stellar mass, increasing the metallicity causes stars to evolve at lower effective temperatures and lower luminosities (Girardi et al., 2000), which increases the M/L ratio. Changing the metallicity also changes the relative numbers of red and blue supergiants. It was shown that the contribution of red supergiants in the color evolution of an SSP depends crucially on metallicity. Increasing metallicity at fixed age was found to have a similar effect to increasing age at fixed metallicity.

In the pixel-z method, degeneracies are therefore inherent in the spectra that we generate and fit to the photometric fluxes in the pixels of galaxies. As well as the above degeneracy, there could also be degeneracies between the other parameters, including between dust obscuration and metallicity as well as between age and dust obscuration. In the first application of the pixel-z technique to galaxies in the HDF-N, Conti et al. (2003) examined the redshift-evolution of the obscuration-metallicity degeneracy, using the best-fit values of $E(B-V)$ and Z in the pixels. They found that at low redshifts, the degeneracy is quite apparent. Pixels whose best fitting SEDs are characterized by solar or above solar metallicities tend to be more obscured than those containing stellar populations with lower metallicites.

The trend flattens off at higher redshift so that by $z \sim 3$, they find that obscuration is not a good indicator of the underlying metallicity.

In Chapter 3, where we apply the pixel-z method to galaxies in the SDSS, we attempt to characterize these degeneracies between the various fitted parameters. Finally, it is also worth noting that there are also uncertainties arising directly from the models themselves. For example, while spectral synthesis models have been quite established for solar metallicity stellar populations in optical photometry, the models are less well defined for very sub-solar or very high metallicity populations.

2.6 SUMMARY

We have described the pixel-z method, which is used to determine the SFR and other properties of the stellar populations within every pixel of a galaxy image. The technique combines stellar population synthesis models with photometric redshift template-fitting on the scale of individual pixels in multi-band galaxy images. Over 2000 spectral energy distributions (SEDs) are constructed, sampling a wide range of properties of the underlying stellar populations, such as star formation rate (SFR), dust obscuration and metallicity. The SEDs are redshifted and convolved with the photometric filters of the detector. They are then compared to the observed fluxes through each pixel in each of the passbands. In the pixel-z technique, however, we fix the redshift of the pixel (which is known since the redshift of the host galaxy is known) and fit for the spectral type only. The best-fit SED is then returned for every pixel within the galaxy. This allows the properties of the stellar populations in that pixel to be determined. We also calculate an associated uncertainty in each of these parameters that arises from the fit. In an initial application to galaxies in the Hubble Deep Field, we showed that the technique allows us to connect features of the galaxy morphology (such as the presence of spiral arms or knots of star formation) with physical properties of the underlying stellar populations (such as the age of the stellar populations, the timescale of star formation decline, the dust obscuration and metallicity). The technique also enables a study of the interplay between these physical properties. In the next chapter, we apply

the technique to a large sample of galaxies in the SDSS, being primarily focused on the star formation within the pixels. Since the method enables a spatial resolution of the star formation distribution *within* galaxies, we can now explore how the SFR of each galaxy – both total SFR and the spatial distribution of SFR within galaxies – varies as a function of the galaxy environment.

3.0 SPATIALLY RESOLVED GALAXY STAR FORMATION AND ITS ENVIRONMENTAL DEPENDENCE I: THE SLOAN DIGITAL SKY SURVEY

3.1 INTRODUCTION

As discussed at the end of Chapter 1, determining the spatial distribution of the star formation rate (SFR) in galaxies as a function of the galaxy environment should provide a novel way to constrain various galaxy formation models. One possible scenario by which galaxy properties can be influenced is described in "infall and quench" models of galaxy formation. This refers to strong physical mechanisms which underly galaxy interactions and which result in a depletion of cold gas that would otherwise have been used to form new stars. There could also be an alternate means by which galaxy evolution can be influenced, other than these strong physical mechanisms. One possible scenario would be that galaxy properties are set by their mass at an early epoch, and since more massive galaxies tend to reside in more dense environments, their evolution would thus be indirectly influenced by their environment.

We argued that we can use the spatial variation of star formation within galaxies to distinguish between the predictions of the "infall and quench" scenario and those of "environmentally-governed evolution". "Infall and quench" mechanisms such as ram-pressure stripping can cause depletion of the cold gas in the disks of galaxies in clusters and thereby truncate star formation in them. These mechanisms would cause the outskirts of galaxies to be affected before the galaxy interiors. "Environmentally-governed evolution" on the other hand should result in star formation that is uniformly suppressed as the galaxy ages, or star formation in the galaxy center being suppressed more than in the outskirts since nuclear star formation

proceeds faster than in the disk due to the elevated gas densities in the former. In this way, we can distinguish between the two scenarios and determine which would be dominant in shaping galaxy properties.

In order to do this, we apply the pixel-z technique, described in Chapter 2, to a large sample of SDSS galaxies to obtain the spatially resolved SFR in these galaxies. The SDSS provides a large sample of galaxies with multi-color imaging in five passbands, and the pixel-z technique can be applied to this galaxy sample. We can then study the spatially resolved star formation in these galaxies in a statistical way, and determine how this varies with the galaxy environment.

3.2 THE SLOAN DIGITAL SKY SURVEY

3.2.1 Background to the SDSS and the Fourth Data Release

The Sloan Digital Sky Survey (SDSS) is an imaging and spectroscopic survey of the sky using a dedicated 2.5m telescope (Gunn et al., 2006) at Apache Point Observatory in New Mexico (see Figure 3.1). It was commissioned in 1998 and aims to map a quarter of the sky, spanning the Northern Galactic Cap (York et al., 2000). Imaging is done in drift-scan mode using a 142 mega-pixel camera (Gunn et al., 1998), which gathers data in five passbands, u, g, r, i, z, spanning wavelengths $3000 < \lambda < 10\,000$ Å. The photometric system and calibration are described in Fukugita et al. (1996); Hogg et al. (2001); Ivezić et al. (2004); Tucker et al. (2006); Padmanabhan et al. (2008). The astrometric calibration is described by Pier et al. (2003) and the data pipelines by Lupton et al. (2001). The Fourth Data Release (DR4) of the SDSS, which was used for this work, is described by Adelman-McCarthy et al. (2006). It includes five-band photometric data for 180 million objects selected over 6670 square degrees, and 673 280 spectra of galaxies, quasars and stars selected from 4783 square degrees of that imaging data using the standard SDSS target selection algorithms. Objects are selected from the imaging data for spectroscopy using a variety of algorithms. These include a complete sample of galaxies with reddening-corrected (Schlegel et al., 1998) Petrosian magnitudes

(Petrosian, 1976) brighter than $r = 17.7$ (Strauss et al., 2002). Spectra are taken using a pair of multi-fiber spectrographs (Adelman-McCarthy et al., 2006) and cover the wavelength range $3800 < \lambda < 9200\,\text{Å}$ with a resolution of $\lambda/\delta\lambda \approx 2000$.

The sky coverage of the imaging and spectroscopic surveys are shown in Figure 3.2. It shows the incremental increases in area of sky covered since Data Release One (Abazajian et al., 2003). The imaging data in DR4 was taken along a series of great circles on the sky with the aim of filling a contiguous area in the Northern Galactic Cap, and three non-contiguous stripes in the Southern Galactic Cap (Adelman-McCarthy et al., 2006; York et al., 2000). Two contiguous regions cover the Northern Galactic Cap, one centered roughly on the Celestial Equator, and the other at around $\delta = +40°$.

3.2.2 Sample Selection

In our study, we use galaxies chosen from the Main Galaxy Sample in the spectroscopic data in DR4. Galaxies are chosen which have a redshift confidence of at least 0.7. We ignore objects with saturated pixels. We exclude galaxies whose spectra has the Z_WARNING_NO_BLUE (no blue side of the spectrum) and Z_WARNING_NO_RED (no red side of the spectrum) flags (Stoughton et al., 2002). We then define a volume-limited sample through the further restrictions $0.019 < z < 0.125$ and $-23.5 < M_r < -20.5$. This gives a sample of 44 964 objects. For each object we obtain the Atlas image (from the SDSS Data Archive Server) which comprises the pixels detected as part of each object in all filters. We use these images in the pixel-z analysis of the final volume-limited sample.

Figure 3.1: The SDSS 2.5m telescope at Apache Point Observatory. Credit: Fermilab Visual Media Services.

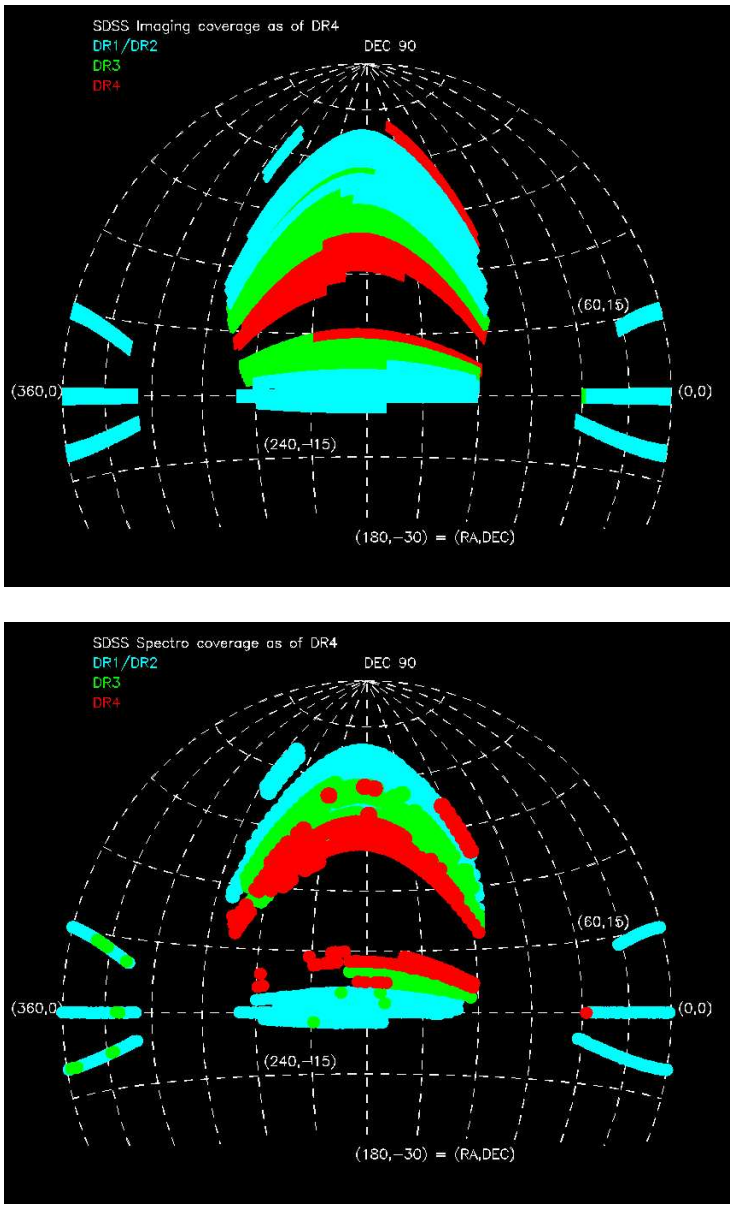

Figure 3.2: The sky coverage in Data Release 4 of the SDSS. The top panel shows the coverage for the imaging survey, showing the incremental increases in area of sky covered by the previous successive data releases (DR1 onwards). The Northern Galactic Cap is covered by two contiguous regions, one centered roughly on the Celestial Equator, and the other at around $\delta = +40°$. Successive data release have tried to close the gap between these two regions: DR1 and DR2 (cyan), DR3(green), DR4(red). The imaging in DR4 covers an area of sky around 6670 deg^2. The bottom panel shows the corresponding incremental sky coverage for the spectroscopic survey. Credit: The Sloan Digital Sky Survey (SDSS) Collaboration, http://www.sdss.org.

3.2.3 The Galaxy Environment

Previous studies have parameterized the local environment of each galaxy using the projected density of galaxies (Gómez et al., 2003; Dressler, 1980). This involves calculating the projected distance to the nth nearest spectroscopically observed neighbor and then converting that into a surface density (in Mpc^{-2}). In our work, we characterize the local density around each galaxy using a 5 $h^{-1}\,Mpc$ sphere centered on the galaxy in question. Each galaxy within that sphere is weighted according to the local completeness as calculated by Blanton et al. (2003d) to account for spectroscopic fiber collisions.

We also need to scale the volume of the sphere according to the fraction of the projected sphere that is contained within the survey area. Since we are using a volume limited sample, we do not need to correct for redshift distribution variations.

There are a few possible caveats associated with this method. Naturally, working in redshift space versus real space opens us up to the possibility of galaxies scattering out of our volume in high density regions where the peculiar velocities would be high and vice-versa in lower density regions. In addition, our calculation of the spherical volume is compromised somewhat by treating masked regions near the center of the projected sphere identically to those on the edges, despite the fact that the former would remove a larger volume from the sphere than the latter. One possible solution for this which can be attempted in the future would be to use cylinders centered on each galaxy (e.g., 5 $h^{-1}Mpc$ in radius and 5 $h^{-1}Mpc$ length along the line of sight) rather than spheres, so that removing any masked regions would take out equal volumes irrespective of whether it is at the center or at the edges.

Between the volume correction and redshift distortions, the latter is more problematic; our sky coverage is sufficiently uniform that tests using an exact spherical volume were not significantly different from those using our method. However, given that redshift distortions are at least equally problematic for any density estimates working in redshift space (Dressler, 1980; Gómez et al., 2003), the more physically-based aspect of this method for measuring local galaxy density makes it the preferred approach. Figure 3.3 shows the distribution of local galaxy densities in our sample.

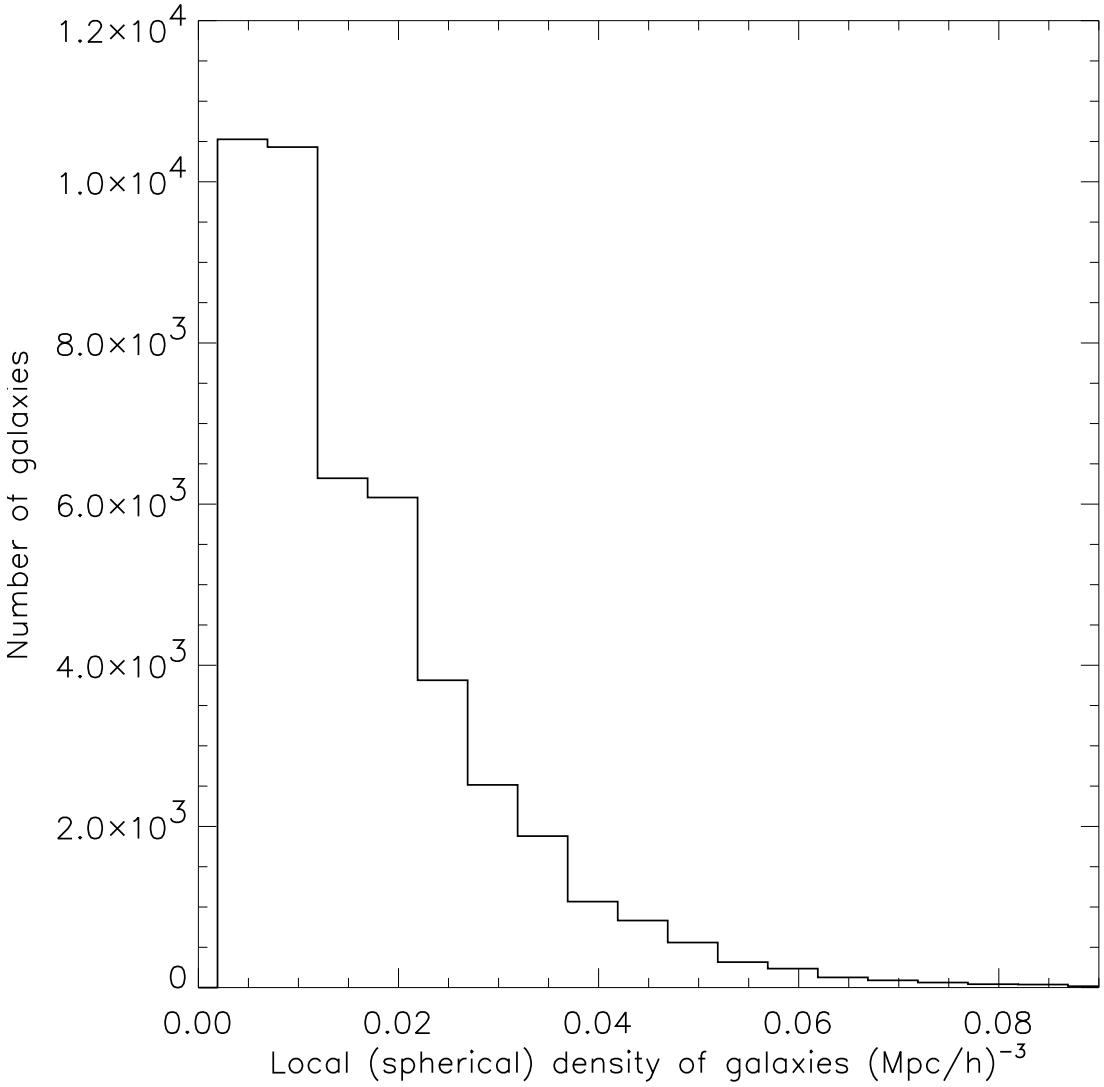

Figure 3.3: Distribution of local galaxy densities in the sample.

3.2.4 SDSS Imaging and the Photometric Calibration of Atlas Images

We utilize one of the photometric data products of the SDSS: the "Atlas images". These are cutouts from the imaging data in all five bands of all detected objects in the survey. Unlike the HDF, no rms error maps in the counts are available for the SDSS galaxies. The photometry in every pixel that belongs to each galaxy of the Atlas image needs to be calibrated to obtain a measured flux in that pixel. In this section, we illustrate the steps that need to be taken to do this. The photometric calibration of the Atlas images was done according to the *asinh* magnitude system developed by Lupton et al. (1999). The photometry is also corrected for foreground Galactic extinction using the extinction values obtained from the dust maps of Schlegel et al. (1998).

We follow the prescription for the photometric calibration of the imaging data as described in the SDSS Photometric Flux Calibration web page [1]. The basic steps are summarized as follows.

We obtain a count rate t/t_0 from the net count N_{DN} (in "Data Numbers", DN) in each pixel in each of the passbands (u,g,r,i,z).

$$\frac{t}{t_0} = \frac{N_{DN} \times 10^{0.4\times(a_0+(k\times A))}}{T} \tag{3.1}$$

where t/t_0 is defined to be the count rate and t_0 is the zero point count rate and is given by $t_0 = 10^{-0.4\times aa}$. T is the exposure time, k is the atmospheric extinction coefficient in that passband and A is the airmass (optical path length relative to zenith for light travelling through the Earth's atmosphere) for that passband. a_0 is the zero-point in each passband.

The count rate is then converted to an SDSS *asinh* magnitude m (and thence to an AB flux) using:

$$m = -\frac{2.5 \times (asinh((t/t_0)/2b) + ln(b))}{ln(10)} \tag{3.2}$$

The error in the counts is calculated from the Poisson error from the photoelectrons which are counted by the CCD detectors, and the total noise contributed by read noise and

[1] http://www.sdss.org/dr4/algorithms/fluxcal.html

dark currents:

$$\delta N_{DN} = \sqrt{(\frac{N_{DN} + N_{sky}}{G}) + N_{pix} \times (D + \delta N_{sky})} \tag{3.3}$$

where N_{sky} is the number of sky counts (in DN) over the area considered, N_{pix} is the area covered by the object in pixels ($N_{pix} = 1$ for one pixel). D is the noise due to dark variance (in DN) and δN_{sky} is the error on the estimate of the average sky level (converted from $maggies/arcsec^2$ to DN/pix) in the frame.

Finally, we work out the error in the SDSS magnitude (from which we can derive an error in the flux):

$$\delta m = \frac{2.5 \times \delta N_{DN} \times 10^{0.4 \times (a_0 + k \times A)}}{2bT \times ln(10) \times \sqrt{1 + (\frac{t}{2bt_0})^2}} \tag{3.4}$$

The Point Spread Function (PSF) is not taken into account in our analysis. The median seeing value reported in DR4 was $1.4''$ so the PSF will be $3 - 4$ pixels across typically. This means that adjacent or nearby pixels are potentially not independent in their pixel-z parameters. We have ignored this effect for now since, as long as the galaxies are well-enough resolved, there will be useful information to be gained regardless of whether the small-scale details of structure (that will be hidden by the PSF) can be extracted.

3.3 PIXEL-Z IMPLEMENTATION: THE SDSS GALAXIES

We fit 2160 SED templates to all pixels in each of the SDSS galaxies in our sample, keeping the redshift of all pixels fixed to the spectroscopic redshift of their host galaxy. As discussed earlier, this effectively removes one degree of freedom in the fit and returns the properties of each of the pixels in terms of their best-fitting template, i.e. the age, SFR e-folding time, dust obscuration and metallicity.

We remove the simplifying assumption used by Conti et al. (2003) that all the pixels are coeval, i.e. that they share a common age over the whole galaxy. The assumption of common age simplifies the interpretation by removing a degree of freedom, and enabling a

clearer vision of the interplay between the remaining fitted parameters. That approach was useful in the analysis of Conti et al. (2003) in comparing maps of SFR, dust obscuration and metallicity for each galaxy with the underlying morphology. This assumption, however, is not consistent with the galaxy formation scenarios we are testing, nor is it required for our current analysis, and so we dispense with it.

The results of applying the pixel-z technique to the SDSS galaxies are described below.

3.3.1 Galaxy Maps

The first two panels of Figure 3.4 show the results of the likelihood decomposition for two galaxies. The image on the left of the top panel shows a SDSS spiral galaxy, NGC 450 (SDSS J011530.44-005139.5) and the middle image shows the distribution of best fitting stellar population ages in Gyr throughout this galaxy. We see an older population in the nucleus of the galaxy (ranging from 5-12 Gyr). In the outskirts there is a younger population whose ages range from 0.001 to 0.2 Gyr. The distribution of this parameter also traces out some of the spiral arm structure. Around the inner spiral arms, some of the "knots" of star formation seen in the original r' band image can be detected in the age image too as yellowish-green regions (with ages between 0.1 and 2 Gyr). The bottom panel shows the results for an edge-on disk galaxy. We detect an older population in the nuclear region (around 12 Gyr) and a mix of intermediate (2-5 Gyr) and old populations (5-12 Gyr) elsewhere in the disk. The stellar populations in the outskirts have a comparatively younger age.

Figure 3.5 is a result of the template decomposition for another SDSS galaxy (SDSS J075642.69+364430.0). There is evidence for a bulge in this disk galaxy - the stellar populations are older - as much as 10 to 15 Gyr, whereas those in the disk are much younger, typically less than 1 Gyr. The population in the core also has a lower e-folding time ($4 < \tau < 5$ Gyr) than in the outer disk. Together these results point to a lower current SFR in the central (bulge) population, compared to the disk population. The nucleus itself has a relatively low obscuration with $E(B-V) \approx 0.0$, while the stellar populations in the outer parts of the disk typically show a higher obscuration ($E(B-V) \approx 0.9$). The central part of the galaxy therefore shows an older population of stars, a faster timescale for SFR decline and a lower

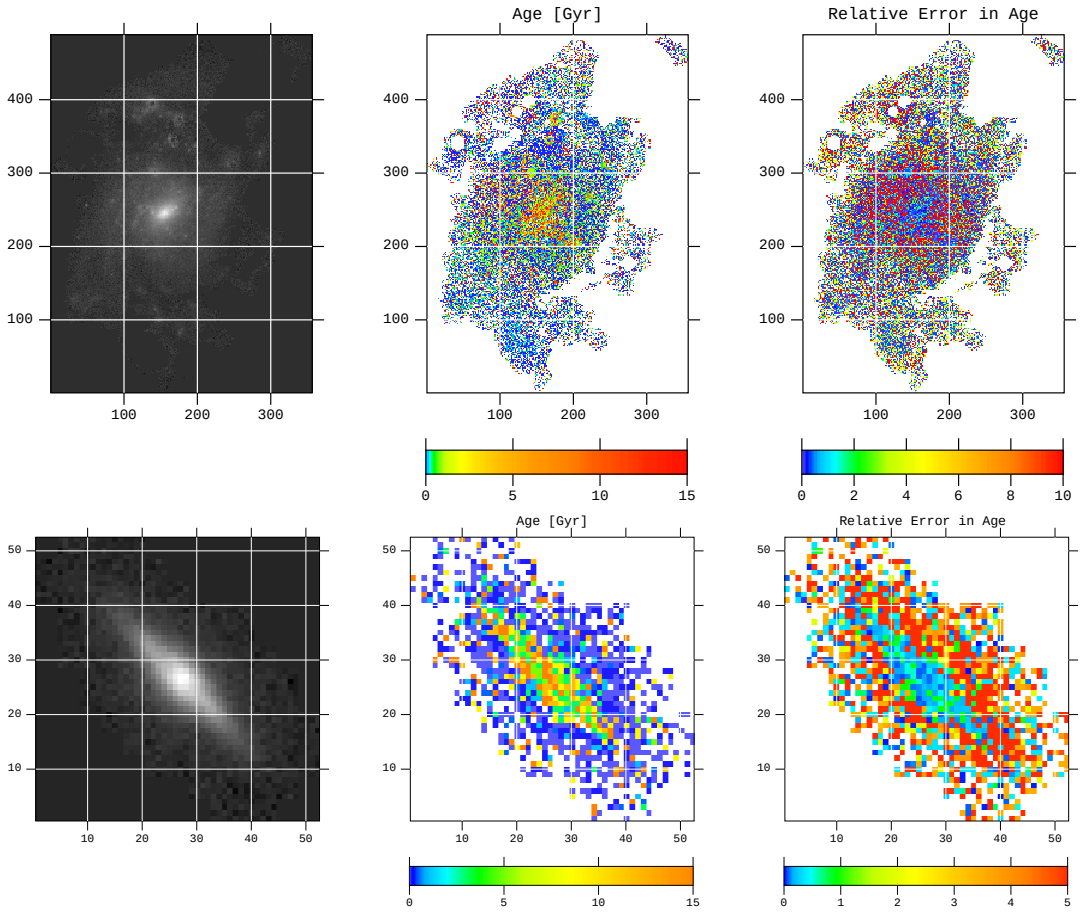

Figure 3.4: Top panel: Result of fitting 2160 SED templates to NGC 450 (SDSS J011530.44-005139.5) in the SDSS. The top left map shows the galaxy in the SDSS *r'* filter. The middle map displays the breakdown of the best-fitting template in each pixel according to the values of stellar population age in Gyr. Blue regions have the lowest age (0.001-0.1 Gyr), then green (0.1-0.6), then yellow (0.6-2 Gyr), then orange (2-7 Gyr), then red (7-15 Gyr). The third map shows the corresponding relative errors in the age for the pixels in this galaxy. As can be seen, the relative errors increase when going from the bulge region to the spiral arms. The map is obtained by computing the marginalized likelihood for each pixel in the galaxy as described in §2.5.3 and §3.3.2. Bottom panel: Another galaxy (SDSS J155919.97+061729.8). The left image shows the image in the *r'* filter. The middle map is the age map and the right image is the corresponding relative error map for the age. The nuclear region, with high flux pixels, shows a lower relative error for the age but the disk has a higher relative error. A substantial number of sky pixels are captured on the outskirts of this galaxy. These have the highest relative errors.

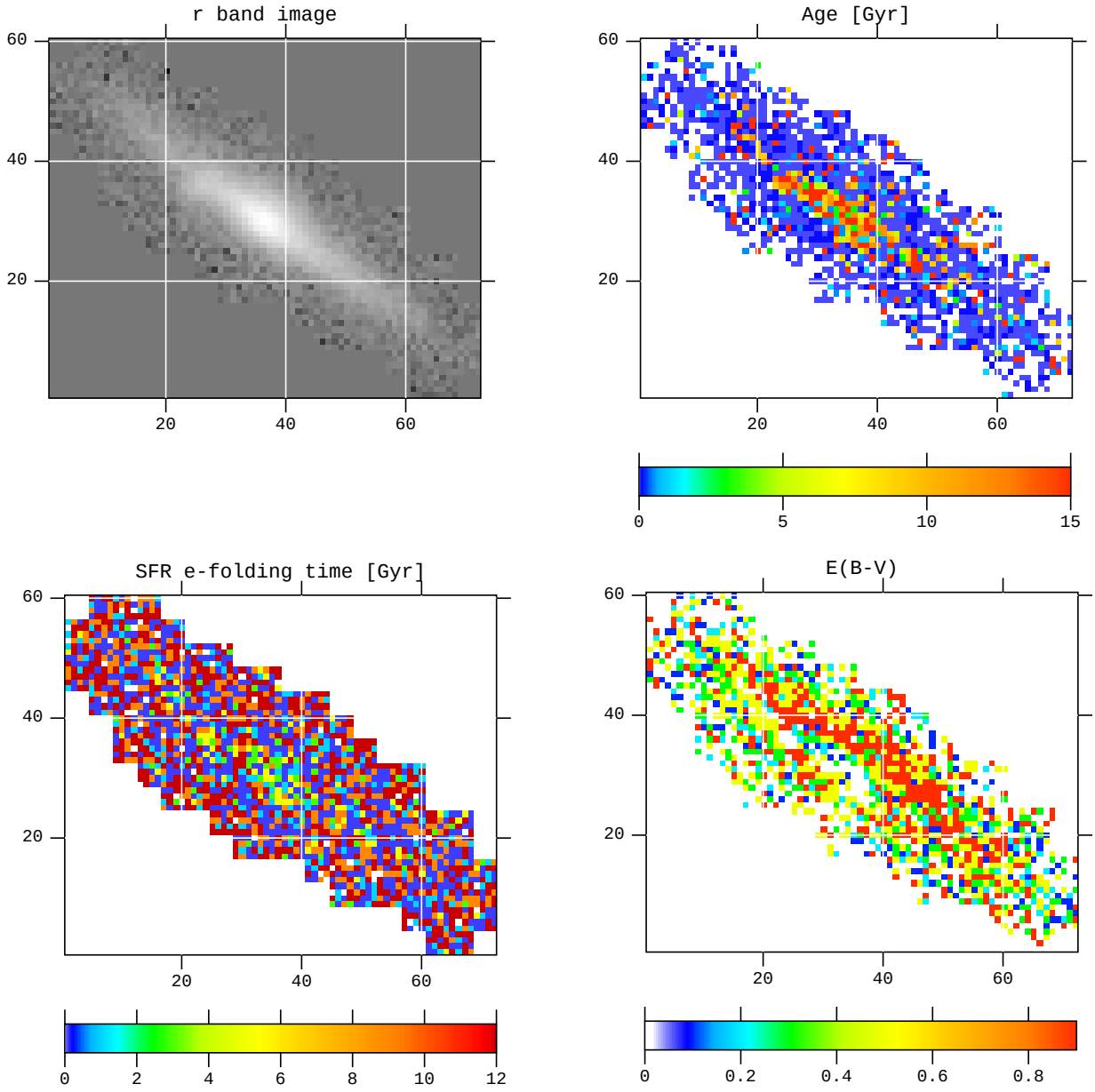

Figure 3.5: Result of fitting 2160 SED templates to each pixel in the SDSS galaxy SDSS J075642.69+364430.0. The top left map shows the galaxy in the SDSS *r'* filter. The other three maps display the breakdown of the best-fitting template in each pixel according to the values of the age of the stellar population, star formation rate e-folding time τ in Gyr and color excess $E(B-V)$ in magnitudes.

level of obscuration than the stellar populations in the outskirts of the disk. As we go further out we expect to be dominated by the sky pixels, which are artificially best fit by our SED templates corresponding to a younger stellar population, a longer timescale for SFR decline and a higher obscuration. Again, this artifact is identified through the large errors in the fitting, an important aspect of the pixel-z analysis, discussed in detail next.

3.3.2 Error Maps

In the top rightmost panel of Figure 3.4, we display the relative error in the age of the stellar populations. The inner arms of the spiral galaxy have a higher relative error in the age than does the central bulge region. In the second galaxy in the lower rightmost panel, the central bulge region has a lower relative error in the age than does the disk region.

In Figure 3.6 the bulge region, which shows an older stellar population, has a lower relative error in the age ($\frac{\Delta t}{t} \approx 0.1$) than the disk region which shows younger stellar populations with much higher relative uncertainties. These higher uncertainties correspond to lower flux pixels. The high values of these relative errors can be reduced somewhat by finer sampling of the age parameter near the low best-fitting age value. Now beyond the disk, the pixel-z technique artificially fits to the sky background, so that the seemingly lower values of the relative error on the age parameter in the outermost pixels are an artifact of the fitting and could also be a product of template degeneracy (discussed below). However, in either the disk or the sky, pixels with a relative error > 1 will have a negligible contribution to the calculated SFR compared to those with very low relative errors.

The bulge also shows a faster e-folding time for star formation, with a lower relative error ($0 < \frac{\Delta \tau}{\tau} < 0.4$) than in the disk ($\frac{\Delta \tau}{\tau} > 1.0$). The pixels in the outer regions within the galaxy generally show the highest relative errors associated with the age and e-folding time. This emphasizes that calculation of the total or local SFR has to be weighted by these fitting uncertainties. Similar trends are seen in other parameters though the bulge population in the obscuration map has a higher relative error in the obscured flux (with $10^{0.4(\Delta E(B-V)-E(B-V))} \approx 1.2$) than does the disk ($\approx 0.5$), although the relative error becomes large again in the furthest outskirts of the galaxy.

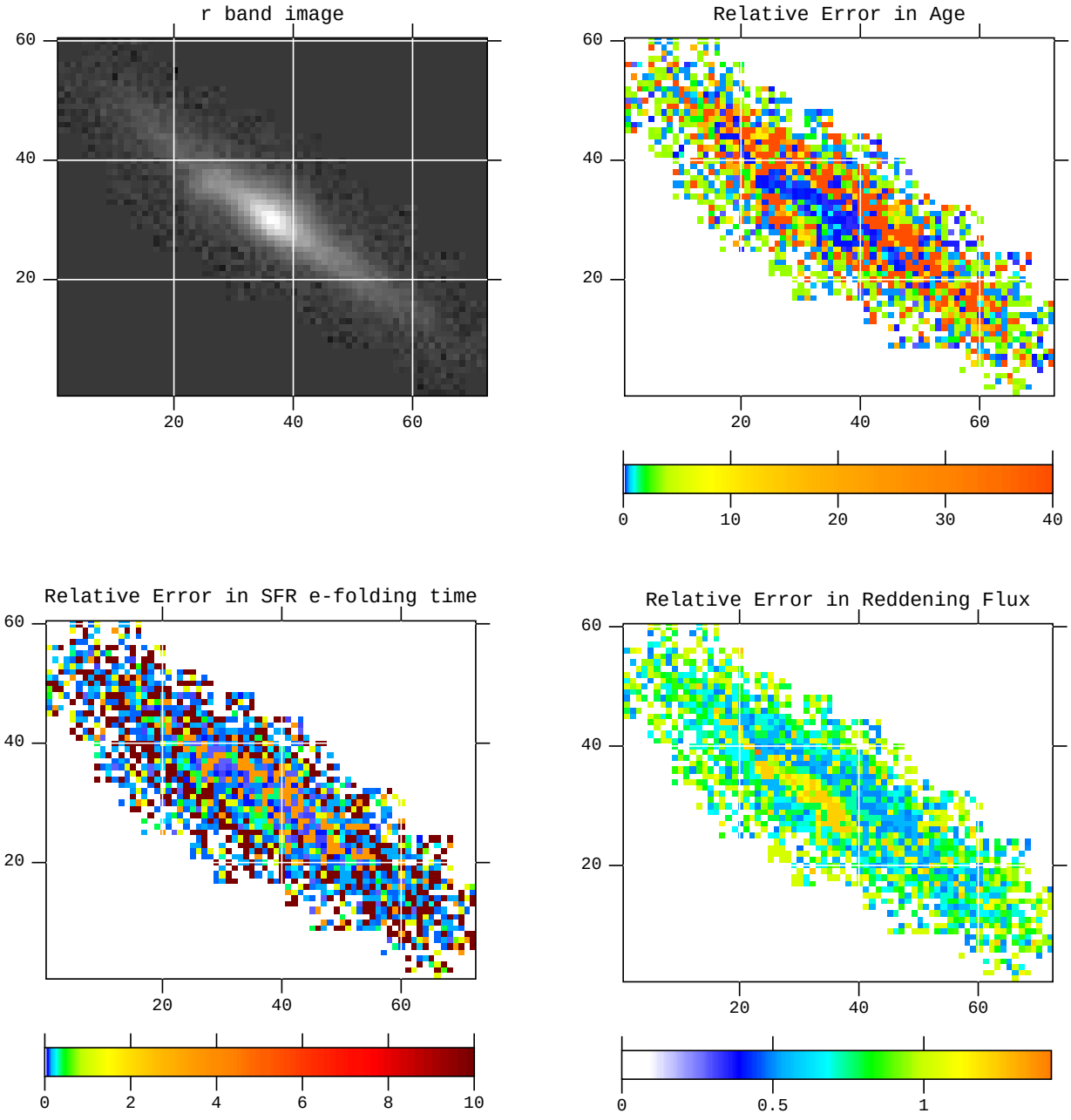

Figure 3.6: Relative error maps for the galaxy shown in Figure 3.5. Original image (top left), relative error in age (top right), relative error in SFR τ (bottom left) and relative error in reddening flux $10^{0.4(\Delta E(B-V)-E(B-V))}$ (bottom right).

In calculating either the total SFR of the galaxy or the mean SFR in radial shells, we weight the SFR in each pixel by its relative uncertainty as calculated from the error maps for the age and τ parameter. The weight of each pixel is proportional to the reciprocal of the fractional error squared in the calculated SFR of each pixel.

3.3.3 SED Degeneracies

Another uncertainty in the method is introduced by degeneracies among the different parameters as discussed in Chapter 2. There is likely to be a correlation between the parameters that determine the best-fit SED. Here, we investigate these correlations by using the 2-dimensional marginalized likelihood function, i.e. collapsing the 4-dimensional function onto the two axes of interest. Example results from this analysis are shown in Figure 3.7. The top panel shows the likelihood contours as a function of age and SFR e-folding time τ for a single central pixel in an SDSS galaxy. This is typical of the degeneracies seen in the fitting of most pixels. The near-elliptical contours indicate that these two quantities are not independent at least in the central region. The likelihood function is double-peaked, with the global maximum corresponding to a 3 Gyr old population and a 1 Gyr SFR e-folding time. As both these quantities are used in determining the star formation rate, we could expect a certain degeneracy in the calculated star formation rate. The bottom panel shows the degeneracy between age and metallicity in a central pixel of another galaxy, with the maximum corresponding to a 0.01 Gyr old populations and a $[Fe/H] \approx 0.01$. Although we have identified such degeneracies, we have not yet exhaustively analyzed their impact through all pixels in all galaxies in the sample. The integrated properties of the whole sample (such as the average total SFR or the average SFR radial profile) are likely to be more robust to such systematics than any individually measured value of a particular parameter.

One of the effects of the degeneracies can be seen directly in the images. Figure 3.8 shows the effect of constraining all the pixels to have a common age. The lower-left image corresponds to the case where no constraint was used and a fit in the full parameter space was done, but the lower-right image shows the case where the common age assumption was used. The reduced number of degrees of freedom enables a more resolved distribution of

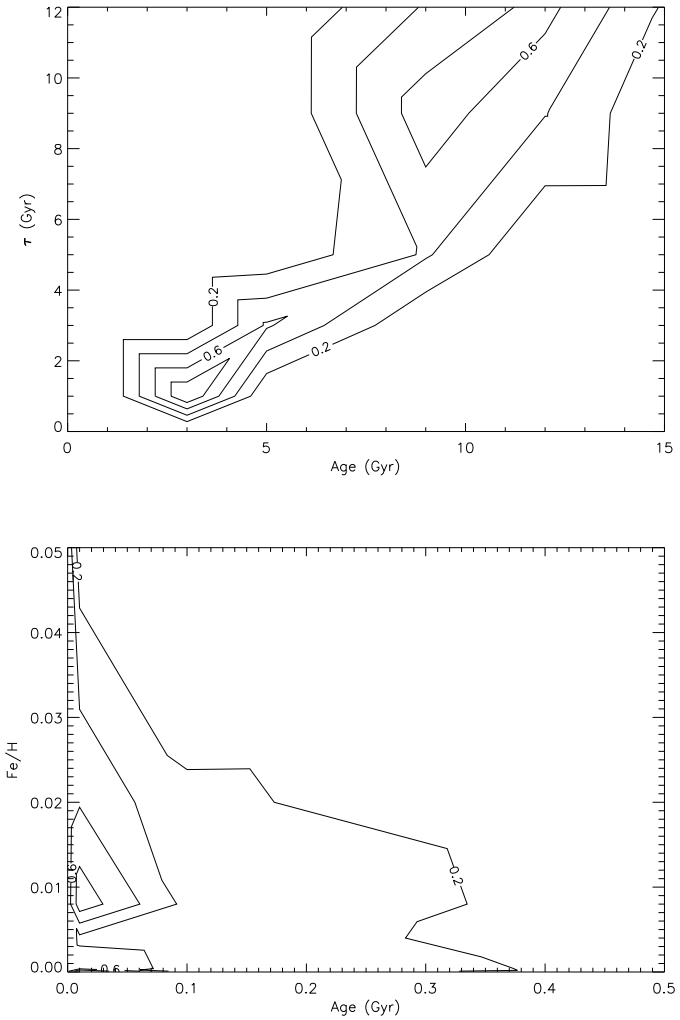

Figure 3.7: Top panel: Age-τ likelihood contours for a pixel in the nucleus of a galaxy. Bottom panel: Age-metallicity likelihood contours for a pixel in the nucleus of another galaxy. Contours are obtained from marginalizing the 4 dimensional likelihood function onto the two dimensions.

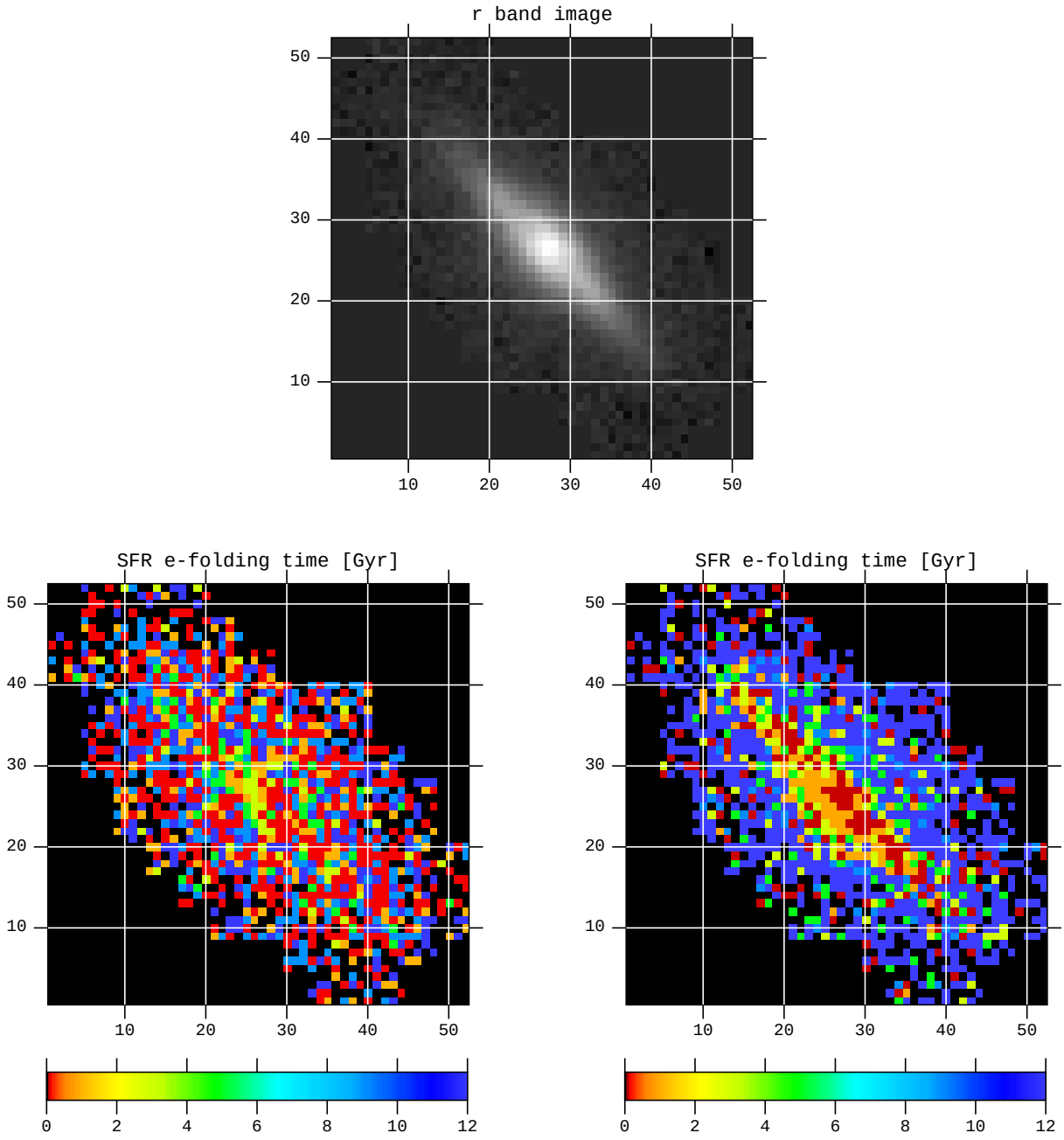

Figure 3.8: Effect of age-τ correlations. Top panel: Image of galaxy in the *r'* band. Lower-left panel: Map of SFR e-folding time τ. Lower-right panel: Map of τ where all the pixels are constrained to have a common age. The reduced number of degrees of freedom enables the central bulge and disk in this τ map to be better resolved.

central bulge and disk in this τ map. As discussed in Chapter 2, some of these degeneracies represent real physical relationships between the parameters, such as the well know age-metallicity degeneracy, while others reflect the choice of templates. Our selected templates cover the majority of parameter space, and since the fitting is done simultaneously over all parameters, the existence of degeneracies between any two parameters is mitigated. A more detailed study of the effect of these degeneracies will be incorporated in future work.

3.4 SFR VARIATION WITH LOCAL DENSITY

In this section, we investigate how the distribution of galaxy SFRs changes as a function of the local (spherical) galaxy density. We study how both the total SFR and the SFR *within* galaxies changes as a function of this galaxy density. As discussed in Chapter 2, the SFR due to stellar populations within each pixel of a galaxy is assumed to follow an exponential functional form $\Psi(t) = \Psi_0 e^{(-t/\tau)}$. The normalization of the SFR in each pixel is based on the scale factor b_j (equation (2.6)), which gives the SFR in units of $M_\odot\, yr^{-1}$.

The total SFR for each galaxy is calculated from the sum of all pixels in the galaxy, summed within consecutive radial annuli from the center of the galaxy up to 1.5 Petrosian radii (R_p), where R_p is a measure of the scale length of the galaxy derived from its surface brightness profile and is measured in the r' band (Petrosian, 1976; Blanton et al., 2001). We construct both unweighted and weighted sums to give a total star formation rate for the galaxy, where the weights correspond to the reciprocal of the square of the fractional error on the SFR in each pixel. The weighting is done to avoid giving undue significance to poorly constrained pixels, such as pixels dominated by the sky background, so that these pixels do not bias our measurements. The unweighted results turn out to be qualitatively the same as the weighted ones, but with some quantitative differences.

We find that doing the summation of SFR in annuli up to $1.5R_p$ captures the vast majority of pixels that actually belong to the galaxy while not including the contribution of a majority of sky pixels surrounding the galaxy. The reason for this is that although low surface brightness, low signal-to-noise pixels in the galaxy outskirts should individually have

only a very small contribution to the total SFR (since we are weighting the SFR in each pixel by the square of the signal-to-noise), galaxies can have a substantially large areas of these low signal-to-noise pixels which extend well beyond the disk scale length. The combined contribution of these pixels could therefore bias the total SFR that is calculated. This appears to be less of a problem for typical disk galaxies than for bulge-dominated systems which can have a large area of these low-surface brightness pixels surrounding the galaxy. Limiting the spatial extent to $1.5R_p$ within which the SFR in the pixels is counted therefore provides a more accurate estimate of the total SFR in the galaxy.

3.4.1 Total Galaxy SFR as a Function of Local Galaxy Density for All Galaxies

Here, we investigate how the total SFR in galaxies varies as a function of the local galaxy density. As described above, the total SFR in each galaxy is calculated as a weighted sum of the SFR over the pixels in the galaxy, where the weights are inversely proportional to the square of the fractional uncertainties in the SFR of each pixel. The local environment is quantified by counting the number of galaxies in a 5 $h^{-1}\,Mpc$ radius sphere centered on each galaxy.

Figure 3.9 shows the variation of the SFR distribution with local density, the three lines corresponding to the 25th, median and 75th percentiles of the SFR distribution. The fluctuations at low densities are characteristic of the size of the systematic uncertainties in these measurements. The SFR decreases with increasing density, with the greatest effect in the highest density environments, $> 0.05\,(h^{-1}\,Mpc)^{-3}$ (densities that correspond to the outskirts of rich clusters).

These results, consistent with the measurements of Lewis et al. (2002) and Gómez et al. (2003), suggest that the total SFR of galaxies in the SDSS is strongly correlated with local density. This is also in agreement with the predictions of various hierarchical galaxy formation models whereby SF in galaxies is suppressed as galaxies fall into more dense environments such as clusters. The range of local densities in our sample allows us track the total SFR in galaxies in a wide range of environments: from the cores of rich clusters and groups into the field. As detailed by Gómez et al. (2003), based on the SDSS Early Data

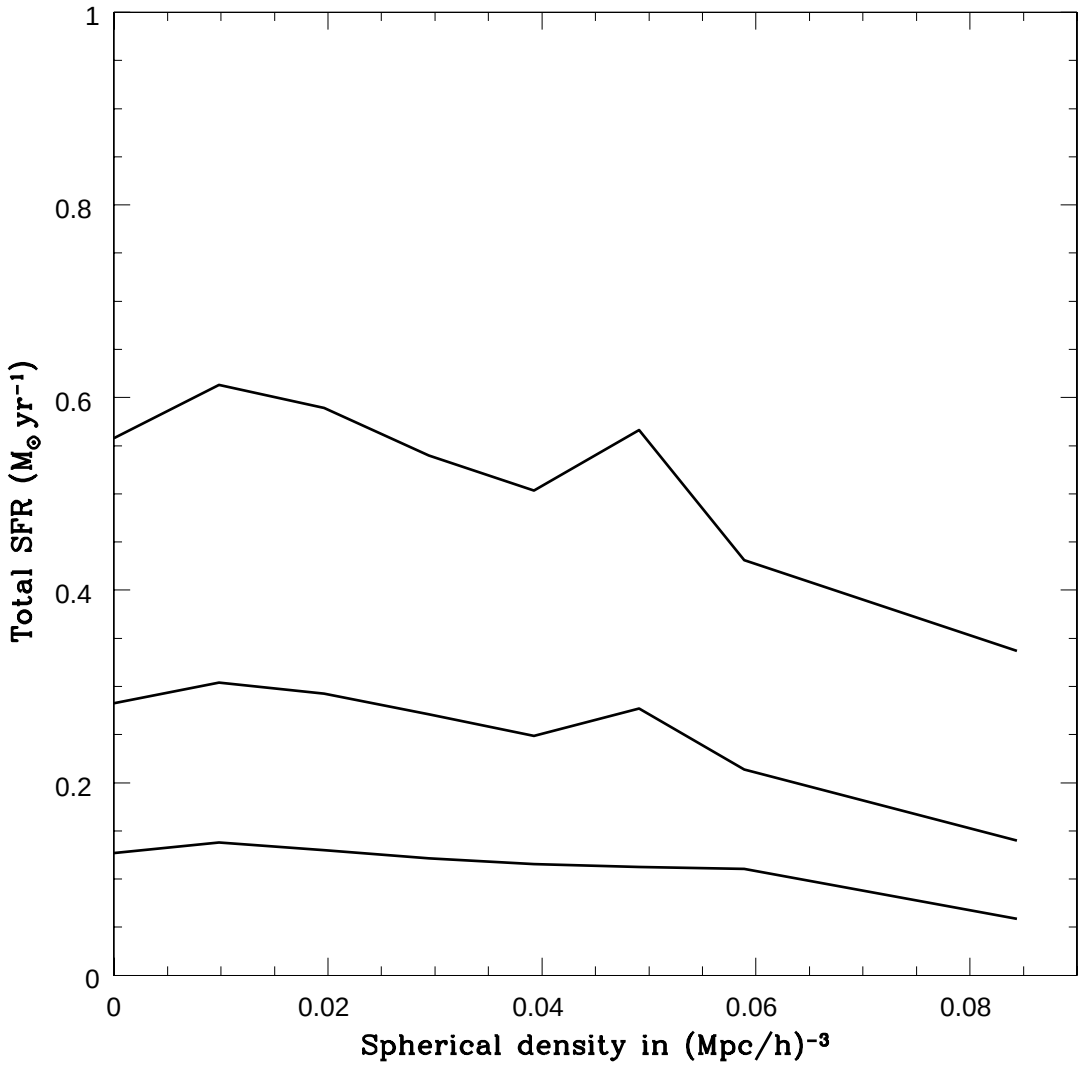

Figure 3.9: Galaxy SFR in $M_\odot\, yr^{-1}$ as a function of density, where the SFR is calculated from a weighted sum over pixels in each galaxy. From top to bottom, the lines indicate the 75th, median and 25th percentiles of the SFR distribution respectively. The fluctuations at low densities correspond to the size of systematic uncertainties in the measurements. The overall SFR distribution which is essentially flat (given the size of these fluctuations) for low densities shifts to lower values at the higher densities. The decrease at higher densities is most noticeable in the most strongly star-forming galaxies, those in the 75th percentile. Finally, the range in the SFR distribution is largest at lower densities and decreases continuously with density.

Release and using Hα EW as a measure of SFR, Figure 3.9 illustrates the effect of environment on SFR. The overall SFR distribution, essentially flat for low densities, shows a decrease or suppression in regions of higher density. The effect is most noticeable in the most strongly star-forming galaxies, i.e. those in the 75th percentile of the SFR distribution. This means that the skewness of the distributions decreases with increasing density. The "break" density, around $0.05\,(h^{-1}\,Mpc)^{-3}$, beyond which the SFR distribution falls rapidly to lower values, occurs well into the regime of rich clusters, the extreme tail of the galaxy density distribution. A comparison between the "break" density seen here using our density estimator and that measured by Gómez et al. (2003) will be explored in future work.

3.4.2 Total SFR-Density Relation for Early and Late Type Galaxies

As discussed in Chapter 1, it is well established that in more dense environments the galaxy population becomes dominated by early-type galaxies (e.g., Dressler (1980); Postman and Geller (1984); Tran et al. (2001)).

We seek to determine whether the SFR of galaxies of a given morphology are also affected by environment, i.e. whether the SFR-density relation holds regardless of morphology. We thus split our sample into two broad morphological bins based on the (inverse) concentration index C_{in} i.e early-types with $C_{in} \leq 0.4$ and late-types with $C_{in} > 0.4$. Consequently, there are 27 993 early-type galaxies and 16 971 late-type galaxies. Figure 3.10 presents the distribution of SFR as a function of the local galaxy density for each of these morphological types. It can be seen that the distribution of SFR for late-type galaxies is skewed towards higher values of SFR, while early-type galaxies populate the lower SFR portion of the distribution in the full sample. This is consistent with early-types having red, older stellar populations and lower SFR, while late-types typically have blue, star-forming populations with consequently high SFR. For early-types, the density-SFR relation is similar to the one observed for the full sample: the overall SFR distribution is relatively flat (compared to the size of systematic fluctuations) for low densities and then shifts to lower values beyond $0.05\,(h^{-1}\,Mpc)^{-3}$. Like the trend for the full sample, the decrease at higher densities is most noticeable in the most strongly star-forming galaxies in the 75th percentile of the SFR distribution, with a

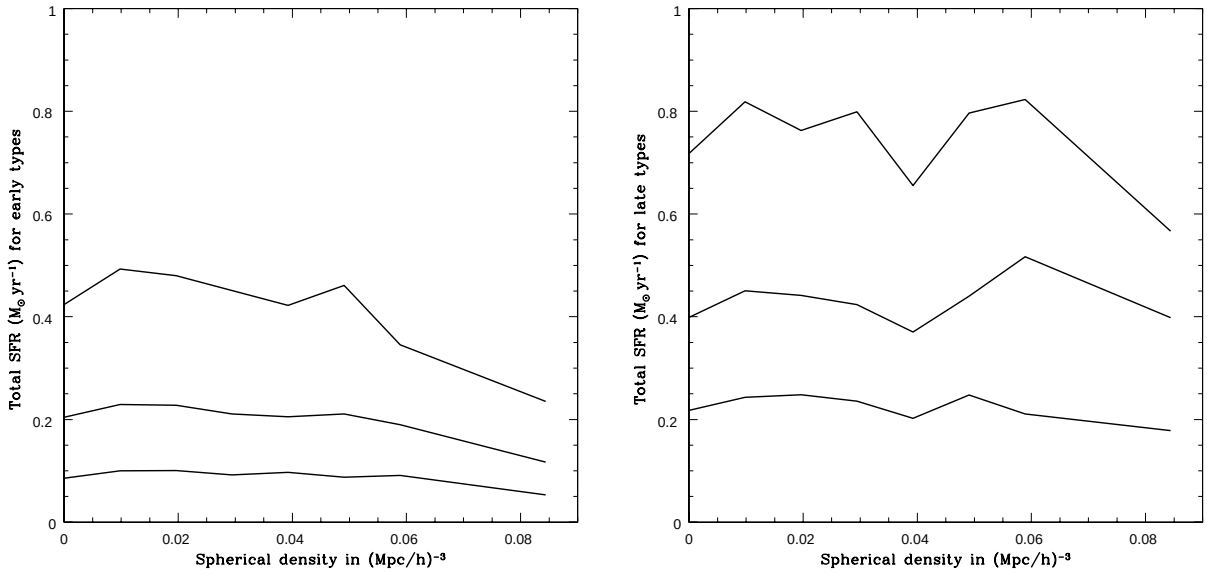

Figure 3.10: Top panel: SFR-density relation for early-type galaxies (with $C_{in} \leq 0.4$ as discussed in §3.4.2). Bottom panel: SFR-density relation for late-types (with $C_{in} > 0.4$). In each panel, the total galaxy SFR is calculated from a weighted sum over pixels in each galaxy. From top to bottom, the lines indicate the 75th, median and 25th percentiles of the SFR distribution respectively. For early-types, the overall SFR distribution is relatively flat (compared to the size of systematic fluctuations) for low densities and then shifts to lower values beyond $0.05\,(h^{-1}\,Mpc)^{-3}$. The decrease at higher densities is most noticeable in the most strongly star-forming galaxies in the 75th percentile of the SFR distribution. For late-types, the overall SFR distribution is also relatively flat at low densities but then falls to lower values beyond $0.055\,(h^{-1}\,Mpc)^{-3}$. The range in the SFR distribution decreases with increasing galaxy density for early-types but is relatively unchanged for late-type galaxies. Finally, late-type galaxies are also seen to be more highly star-forming than early-types at all densities.

sharp decrease beyond $0.05\,(h^{-1}\,Mpc)^{-3}$. The scatter in the SFR distribution decreases with increasing galaxy density for early-types. For late-types, the overall SFR distribution is also relatively flat at low densities but then falls to lower values beyond $0.055\,(h^{-1}\,Mpc)^{-3}$. However, even in the highest density environments, the SFR of these high-SF late-type galaxies is higher than for the early-types. Finally, unlike the early-types, the scatter in the relation is relatively unchanged for late-type galaxies across all densities.

The results are broadly consistent with the findings of Gómez et al. (2003) who also split their sample based on the parameter C_{in}. They found that early and late-type galaxies each obey a SFR-density relation although it is a shallow one for early-types (which have low SFR) while for late-types (which dominate the galaxies in their sample with high SFR), the relation is similar to that for the full sample.

3.4.3 Radial Variation of SFR as a Function of Local Galaxy Density

Although we have established a correlation between the total galaxy SFR and galaxy density, we can now explore where within the galaxies this suppression is taking place. In particular, we are interested in finding out if the suppression is primarily in the outskirts of galaxies or if it is in their inner regions. The former would support the predictions of hierarchical ("infall and quench") models of galaxy formation, as the SF in the outskirts of the galaxies would be expected to be first affected by encountering an increasingly dense environment, while the latter would favor an "environmentally-governed evolution" scenario. By using pixel-z to study the spatial distribution of SF, we will be able to distinguish between these two models.

For each galaxy we calculate a weighted mean SFR Ψ_w within successive annuli:

$$\Psi_w = \frac{\sum_{i=1}^{N_a} w_i \times \Psi_i}{\sum_{i=1}^{N_a} w_i} \tag{3.5}$$

where w_i is the weight corresponding to Ψ_i, the SFR in pixel i, and N_a is the number of pixels within that annulus a. The weight w_i is inversely proportional to the square of the fractional error on the SFR for the pixel i. The SFR in each annulus is thus normalized by the number of pixels, accounting for the larger total SF at larger radii due to a greater

number of pixels. Scaling the radius of each annulus by the Petrosian radius (R_p) of the galaxy allows us to stack annuli for different galaxies (which have different Petrosian radii) together. The center of the galaxy is chosen as the brightest pixel in the galaxy.

We examine the annular distribution of Ψ_w for the stacked galaxies, spanning a range of local densities: $0.0 < \rho \leq 0.01\,(h^{-1}\,Mpc)^{-3}$, $0.01 < \rho \leq 0.04\,(h^{-1}\,Mpc)^{-3}$, $0.04 < \rho \leq 0.09\,(h^{-1}\,Mpc)^{-3}$. Figure 3.11 shows the median and 75th percentiles of this distribution. The inner annuli are more finely binned with $\Delta\,(r/R_p) = 0.125$ for $r/R_p \leq 0.25$, while $\Delta\,r/R_p = 0.25$ for $r/R_p > 0.25$. Errors in Ψ_w are calculated for each annulus by propagating the errors in all the SFRs Ψ_i of the pixels within that annulus. The typical size of $0.125r/R_p$ is 2-3 pixels. There are 2785 galaxies where $0.125r/R_p$ is below the pixel resolution. Removing these galaxies neither significantly changes the radial profile of SF nor affect its dependence on local density.

Star formation in galaxies on average is higher in the the mid-annular region than in the core or outskirts. It is lower (averaged over all morphological types and inclinations) in the nucleus than in the circumnuclear regions. We find that in dense environments this low SF in the nuclear regions appears lower still. The higher SF in the circumnuclear region ($0.125 < r/R_p \leq 0.25$) is also lessened in more dense regions. It is this depression in the innermost annuli that accounts for the dependence of total galaxy SFR on density.

The effect can be seen most prominently in the 75th percentile of the distribution of Ψ_w. The density dependence in the 75th percentiles of Ψ_w is most evident in the first two innermost annuli up to $r/R_p = 0.25$, where there is a clear suppression of Ψ_w between the lowest and highest density intervals: by $8.2 \times 10^{-4} M_\odot\,\mathrm{yr}^{-1}$ (with $4\,\sigma$ significance) in the nuclear region and $2.6 \times 10^{-3} M_\odot\,\mathrm{yr}^{-1}$ (with $3\,\sigma$ significance) in the circumnuclear region. A Kolmogorov-Smirnov (KS) test on the distribution of Ψ_w of these two innermost annuli in the lowest density interval ($0.0 < \rho \leq 0.01\,(h^{-1}\,Mpc)^{-3}$) and the highest density interval ($0.04 < \rho \leq 0.09\,(h^{-1}\,Mpc)^{-3}$) rules out the hypothesis that the populations in the two density ranges are derived from the same underlying distribution at more than 99.9% confidence level. The suppression of SF in the central regions of the galaxies is therefore an effect of the environment rather than being due to stochastic fluctuations.

Beyond $r/R_p = 0.25$ there appears to be no clear dependence of the mean SFR on the

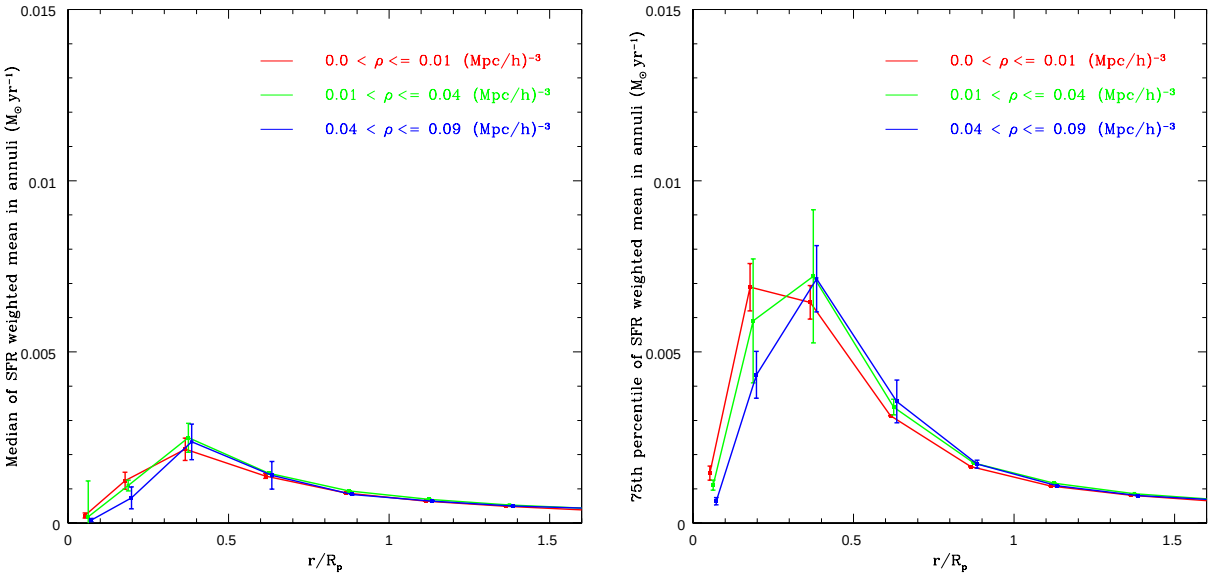

Figure 3.11: Top panel: Median of the weighted mean SFR Ψ_w $(M_\odot\, yr^{-1})$ within successive radial annuli for 3 different intervals of galaxy density ρ: $0 - 0.01\,(h^{-1}\,Mpc)^{-3}$ (red), $0.01 - 0.04\,(h^{-1}\,Mpc)^{-3}$ (green), $0.04 - 0.09\,(h^{-1}\,Mpc)^{-3}$ (blue). Bottom panel: 75th percentile of Ψ_w $(M_\odot\, yr^{-1})$. The mean SFR in each annulus for each galaxy is a weighted mean of the SFRs in all the pixels in the annulus. For galaxies in each local density interval, these radial annuli are then stacked. The percentiles are obtained from the distribution of the mean SFR in these stacked annuli. The inner annuli are more finely binned with $\Delta\, r/R_p = 0.125$, while $\Delta\, r/R_p = 0.25$ for $r/R_p > 0.25$. The density dependence in the 75th percentiles of Ψ_w is most evident in the first two innermost annuli up to $r/R_p = 0.25$, where there is a clear suppression of Ψ_w between the lowest and highest density intervals. The same is true to a lesser extent in the median. Beyond $r/R_p = 0.25$, no dependence on the local density of galaxies is detected. Errors in Ψ_w are calculated for each annulus by propagating the errors in all the SFRs Ψ_i of the individual pixels within that annulus.

local density of galaxies. We see a similar, though less pronounced, trend in the median of the distribution of Ψ_w. Again, there is no statistically significant dependence of the mean SFR on local density in galaxy outskirts.

3.4.4 Radial Variation of SFR with Environment for High and Low Star Forming Galaxies

The suppression of the total galaxy SFR with increasing local density is most noticeable in the 75th percentile curve of Figures 3.9. In other words, at progressively higher densities, the distribution of galaxy SFRs is truncated at lower SFR values, and it is the population of the most highly star forming galaxies that are being affected. Here we investigate whether the radial variation we observe in Figure 3.11 is seen only in these high SFR galaxies or whether such a trend also exists in more quiescent galaxies. We examine the galaxy populations comprising the upper and lower quartile of the SFR distribution, and the results are shown in Figure 3.12 for the high SFR galaxies (with SFR $> 0.60\,\mathrm{M}_\odot\,\mathrm{yr}^{-1}$) and in Figure 3.13 for the low SFR galaxies (SFR $< 0.14\,\mathrm{M}_\odot\,\mathrm{yr}^{-1}$). For the high SFR population, up to a radius of $0.25R_p$, the suppression of Ψ_w with environment is clearly evident, and as with the total galaxy population, there is no dependence beyond this radius. Again, as before, the effect is most pronounced for the 75th percentile of Ψ_w (in the range $0 < r/Rp \leq 0.25$), where there is a $2\,\sigma$ difference between the highest and lowest density intervals in the range $0 < r/Rp \leq 0.125$ and a $3\,\sigma$ difference in the range $0.125 < r/Rp \leq 0.25$. But it can also be seen in the median of the distribution (in the range $0.125 < r/Rp \leq 0.25$), where the difference is $2.5\,\sigma$. This is consistent with the dependence of the radial variation of the mean radial SF on environment for the total galaxy population in the sample (averaged over all star formation rates) in §3.4.3. A KS-test on the distribution of Ψ_w of these two innermost annuli in the lowest density interval ($0.0 < \rho \leq 0.01\,(h^{-1}\,Mpc)^{-3}$) and the highest density interval ($0.04 < \rho \leq 0.09\,(h^{-1}\,Mpc)^{-3}$) once again rules out the hypothesis that the populations in the two density ranges are derived from the same underlying distribution, at more than 99.9% confidence level.

For the low star forming galaxies a small, although not statistically significant, depen-

dence on environment is seen. It is thus the population of strongly star forming systems that account for the observed relation between the radial mean SFR and the local density of galaxies shown in Figure 3.11. The suppression of SFR in the innermost annuli of the most strongly star-forming systems accounts for the observed SFR-density relation in the overall galaxy population.

It should be noted that the innermost annulus ($r \leq 0.125R_p$) is resolved (i.e. larger than the pixel resolution) for the majority of galaxies. For over 53% of galaxies, the innermost annulus is also larger in angular scale than the median PSF width in the SDSS (1.4").

3.4.5 Physical Interpretation

In §3.4.1 and §3.4.2, we find evidence for a suppression of total SFR as we go to higher density environments, and this relation seems to be preserved independent of morphology. So the total SFR-density relation is a result of SFR suppression at higher densities, not just a result of the morphology-density relation (at least not solely). The suppression is evident at the highest densities, beyond $0.05\,(h^{-1}\,Mpc)^{-3}$, in the regime of clusters. In these high density environments, there are a number of physical mechanisms responsible for the suppression of total SFR. These include ram-pressure stripping, galaxy harassment and tidal disruptions, mechanisms that are known to be dominant in cluster cores.

However, in §3.4.3, we find that the suppression of mean radial SF takes place in the cores of galaxies (particularly in the nuclear and circumnuclear region) while the outskirts are not affected by their changing environment. This implies that the environment itself is not impinging on galaxies to suppress the SFR, as the outer regions should otherwise be most affected according to "infall and quench" models. Any physical mechanism cannot therefore be solely responsible for this drop in the nuclear SF. By extension, they cannot therefore be governing the suppression in total SFR in galaxies in high density environments.

This seems to point to an evolutionary rather than an environmental origin for the SFR-density relation. If galaxies in more dense environments formed their stars earlier and faster than those in less dense environments, that would be consistent with either a uniformly depressed SFR as a function of galaxy radius, or a depressed nuclear SFR, given that higher

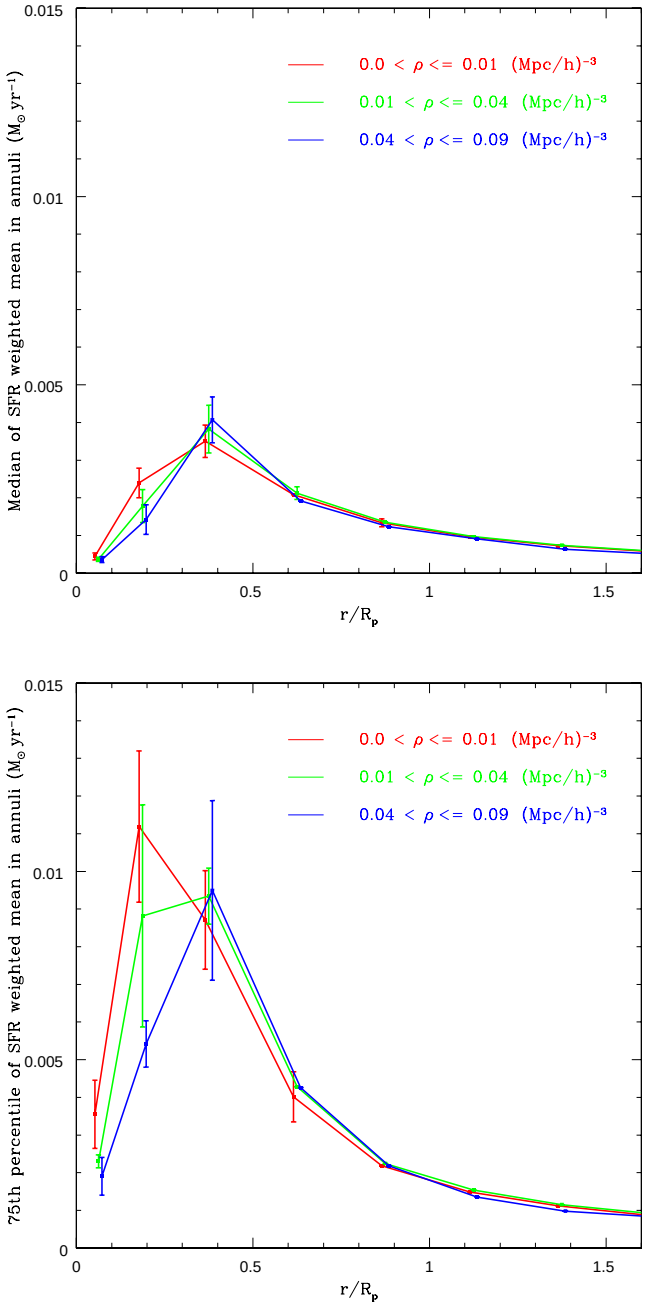

Figure 3.12: Top panel: Median of the distribution of weighted mean SFRs Ψ_w $(M_\odot\, yr^{-1})$ within successive radial annuli as a function of the local galaxy density ρ for high star forming galaxies ($> 0.60\, M_\odot\, yr^{-1}$). There are 3 different intervals of ρ, as in Figure 3.11. Bottom panel: 75th percentile of Ψ_w $(M_\odot\, yr^{-1})$.

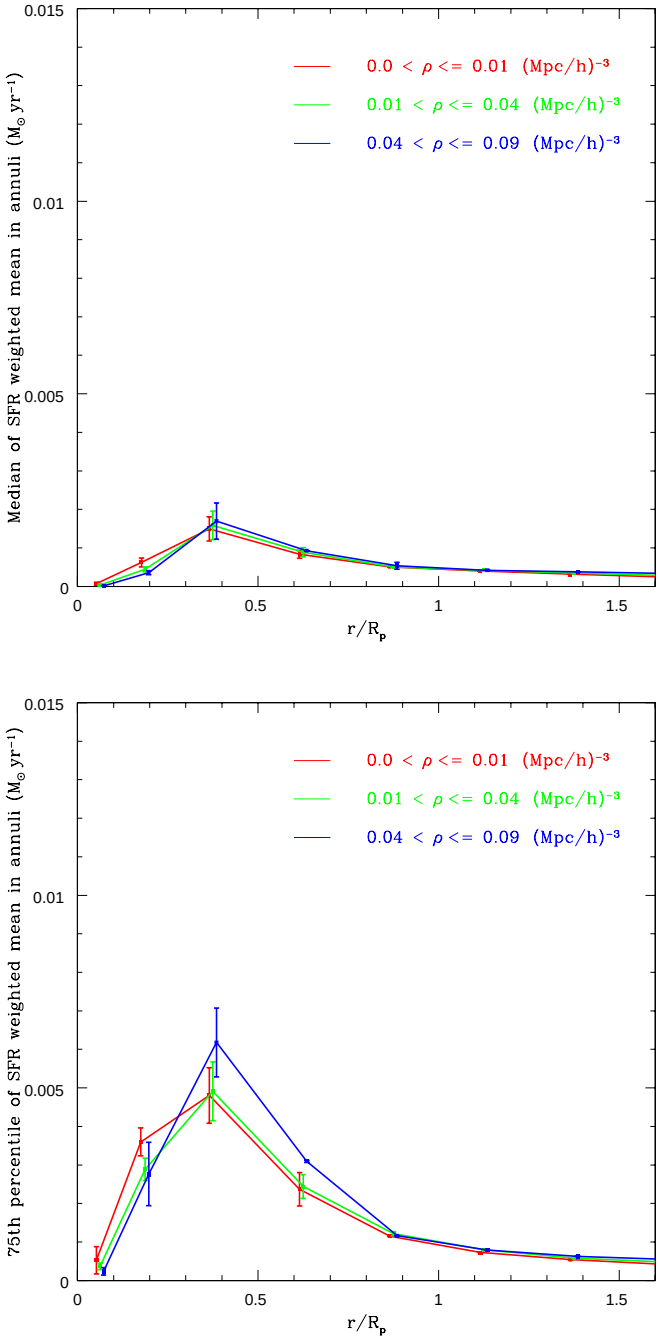

Figure 3.13: Top panel: Median of the distribution of weighted mean SFRs Ψ_w ($M_\odot\, yr^{-1}$) within successive radial annuli as a function of the local galaxy density ρ for low star forming galaxies ($< 0.14\, M_\odot\, yr^{-1}$). There are 3 different intervals of ρ, as in Figure 3.11. Bottom panel: 75th percentile of Ψ_w ($M_\odot\, yr^{-1}$).

gas densities in the nuclear regions are likely to drive star formation more rapidly (supported by the fact that star forming disk galaxies typically show bulges dominated by old, red stellar populations).

These results seem to be consistent with the idea of "downsizing" in galaxy formation (Cowie et al., 1996), discussed in Chapter 1, whereby the more massive galaxies form at earlier epochs. Downsizing is characterized by a decline in the mass of the galaxies that dominate the star-formation rate density with decreasing redshift ("downsizing of star formation"). This is supported by recent measurements of star-formation histories in both local galaxies from the SDSS (Heavens et al., 2004) and distant galaxies from the Gemini Deep Deep survey (Juneau et al., 2005). This is distinct from the "downsizing with quenching" which follows a different timescale - spheroidal galaxies have been known to have a second star-formation timescale, namely that of "quenching": it becomes easier to keep galaxies gas-free with time. In fact, recent studies of the galaxy luminosity function at $z \approx 1$ (Bell et al., 2004; Faber et al., 2007) conclude that massive red galaxies observed at $z \approx 0$ migrated to the bright end of the red sequence by a combination of two process: the quenching of star formation in blue galaxies and the merging of less-luminous, previously quenched red galaxies. Faber et al. (2007) conclude that the typical mass at which a blue, star-forming galaxy is quenched (and therefore enters the red sequence) decreases with time. Our radial result is evidence for the "downsizing of star formation" as opposed to this "downsizing with quenching".

In §3.4.4, we have also found that whereas the quiescent galaxies (corresponding to the bottom quartile of the total SFR distribution) in the sample show no significant dependence of SFR on environment at any radius, the radial dependence of the mean annular SFR for the highest star-forming galaxies (top quartile of the total SFR distribution) mirrors the trend for the full sample. In addition, while the decrease of total SFR with density is dominated by the high-SFR galaxies, the quiescent galaxies show hardly any dependence of their total SFR on environment. The radial result in §3.4.4 confirms that the total SFR-density relation is largely due to the decline of nuclear SF in these high SF galaxies as we go to higher density environments. The overall radial result can therefore be explained if we consider a population of active, star-forming galaxies which formed at high redshift. The SF in this population of

galaxies is dominated by the nuclear SF. Out of this population, the more massive systems which formed in more dense environments also formed their stars earlier and faster than those in less dense environments. By $z \approx 0$, this sub-population (which originated from more massive systems) has a lower nuclear SF than the sub-population which formed in less dense environments. This supports the idea that the "downsizing of star formation" in galaxies as described by Cowie et al. (1996) apples only to the actively star-forming galaxies in our sample.

It could also be possible that this SFR suppression in galaxy cores may be a consequence of feedback from an active galactic nucleus (AGN). In particular, if AGN feedback in more massive systems is more efficient than in lower mass systems, and since dense environments are known to host more massive galaxies on average (Dressler, 1980; Postman and Geller, 1984), this could perhaps lead to preferential suppression of nuclear star formation in more dense environments. This mechanism could be explored further by looking into the mass dependence of the SFR suppression in galaxies, although this is beyond the scope of our current analysis. The radius out to which such a feedback mechanism could suppress SF also needs to be quantified. The complete explanation may be a combination of this "downsizing" in SF together with more efficient AGN feedback in galaxies in more dense environments.

3.4.6 Effect of Probing the Full PDF: Systematic Uncertainties in Annular SFR Estimates

In the pixel-z method, we compare the observed fluxes in five passbands in every pixel in a galaxy to the filter-convolved SED fluxes through the same passbands (see §2.4.1). We chose a best-fitting template SED using χ^2 minimization on a discrete grid of stellar population parameters: age t, SFR e-folding time τ, $E(B-V)$ and the metallicity Fe/H. The SFR in every pixel is calculated from the values of t and τ that correspond to the best-fit SED. We now study the effect of sampling the full probability distribution defined by the grid of stellar population parameters. We use Markov Chain Monte Carlo (MCMC) to sample the full probability distribution defined by these parameters. This involves constructing a Markov Chain that approximates its stationary distribution. The aim of this work (Welikala

et al. 2008, in preparation) is to determine whether the estimates of the mean annular SFR Ψ_w derived from MCMC differ substantially from those derived from the pixel-z method that relies on χ^2 minimization.

We chose pixels in the annulus $0.125 < r/R_p \leq 0.25$ to perform our analysis since this is where the most significant suppression in the SF in the highest density environments takes place. Yip et al. (2008, in preparation) used the "Metropolis" algorithm (Gamerman, 1997). This has been shown to converge to an equilibrium probability distribution after sampling a sufficiently long chain. The transition probability at a particular step in the algorithm depends only on the ratio between that step and its previous step. In forming the chain, the probability density at a particular parameter combination $[t,Z,\tau,E(B-V)]$ is assumed to be (Yip et al. 2008, in prep.):

$$\rho(t, Z, \tau, E(B-V)) = Ae^{-s\chi^2(t,Z,\tau,E(B-V))} \quad (3.6)$$

where χ^2 is defined as in equation (2.5). A is a normalization constant and s is fudge factor used to decrease the acceptance rate when making the Markov chain.

In this study, we use 450 pixels from 9 annuli belonging to 9 galaxies (5 early-type and 4 late-type), the pixels being located in the radial annulus defined by $0.125 < r/R_p < 0.25$. An SFR (in $M_\odot\, yr^{-1}$) is calculated for every pixel in each galaxy before doing a weighted sum over the pixels within the annulus, as described in §3.4.3, in order to calculate Ψ_w for each annulus. The results are shown in Figure 3.14. The left panel shows the result of comparing the values of Ψ in the annulus that were obtained by template SED-fitting via the pixel-z method with those obtained from sampling the full probability function via the Markov Chains. It can be seen that there is a correlation between the SFR estimates calculated by each method, although the scatter becomes large for $\Psi > 0.0065\, M_\odot\, yr^{-1}$. The next panel shows the residual (the difference between the MCMC and pixel-z value) for each value of Ψ_w estimated by pixel-z. Up to $0.006\, M_\odot\, yr^{-1}$, there is good agreement between the two methods

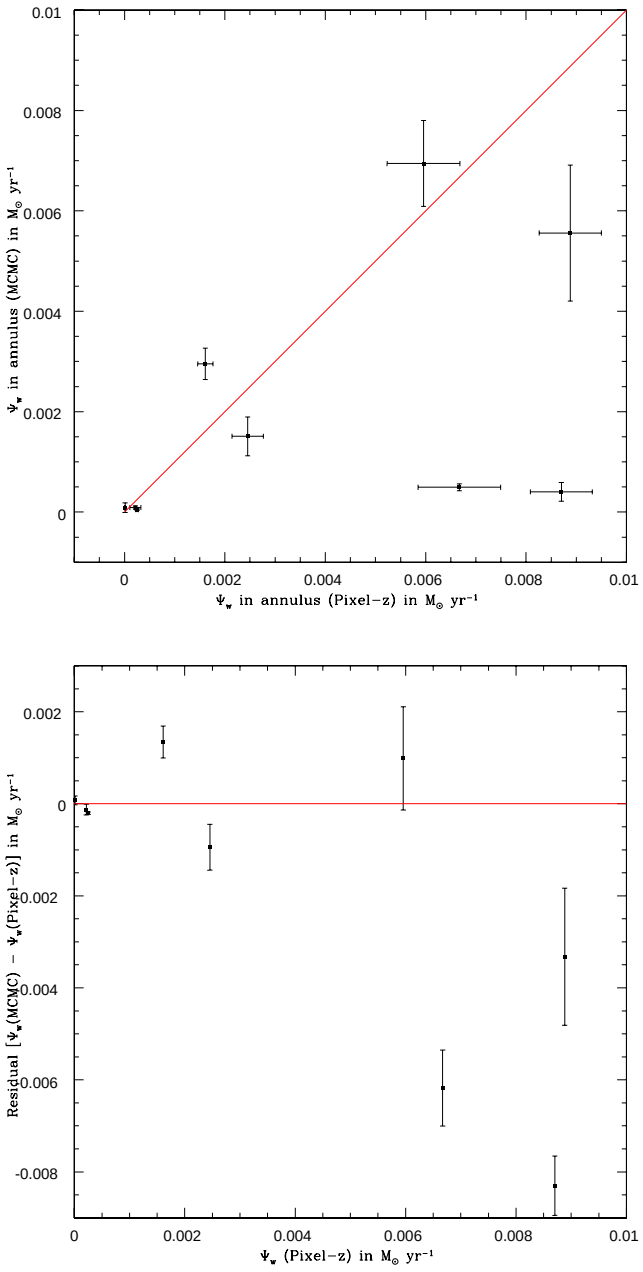

Figure 3.14: Top panel: A comparison of the estimated weighted mean SFR Ψ_w in the annulus $0.125 < r/R_p < 0.25$ in 9 galaxies which are obtained from two different methods: the pixel-z method (via template SED-fitting to the photometric u,g,r,i,z fluxes in the pixel and using χ^2 minimization to obtain the best-fit values of t and τ) and the Monte Carlo Markov Chain (MCMC) method that samples the full probability function. Bottom panel: The difference between the MCMC value of Ψ_w and the value obtained from the pixel-z method, as a function of the pixel-z measurement.

but beyond $0.0065\,M_{\odot}\,yr^{-1}$, the pixel-z based value of Ψ is increasingly overestimated relative to the MCMC value. At $\Psi_w = 0.009\,M_{\odot}\,yr^{-1}$, the offset is $0.008\,M_{\odot}\,yr^{-1}$.

The study, based on a very small number of galaxies, shows that the pixel-z measurement of mean SFR in annuli is generally consistent with the MCMC method that samples the full probability function, at least for values of mean SFR less than $0.0065\,M_{\odot}\,yr^{-1}$. Beyond that SFR, there is some suggestion that the pixel-z value becomes an increasing overestimate (relative to the MCMC value). This may thus affect the most highly star-forming systems. A larger sample of galaxies is needed to explore this offset further and possibly to apply it to make a correction to the measured values of Ψ_w in the radial annuli. This would be particularly interesting to do for those central annuli where we do detect a suppression of mean SFR due to an increasingly dense galaxy environment.

3.5 SUMMARY

Pixel-z is a useful technique for exploring spatially distributed galaxy properties, including the star formation rate. Although it has inherent limitations (described in this work), it can provide insights to direct more detailed exploration, and when applied to large samples, many of those limitations can be overcome. We draw several conclusions about the environmental dependence of spatially resolved galaxy star formation:

1. By summing the SFRs in individual pixels, a total SFR-density relation is established. The SFR-density relation measured from emission lines (Gómez et al. (2003), Lewis et al. (2002)) is confirmed based on SFRs inferred from SED template-fitting to pixel fluxes across five bands.

2. The total SFR-density relation is found to be independent of the morphological type of the galaxy. Therefore, the SFR-density relation for galaxies in the SDSS is not solely a result of having a larger fraction of early-type galaxies as we go to higher densities (the morphology-density relation). So there is indeed a SFR suppression in more dense environments.

3. Within galaxies, star formation, averaged over all morphological types and inclinations, is highest in a region spanning $0.125 < r/R_p < 0.5$, with the specific location of the peak dependent on local density. It is lower in both the nucleus and the outskirts than in the circumnuclear region. In denser environments, the low mean SFR in the nuclear regions appears lower still. The higher mean SFR in the circumnuclear region is also lessened in more dense regions, with the peak SFR moving towards larger radii. The SFR beyond $r/R_p \approx 0.25$ and in the outskirts of galaxies is not affected by a changing environment. It is thus a depression of SF in the innermost annuli that accounts for the dependence of total galaxy SFR on density. This suggests that quenching mechanisms such as ram-pressure stripping are not the sole driver of the observed SFR-density relation in galaxies.
4. When the sample is split based on the total SFR of galaxies, it is the highly star-forming systems that are found to be responsible for the dependence of radial SFR on local density. The low star-forming galaxies show little dependence of radial SFR on environment.

Although the density-morphology relation is seen to be independent of the total SFR-density relation, the relationship between the density-morphology relation and the radial result has yet to be explored. We know that in addition to the nuclear SF declining in more dense environments, the location of the SF peak within galaxies is shifted to larger radii at higher densities. Is this telling us that the signal from early-type galaxies is just becoming stronger as we go to higher densities because there is a higher proportion of early types in those environments? At lower densities, the nuclear SF is higher, so could this be due to a predominance of star-forming late-types which are known to reside in these low density environments? We know that by the "downsizing" argument, the more massive galaxies at high redshift form their stars early and rapidly. But these more massive systems tend also to be elliptical galaxies, so to some degree, the radial trend (and its dependence on density) for the full sample could still be a result of the density-morphology relation. To disentangle this, we wish to find out first what the radial SFR-density trends look like for each morphological type within our sample. Next, given these separate radial profiles, together with the fact that the proportion of early-type galaxies is expected to increase as we go to intervals of higher density, we wish to establish what the contribution of each type is to the radial SF-density relation for the full sample.

In the next chapter, we explore in the detail the effect of the density-morphology relation on the spatial distribution of star formation in galaxies.

4.0 EFFECT OF THE MORPHOLOGY-DENSITY RELATION

4.1 INTRODUCTION

In dense environments, for example in the cores of rich clusters, the galaxy population is dominated by early-types, as discussed in §1.3.3. In fact, the fraction of early-type galaxies has been shown to increase with increasing galaxy density (Dressler, 1980; Postman and Geller, 1984; Tran et al., 2001). The same physical mechanisms that are proposed to explain the relation between SFR and environment have also been proposed to explain the morphology-density relation as well. These mechanisms include ram pressure stripping of gas (Gunn and Gott, 1972), gravitational interactions between galaxies (Byrd and Valtonen, 1990), galaxy harassment via high-speed encounters (Moore et al., 1996) and galaxy mergers. However, little observational evidence exists to suggest that these processes drive the evolution in galaxies. On the theoretical front, the combination of semi-analytic models with N-body simulations of cluster formation has enabled the density-morphology relation to be simulated. Diaferio et al. (2001) derived the relation assuming that galaxy morphologies (determined in the simulation using a bulge-to-disc ratio) in clusters are solely determined by their merging histories. They found good agreement with data from the CNOC1 sample (Yee et al., 1996) for bulge-dominated galaxies. Benson et al. (2001) found that a strong density-morphology relation was established at $z = 1$ which was similar to that at $z = 0$ but their results suggested that more than one of the physical mechanisms mentioned above may have to be used to explain the relation.

In Chapter 3, I studied the spatial variation of SF within galaxies as a function of the galaxy environment, for 44 964 galaxies in the SDSS. I showed that the SFR in galaxies in high-density regions is suppressed compared to those in lower-density regions. I showed that

this suppression occurs in the innermost regions within galaxies ($r < 0.25R_p$ where R_p is the Petrosian radius). The study dealt with galaxies of all morphologies. I now aim to extend that investigation by focusing on the following three questions:

1. Do early-type and late-type galaxies, which have distinct radial light profiles, also have distinct radial distributions of SF? This may be associated with different formation mechanisms or evolutionary histories in either galaxy type.
2. Does any type-dependent change in the spatial distribution of SFR occur for all galaxies of that type uniformly? Or is it restricted to a sub-population, such as the highly star forming systems? In Chapter 3, we established that the suppression of SF seen in high density environments for the full sample is a consequence of suppression only in the highly star forming sub-population of the sample. We want to establish whether the trends in early-type and late-type galaxies separately are also dominated by this active sub-population.
3. Is the observed environmental dependence of SFR in galaxies a consequence of, or in addition to, the reduced average SFRs expected simply from the higher proportion of low star-forming early-types in high density environments?

We describe our method and approach in §4.2, and our results in §4.3. The implication of the results are discussed in §4.4, where we explore an evolutionary explanation for the observed trends. We present our conclusions in §3.5. We assume throughout that $\Omega_\Lambda = 0.7$, $\Omega_\mathrm{M} = 0.3$, and $H_0 = 75\,\mathrm{km\,s^{-1}\,Mpc^{-1}}$.

4.2 METHOD

We retain the same two morphological classes as in Chapter 3, as used also by Goto et al. (2003b), based on discriminating galaxies according to their inverse concentration index C_{in}. This is defined as the ratio of the Petrosian 90 percent light radius to the Petrosian 50 percent light radius. The selection results in 27 993 early-type galaxies ($C_{in} \leq 0.4$) and 16 971 late-type galaxies ($C_{in} > 0.4$) classified according to this parameter.

To establish that our results are not sensitive to, or biased by, this choice of morphology proxy, we duplicate our analysis using the Sersic index. The Sersic model for the surface brightness in a galaxy is given by $I(r) = I_0 e^{(-r/r_0)^{1/n}}$, where $I(r)$ is the intensity at an angular radius r, I_0 is the central intensity, r_0 is the characteristic radius and n the Sersic index or profile shape parameter. An exponential profile, which typically describes the light profile of late-type galaxies, is recovered with $n = 1$, while $n = 4$ gives the traditional de Vaucouleurs profile which is best fit to bulge-dominated, early-type systems. The Sersic index values calculated for the SDSS galaxies used in our sample have been corrected for the effects of seeing. In our analysis we classify galaxies with $n < 2$ as late-types and those with $n > 2$ as early-types.

4.3 RADIAL AND ENVIRONMENTAL TRENDS IN SFR

4.3.1 The Density-Morphology Relation

Figure 4.1 illustrates the density-morphology relation in this sample of SDSS galaxies. The proportion of early-type galaxies, with $C_{in} < 0.4$, is shown to be increasing as a function of local galaxy density. In the low-density environments, around 50 percent of galaxies are early-types, while in the highest density environments this increases to around 75 percent. The bottom panel gives the total number of galaxies found in each density interval. These plots sample the local galaxy density more finely than in the analysis described in Chapter 3 or in subsequent analyses herein, where only three intervals of local density are used. We use the results of the density-morphology relation below in §4.3.4 when assessing whether the observed suppression in SF can be recovered simply by mimicking this effect. Before we can do this, though, we need to establish the radial variation of SFR for each morphological type as a function of environment.

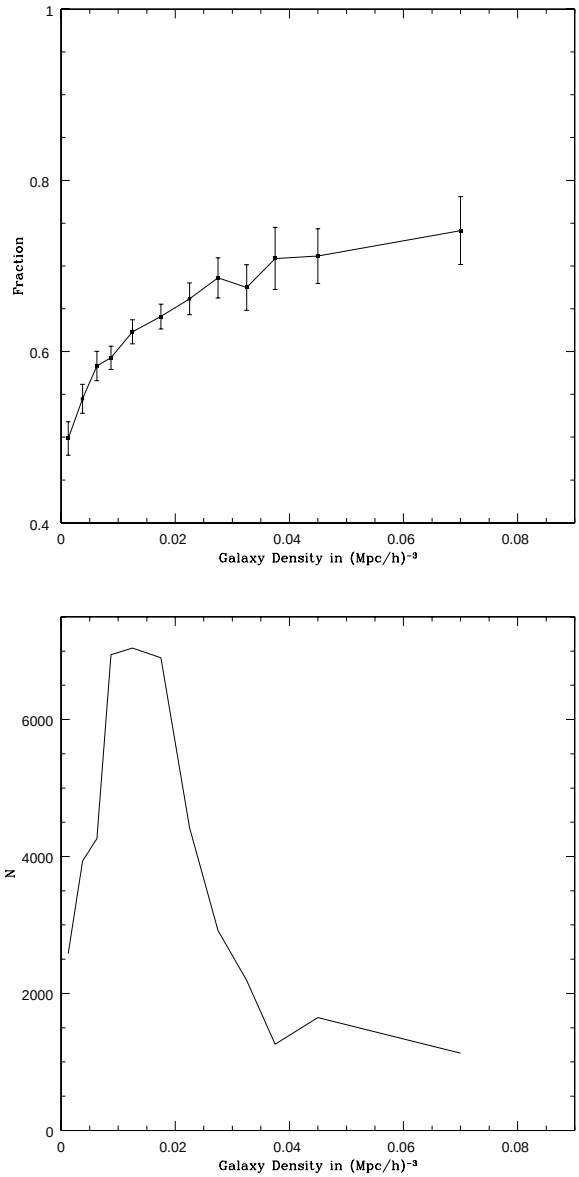

Figure 4.1: Top panel: The density-morphology relation, showing the fraction of early-type galaxies (with $C_{in} < 0.4$). Error bars are Poisson. Bottom panel: Number of galaxies in each interval of local galaxy density. The local galaxy density is sampled more finely in these bins that in the subsequent analysis in the paper, where only three intervals of local density are used.

4.3.2 Radial Variation of SFR as a Function of Environment

Here we examine the radial distribution of SFR in both early-type and late-type galaxies as a function of their environment for galaxies (a) spanning the entire range of (total) SFR and (b) within the highly star-forming population only.

We calculate the weighted mean SFR ψ_w for each radial annulus in every galaxy (see Chapter 3 for details). For a sample of galaxies this gives a distribution of ψ_w for each annulus. Figure 4.2 shows the 75th percentile of ψ_w for the early-types, late-types and for the full sample, within three intervals of galaxy density (corresponding to the three panels in the Figure). As shown in Chapter 3, the effect of environment is most pronounced for the 75th percentile of ψ_w, rather than the median of ψ_w. In determining the radial variation of SFR and its dependence on environment, we focus on the 75th percentile of ψ_w in this study.

Both early and late-type galaxies have distinct radial SFR profiles. This answers the first of the questions we posed above. The peak of ψ_w in early-types is significantly lower than in late-type galaxies. The SF in the center is very low, reflecting the fact that in early-type systems, which are typically bulge-dominated, the stellar populations in the center of the bulge are old and there is consequently little ongoing SF. In contrast, the stellar populations with higher SFR are further out in the bulge and the mean SF in this region is also better sampled. The early-type galaxies show a more extended distribution of SF which peaks further out in radius than in late-type galaxies. This reflects the fact that late-type galaxies have a smaller bulge compared to early-types.

In the late-types most of the SF takes places in the inner part of the disk, closer to the center. There is thus a very sharp increase in SFR as we go from the center ($r \leq 0.125\,R_p$) to the inner part of the disk ($r \approx 0.25\,R_p$) followed by a rapid decline in the SFR throughout the disk to the outskirts. Disk galaxies have, on average, a much higher SFR up to to $r \approx 0.25\,R_p$ (by as much as $0.014\,M_\odot\,\mathrm{yr}^{-1}$ in the lowest density environments and $0.012\,M_\odot\,\mathrm{yr}^{-1}$ in the highest density environments) than do the early-types. This reflects the younger star-forming stellar populations in the disks of these galaxies.

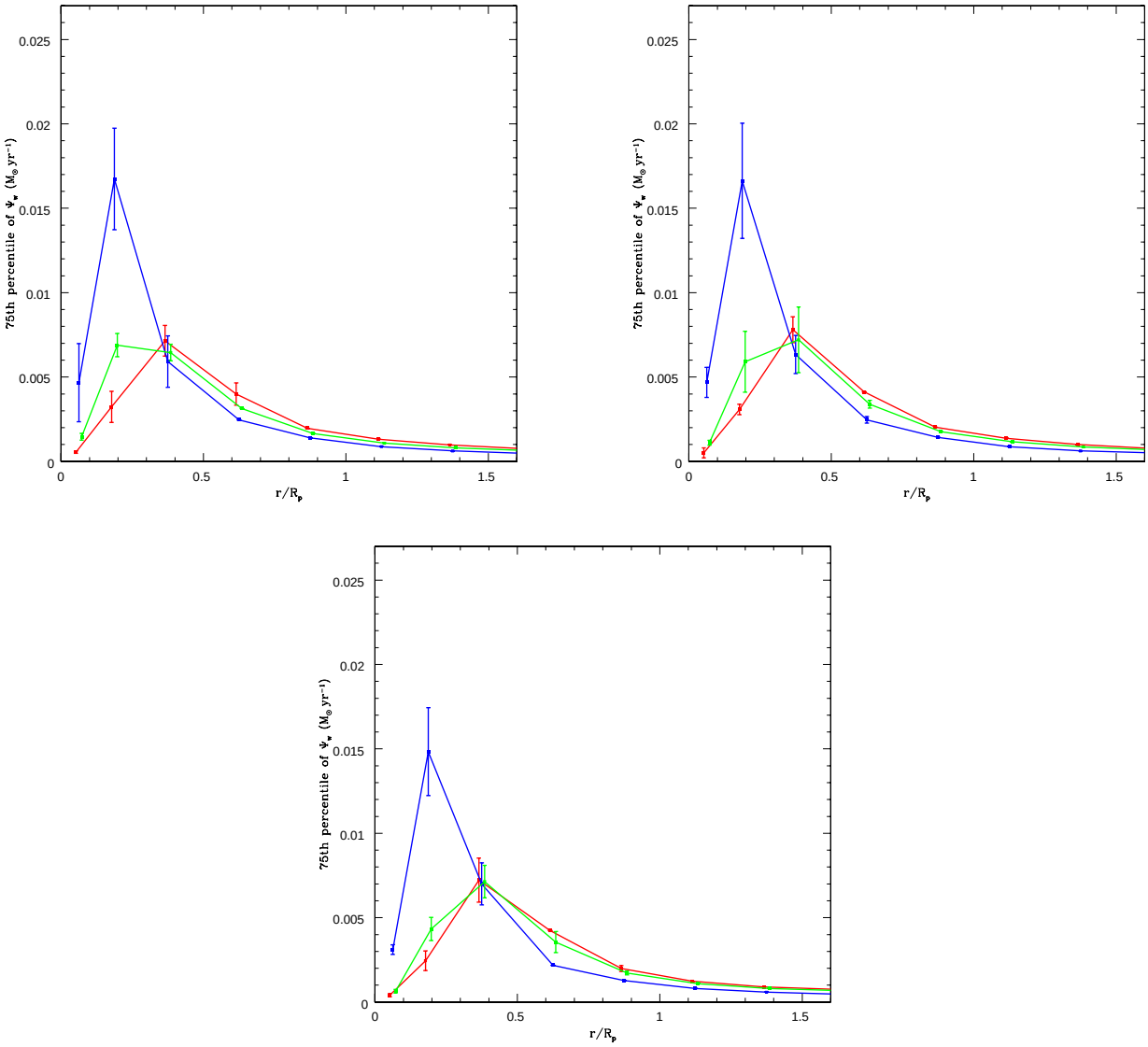

Figure 4.2: Top panel: 75th percentile of the distribution of weighted mean SFRs Ψ_w $(M_\odot\, yr^{-1})$ within successive radial annuli for early-type galaxies (red), late-type galaxies (blue), and all galaxies (green) which have local galaxy densities ρ in the range $0.0 < \rho \leq 0.01\,(h^{-1}\,Mpc)^{-3}$. Middle panel: $0.01 < \rho \leq 0.04\,(h^{-1}\,Mpc)^{-3}$. Bottom panel: $0.04 < \rho \leq 0.09\,(h^{-1}\,Mpc)^{-3}$. The three density intervals are the same as those used in Chapter 3, Figure 3.11.

4.3.3 The Significance of Highly Star Forming Galaxies

Figure 4.2 shows that the effect of the environment on the full sample of galaxies (early-types and late-types together, green curve) is to push the peak of the SFR profile to larger radii. A straightforward explanation in terms of the density-morphology relation presents itself, namely that at low densities there is almost an equal fraction of early and late-type galaxies, while at higher densities the profile is progressively more dominated by the higher contribution from early-types. It is important to note that while the shifting of the peak mean SFR in the full sample of galaxies can indeed be explained simply by the increasing fraction of early-type galaxies in higher density environments, there are other aspects of the density dependence that are not.

In Chapter 3, it was shown that the most significant decrease in the total SFR with increasing local galaxy density takes place for galaxies in the top quartile of the total SFR distribution. Here we explore the radial SFR profiles for the galaxies that are in the top and second quartile of the total SFR for each galaxy type, to identify whether the trends with environment are driven only by the most active star-forming galaxies. In §4.3.5, we also examine the proposal by Park et al. (2007) that the trends are instead driven primarily by luminosity, with the most luminous late-type galaxies having the highest SFRs.

We refer to the top quartile of the total SFR distribution, for both morphological types, as the "highest SF galaxies," and the second quartile as the "the next highest SF galaxies". We examine the distribution of ψ_w for these subpopulations for early and late-types separately, determining the quartiles of ψ_w of these distributions as above in the same intervals of local galaxy density. The results, as before, are most prominent in the 75th percentile of ψ_w (compared to the median or 25th percentile) and only radial trends for this quartile are shown.

The results of this analysis are presented in Figure 4.3, with the full sample spanning all SFRs shown for comparison in Figure 4.4. Figure 4.3 shows the 75th percentile of ψ_w for the highest and next highest SF galaxies for both galaxy types. In the early-type highest-SF galaxies there is a relatively small suppression (just under 1.5σ) in ψ_w between the least and most dense environments but only in the region $0.125 \leq r/R_p \leq 0.25$. We do not see a

significant effect of environment on the SFR in early-types in the center ($0.0 \leq r/R_p \leq 0.25$) or in the outskirts. In the next highest SF early-types, we do not detect a similar suppression in the SF, suggesting that this is a phenomena that affects only the most active early-type systems. In the highest-SF late-type galaxies, we detect a suppression of 3σ in the mean SFR in the center ($r/R_P \leq 0.125$) while there is no significant suppression of SF at other radii. In the next highest SF late-types, we find a slightly lower suppression in ψ_w of 2σ in the SFR in the center ($r/R_P \leq 0.125$), and again, no significant effect of the environment at other radii. The cores of late-type galaxies thus have their SF reduced in more dense environments while the SF in the remainder of the disk and outskirts is largely unaffected by a changing environment. Further, unlike the early-type systems, this affects a larger proportion of star-forming late-types. All late-types in the top two quartiles of the total SFR have their central SFR suppressed in the highest densities. In contrast, in the early-types, we detect a suppression only in galaxies in the highest quartile of the total SFR distribution.

Figure 4.4 shows the results of performing a similar analysis for the full sample of early and late-type galaxies, without making any cuts in total SFR. Neither galaxy type shows any statistically significant variation in the 75th percentile of ψ_w with environment at any radius when the full sample of galaxies of each type is considered. *The suppression of SF in the highest density environments is therefore driven by the most active, highly SF galaxies.* This answers the second of the questions posed above. It is also worth noting that, as found for the full sample in Chapter 3 when considering both morphological types together, the SFR in the outskirts of either the early or late-type galaxies is not affected by a changing environment. In fact, despite the relatively low values of ψ_w in the outskirts of the galaxies of either type, the signal-to-noise in the outskirts remains relatively high ($S/N \approx 10$) as long as the radius does not exceed $1.5R_p$.

The right-hand panels of Figure 4.4 also show the radial SFR profiles when the Sersic index is used as a proxy of galaxy morphology. It is clear that these results hold independent of the choice of inverse concentration index C_{in} or the Sersic index as the morphological proxy.

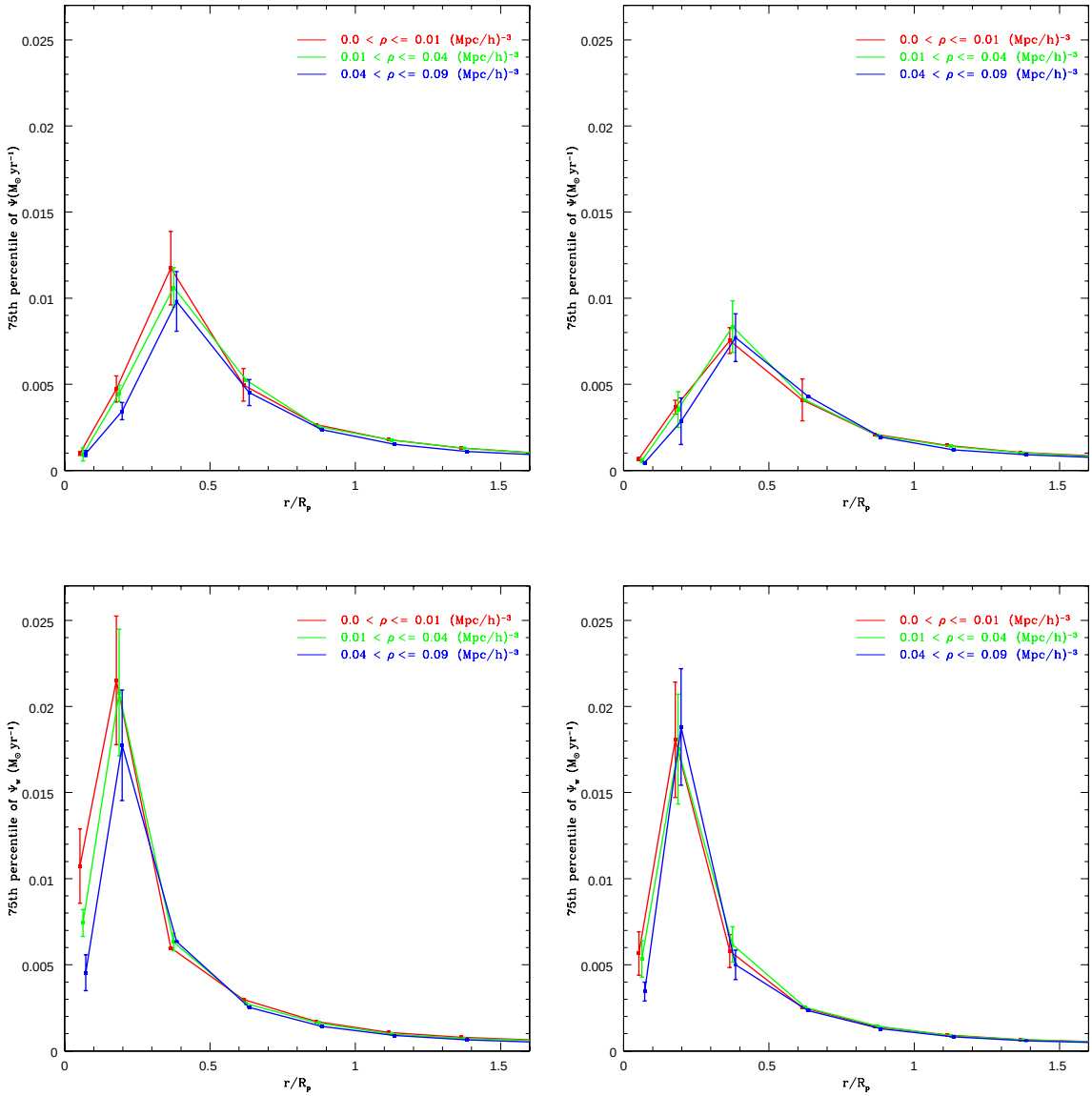

Figure 4.3: 75th percentile of the distribution of weighted mean SFRs Ψ_w $(M_\odot\, yr^{-1})$ within successive radial annuli as a function of the local galaxy density ρ for the highly SF populations of either galaxy type. The intervals of local galaxy density ρ considered are $0.0 < \rho \leq 0.01\,(h^{-1}\,Mpc)^{-3}$ (red), $0.01 < \rho \leq 0.04\,(h^{-1}\,Mpc)^{-3}$ (green), $0.04-0.09\,(h^{-1}\,Mpc)^{-3}$ (blue). Top left panel: For the early-type galaxies in the highest quartile of the total galaxy SFR ('the highest SF galaxies'). Top right panel: For early-type galaxies in the second highest quartile of the total galaxy SFR ('the next highest SF galaxies'). Bottom left panel: For the highest SF late-type galaxies. Bottom right panel: For the next highest SF late-type galaxies.

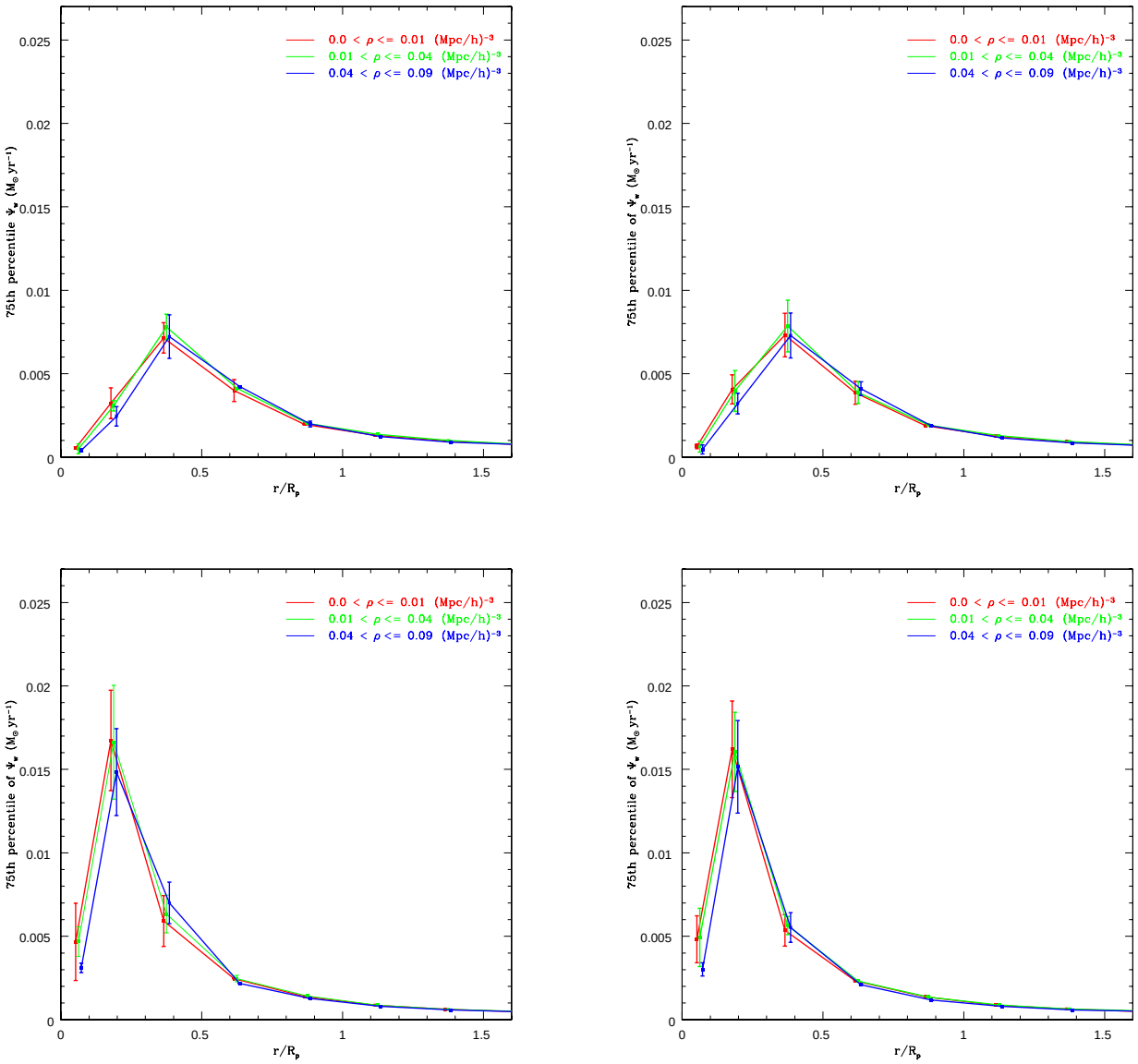

Figure 4.4: 75th percentile of the distribution of weighted mean SFRs Ψ_w $(M_\odot\, yr^{-1})$ within successive radial annuli as a function of the local galaxy density ρ for the full sample of galaxies of either type. No cuts in total SFR are made here. Top left panel: For all early-type galaxies chosen according to the concentration index ($C_{in} < 0.4$). Top right panel: For all early-type galaxies chosen according to the Sersic index ($n > 2$). Bottom left panel: late-type galaxies chosen using $C_{in} > 0.4$. Bottom right panel: late-type galaxies chosen using $n < 2$.

4.3.4 Can the density-morphology relation alone explain the suppression of star formation?

The results for the high SF populations of either galaxy type suggest that the suppression of SF is not due solely to the density-morphology relation. In order to determine definitively whether the suppression in SF is a result of the density-morphology relation or if another, perhaps evolutionary, mechanism is at work, we carry out a further test. We have determined the radial SFR profiles for the early and late-types in the lowest density environments, together with the fraction of early and late-types as a function of density. So we can now ask how the radial SFR profile for the full sample (all types) in the highest density environment compares with a profile constructed by combining the low-density profiles for each morphological type in the proportions appropriate to the high-density environment.

Let $\Psi(r,\rho)_E$ be the mean SFR profile of early-types at density ρ, $\Psi(r,\rho)_L$ the mean SFR profile of late-types at density ρ and $\Psi(r,\rho)_T$ the mean SFR profile of all types at density ρ. We will use ρ_1, ρ_2, ρ_3 to refer to the lowest, intermediate, and highest density environments respectively. Figure 4.5 shows the radial variation of $\Psi(r,\rho)_E$ and $\Psi(r,\rho)_L$. The high value of the mean, compared to the 75th percentile, reflects an underlying distribution of ψ_w that is skewed towards higher values of SFR. The trends in the mean reflect many of those observed with the 75th percentile in that there is little effect of environment on the outskirts of the galaxies of either type, but there is a more marked suppression in the mean of Ψ in the galaxy center in either type. This is true for both the highest SF galaxies and for the full sample of early and late-types (the mean being more sensitive to the high SFRs in the most active galaxies). For the highest SF late-types, there is a relatively high mean Ψ in the galaxy center ($r/R_p \leq 0.125$) and this is suppressed by about 2σ in the highest density environment ρ_3. In the highest SF early-type galaxies, there is a 2σ suppression in the first two inner annuli, up to $r \leq 0.25R_p$.

Suppose the suppression of SF is just due to the density-morphology relation, simply a higher fraction of early-types in high-density environments. We can use the individual SF profiles of early and late-type galaxies at low densities ρ_1 to determine what the profile for the composite sample would be at the highest densities ρ_3. To do this we take $\Psi(r,\rho_1)$ for early

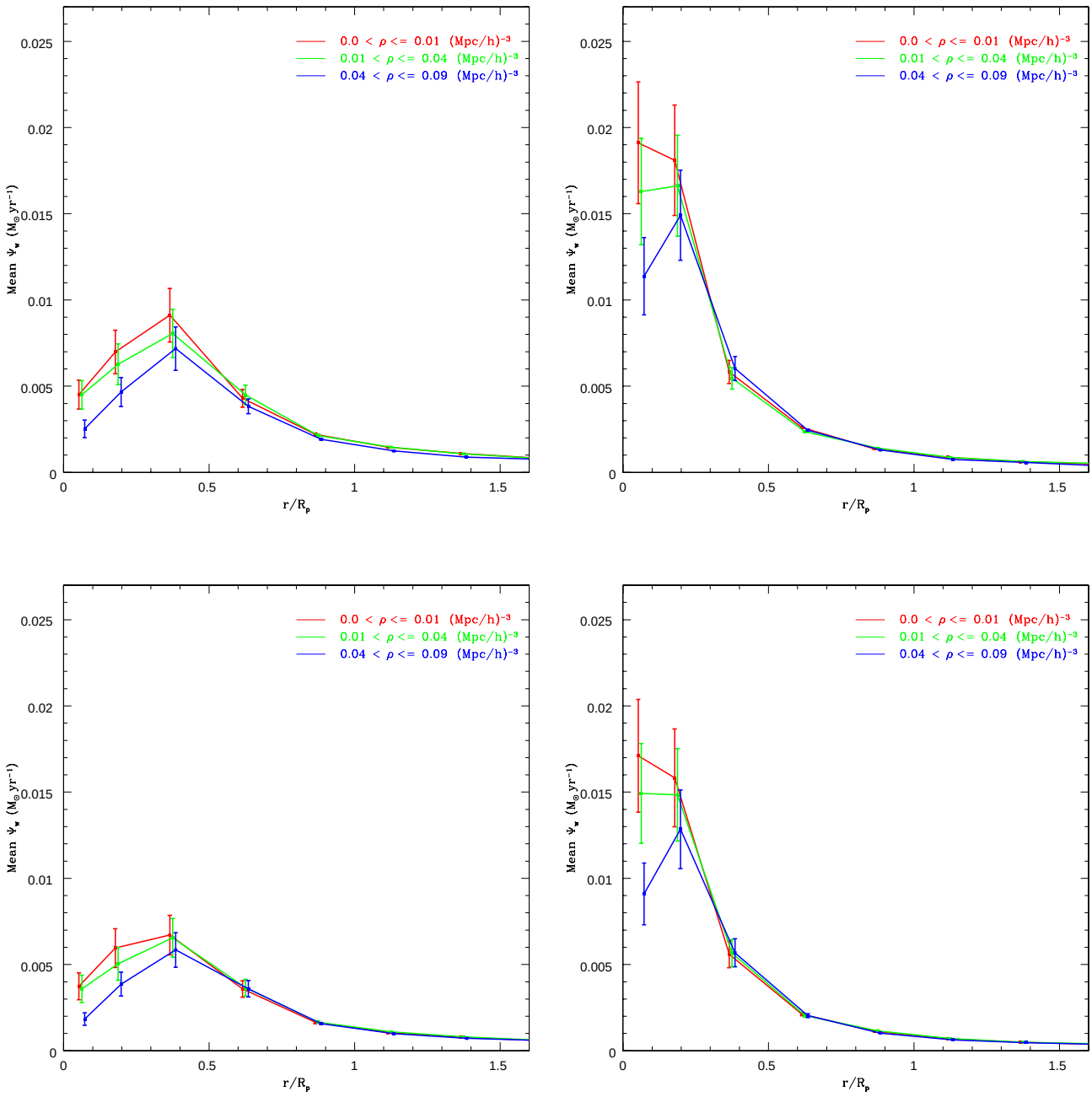

Figure 4.5: Mean of the distribution of weighted mean SFRs Ψ_w $(M_\odot\, yr^{-1})$ within successive radial annuli as a function of the local galaxy density ρ. Top left panel: For the highest SF early-type galaxies. Top right: For the highest-SF late-type galaxies. Bottom left panel: For all early-types in the full sample (no cuts in the total SFR are made). Top right panel: For all late-type galaxies in the full sample.

and late-types, explicitly assuming these remain the same within different environments, and average them, weighted by the relative proportion of early and late types at $\rho = \rho_3$. This produces an artificial composite profile at $\rho = \rho_3$ that reflects the profile expected if it arose solely from the density-morphology relation:

$$\Psi(r, \rho_3)_{\text{artificial}} = \frac{N_E}{N_E + N_L}(\rho_3) \times \Psi(r, \rho_1)_E + \frac{N_L}{N_E + N_L}(\rho_3) \times \Psi(r, \rho_1)_L. \tag{4.1}$$

We compare this artificial profile at $\rho = \rho_3$ to the one actually observed at $\rho = \rho_3$:

$$\Psi(r, \rho_3)_{\text{observed}} = \frac{N_E}{N_E + N_L}(\rho_3) \times \Psi(r, \rho_3)_E + \frac{N_L}{N_E + N_L}(\rho_3) \times \Psi(r, \rho_3)_L. \tag{4.2}$$

$\Psi(r, \rho_3)_{\text{observed}}$ is of course simply equal to $\Psi(r, \rho_3)_T$.

The result of this composite SFR profile is shown in Figure 4.6 for both the highest SF galaxies and for the full sample. The observed SFR profile in both cases is significantly below the artificial SFR profile, particularly in the innermost annulus $r \leq 0.125 R_p$ where there is a 2σ result. *This shows directly that the density-morphology relation alone cannot give rise to the observed suppression in SF in centers of galaxies in high density environments.* This answers the third of the questions we initially posed, but raises another. Since the effect is not due to the density-morphology relationship alone, what is the mechanism or mechanisms that drive the observed suppression in SF? Before addressing this, we briefly investigate the possibility that our results, which as we have shown are a consequence of the highest SF galaxies, are a simple consequence of higher SFRs in more luminous galaxies.

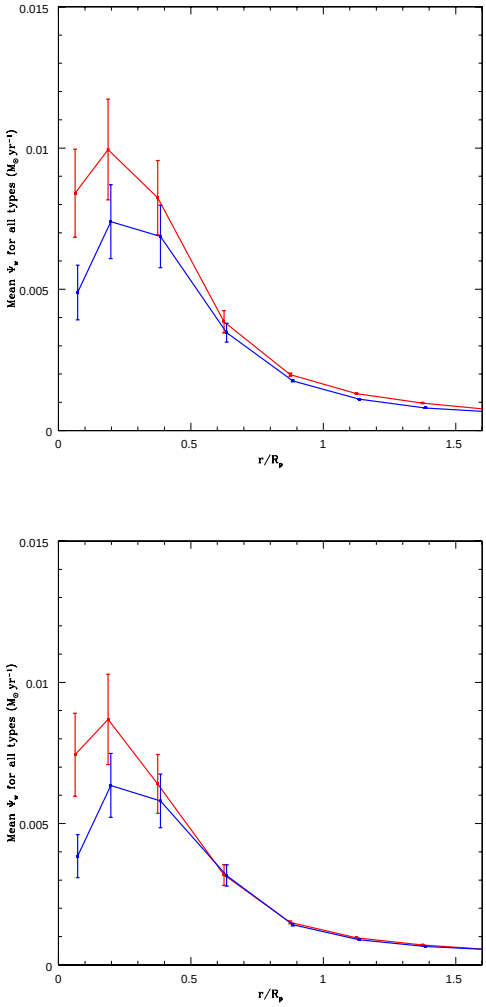

Figure 4.6: Testing how much the density-morphology relation is responsible for the observed dependence of SFR on galaxy density. The red line is the artificial composite SFR radial profile (for both early and late-types) in the highest density interval for the highest SF galaxies. The profile is obtained by using the SFR profile of the highest SF early and late-types in the lowest density interval and propagating this to the highest density environment using the density-morphology relation. This artificial composite profile then predicts what the SFR profile would look like in the highest density environment if the SFR-density relation was just due to the density-morphology relation alone. This profile can then be compared to the observed composite profile in the highest density environment (in blue). The bottom panel shows the composite artificial and observed SFR profiles for the full sample of galaxies (not just the highly star-forming ones).

4.3.5 The Effect of Luminosity

Here we investigate the effect of galaxy luminosity on the radial variation of SF and its dependence on environment. Park et al. (2007) studied the color gradients of galaxies brighter than $M_r = -18.5$ as a function of the local galaxy density in the SDSS. For early-type galaxies, they found no environmental dependence of the color gradient at a given absolute magnitude, and in addition found that the gradient is almost independent of the luminosity as well. They also found that for late-type galaxies which are bright, there is no dependence of the gradient on environment, while for fainter late-types, there is a weak dependence on environment - fainter galaxies were seen to become bluer at the outskirts (relative to the galaxy center) at low densities while the color gradient vanishes in high density environments. In order to determine if the luminosity of galaxies has some effect on the radial variation of SF and the way it depends on the galaxy environment, we split our galaxies into narrower intervals of absolute magnitude and examine the radial distribution of SF within the early and late-type galaxies in each interval, across the same range of densities. Absolute magnitudes are k-corrected according to Blanton et al. (2003a). The top panel of Figure 4.7 shows the SFR profiles (75th percentile of ψ_w) for early-type galaxies in the absolute magnitude intervals $-22.5 < M_r < -21.5$ and $-21.5 < M_r < -20.5$ respectively, and the bottom panel is for the late-type galaxies for the same absolute magnitude intervals. The general characteristics of the profiles for both types remain unchanged when we split our sample into these narrower intervals of luminosity. We detect no effect of the environment on the SF in the brighter sample but do recover the suppression of SF with increasing local density in the fainter sample.

For the brighter early-type galaxies we find no significant change in the variation of SF with galaxy density in either the center or outskirts of the galaxies, which is consistent with the findings of Park et al. (2007). But for the fainter early-type galaxies we do detect a suppression of SF at higher densities. There is a decrease of 2.5σ in $0.125 \leq r/R_p \leq 0.25$ between the lowest and highest local density intervals, while there is no change in the SFR with increasing density in the outskirts.

For the late-type galaxies, just as for the early-types, there is no change in the mean

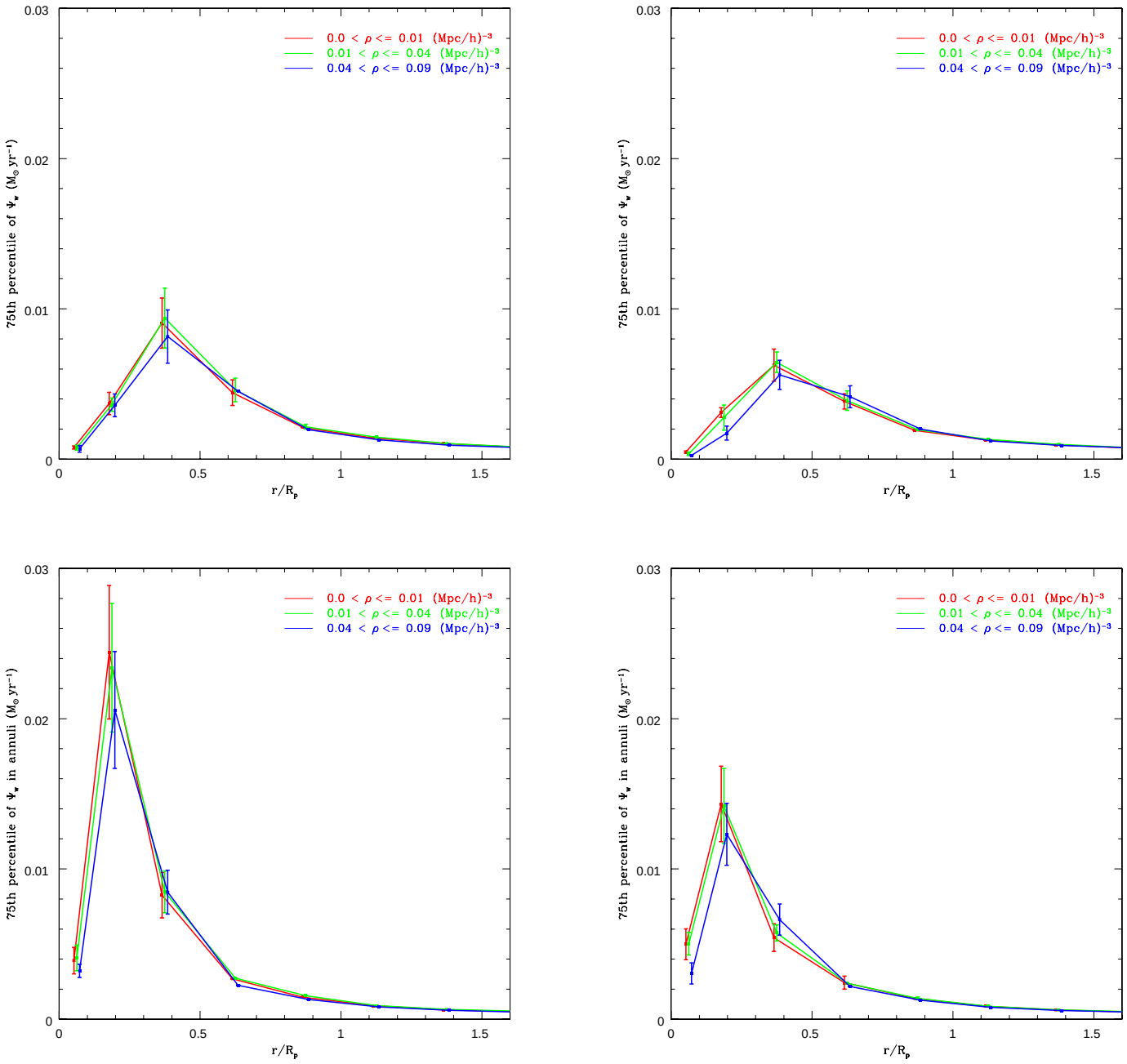

Figure 4.7: Top panel: 75th percentile of the distribution of weighted mean SFRs Ψ_w ($M_\odot\, yr^{-1}$) within successive radial annuli as a function of the local galaxy density ρ for early-type galaxies in our sample in intervals of absolute magnitude: $-22.5 < M_r < -21.5$ (top left) and $-21.5 < M_r < -20.5$ (top right). Bottom panel is for late-type galaxies for the same two absolute magnitude intervals.

SFR at any radius with environment for the brighter sample, which is consistent with the Park et al. (2007) result. For the fainter sample, there is a decrease in the mean SFR (approximately a 2σ difference) in the region $r/R_p \leq 0.125$, while the mean SF in the outskirts is again unchanged. Park et al. (2007) finds that at the highest densities, both the center and the outskirts become redder (giving zero color gradient). This is inconsistent with our findings which suggest that the suppression of SF in the faint late-types occurs only in the center.

There are some conclusions to be drawn here. First, there is no indication that our primary results are a direct consequence of a SFR-luminosity relation, since it is the fainter subsample that contributes primarily to the trends with environment that are observed. There remains the caveat that the sample selection was very different between the two groups: Park et al. (2007) classified galaxies based on their locations in u-r versus g-i color gradient space as well as concentration index space (Park and Choi, 2005) whereas we use concentration alone. Finally, the disparity between our results and those of Park et al. (2007) may be explained to some extent by the inclusion of dust obscuration in the pixel-z analysis. SFR gradients may be observed in the absence of color gradients, as the effect of dust will be to redden otherwise bluer star forming stellar populations.

4.4 DISCUSSION

The distinct radial SF profiles separate the two galaxy types cleanly. Early-types have a lower mean SFR throughout compared to the late-type galaxies. The environment is found to affect the highest SF early-type galaxies only while affecting the late-type galaxies in both the highest and second highest quartiles of their total SFR distribution. In the highest SF early-type galaxies, the suppression of SF takes place in $0.125 \leq r/R_p \leq 0.25$ while in the the late-type galaxies, the suppression takes place at $r/R_p \leq 0.125$. This suggest that the suppression of SF in these active galaxies of either type is independent of the established density-morphology relation.

It is worth noting that, as found for the full sample in Chapter 3, the outskirts of galaxies

in either the early or late-type galaxies are not affected by a changing environment. This implies that the outskirts of either type of galaxy are not significantly affected by processes such as ram-pressure stripping and galaxy harassment, processes which remove cold gas available for star formation, and which should primarily affect the outskirts of galaxies before they affect the inner regions. The lack of effect in the outskirts could alternatively be due to the fact that these processes affect only a small fraction of the population. The short timescales for the physical mechanisms of SFR quenching would also make them difficult for our method to detect as they will only be detectable for a small fraction of the sample at any given redshift (e.g., only a small fraction of galaxies will be undergoing ram-pressure stripping at the time of observation) and this will be hidden by our quartile sampling statistics. This is supported by the results of Doyle and Drinkwater (2006) who find a reduction in the *number* of galaxies with neutral hydrogen (HI) in high-density environments, but no significant trend with environment in the star formation rate or efficiency of star formation in HI galaxies. There is also the possibility that some of these processes could be taking place at much lower densities than we are probing.

The results of §4.3.4 suggest that the suppression of SF cannot be due to the density-morphology relation alone. Given that both physical "infall and quench" mechanisms and the density-morphology relation are unlikely to be the main mechanisms of SF suppression in either type of galaxy, we explain the trends observed by extending the "downsizing of SF" hypothesis laid out in §1.5 in terms of galaxy morphology.

As discussed in §1.5, downsizing is characterized by a decrease in the mass of galaxies that dominate the SFR density with increasing cosmic time, as was first suggested by Cowie et al. (1996). Heavens et al. (2004) observed that the most massive local galaxies seen in the SDSS also appear to be dominated by stars which formed at early epochs. Juneau et al. (2005) studied the cosmic SFR and its dependence on galaxy stellar mass in galaxies in the Gemini Deep Deep Survey (GDDS) and found that the SFR in the most massive galaxies ($M > 10^{10.8} M_{\odot}$) was 6 times higher at $z = 2$ than at present and that the SFR at $z = 2$ falls sharply to reach its present ($z = 0$) value by $z \approx 1$. Mobasher et al. (2008) used a mass-selected sample of 66 544 galaxies with photometric redshifts from the Cosmic Evolution Survey (COSMOS) to study the evolution of star formation activity as a function of stellar

mass in galaxies over the redshift range $0.2 < z < 1.2$. They found that the SFR is a strong function of stellar mass at any given redshift. They then combined this data with galaxies from the GDDS, thereby extending the cosmic SFR density (SFRD)-redshift relation as a function of stellar mass to $z \approx 2$. For massive systems, they found a steep increase in the SFRD-z relation to $z \approx 2$, while for less massive systems, the SFRD which also increases from $z = 0$ to $z \approx 1$, levels off at $z \approx 1$. This implies that massive systems had most of their star formation activity occur at earlier epochs ($z > 2$) compared to less massive systems. Panter et al. (2004) found no evolution in the stellar mass function of galaxies in the SDSS in the redshift range $0.05 \leq z \leq 0.34$ indicating that almost all stars were formed at $z \approx 0.34$ with little SF activity since then. In a radio-selected survey, Seymour et al. (2008) also determined that the majority of the observed SF occurs in the highest mass galaxies at high redshift, then moving to lower mass galaxies at lower redshifts.

To interpret our results we consider a population of galaxies that is active and highly star forming at high redshifts. Some of these become early-type galaxies and include in particular the most massive systems that form within the more massive dark-matter halos in dense environments. As the SF, in the "downsizing" scenario, is progressively associated with less massive galaxies in lower-mass halos and less dense environments, the SF moves from being dominant in cluster regions at high redshift to being dominant in low-density regions at low redshifts. This explains the density-morphology relation – at low redshift, there is a predominance of passive early-type galaxies with little SF, residing in clusters. To explain the central suppression of SF in the high-SF galaxies, we consider that bulges within late-type galaxies may form and evolve similarly to early-type galaxies (Driver et al., 2007). This will result in late-type galaxies in high-density environments having bulges that formed the bulk of their stars earlier than similar late-types in lower-density environments. These will consequently show the same kind of reduced current SF, purely as a consequence of their rapid early evolution, compared to late-types in lower-density environments. This is also consistent with the observed reduction in the SFR of early-types in high-density environments.

A natural consequence of downsizing in galaxies would be that the SFR-density relation should invert at higher redshifts, with increased SFR in the more dense environments. This

has been measured by Elbaz et al. (2007) using data from the Great Observatories Origins Deep Survey (GOODS) at $z \approx 1$. They found that the SFR-density relation observed locally was reversed at $z \approx 1$, with the average SFR of galaxies increasing with increasing local density. This adds additional support to the interpretation of our observed SFR suppression at low redshifts in terms of the downsizing in galaxies.

Reproducing the radial SFR profiles and their density dependence may require some addition to current models. It has recently been shown (Neistein et al., 2006) that downsizing could be a natural outcome of hierarchical structure formation if mass assembly and star formation are treated as distinct processes that proceed in opposite directions, and if a characteristic mass for SF truncation is introduced. Stars can form first in the small building blocks of today's massive galaxies. If gas processes limit galaxy formation to dark matter halos above a minimum mass, a certain downsizing arises naturally from the mass assembly process itself. Cattaneo et al. (2008) who studied the origin of downsizing of elliptical galaxies using the mean stellar ages of galaxies, showed that this could result naturally from a shutdown of star formation in dark matter halos above a critical mass of $10^{12} M_{\odot}$. Above this mass there is stable shock heating which truncates the star formation.

Our observations could well be driven by the downsizing of SF together with a treatment of late-type galaxy bulges in a similar fashion to those of early-type galaxies, resulting in the observed central suppression of SF in high density environments. More work needs to be done on the theoretical front, however, if the observed dependence of radial SF on environment is to be reproduced in the models.

4.5 THE POST-STARBURST POPULATION

In a visual inspection of a randomly selected sample of galaxies (of both types), we observe a very small number of red disk galaxies in both the field and cluster environments. Some of these could well be candidates for the elusive post-starburst ("K+A") population – galaxies that have undergone a recent burst of star formation, followed by relative quiescence. The spectrum of these galaxies are characterized by a strong H_δ absorption line. Post-starburst galaxies have recently been detected in both the SDSS and in the DEEP2 Galaxy Redshift Survey primarily in low density environments (in the field). They were identified in the SDSS by Goto et al. (2003a) and Quintero et al. (2004) and in both the SDSS and DEEP2 by Yan et al. (2008). As a first step towards possibly identifying this population with a view to determining if it has a contribution to the radial SF-environment relation, we examine the distribution of the equivalent width (EW) of H_δ. This line indicates that the spectral energy distribution of a galaxy is dominated by A stars. In fact, strong H_δ absorption is consistent with models of galaxy evolution that include a recent burst of star formation followed by passive evolution (any on-going star formation would hide the H_δ absorption line due to emission-filling of the line and the dominance of hot O and B stars which have weaker H_δ absorption compared to A stars (Balogh et al., 1999; Poggianti et al., 1999)). The exact mechanism by which the star formation history changes abruptly remains unclear.

Goto et al. (2003b) selected a sample of 3340 galaxies from the SDSS based solely on the observed strength of their H_δ line. More recently, post-starburst galaxies have been selected based on the excess A/K ratio relative to the H_α EW (Quintero et al., 2004; Hogg et al., 2006), where the A/K ratio is found by fitting a linear sum of an average old stellar population spectrum (K) and an average A star spectrum (A) to the galaxy spectrum. The post-starburst population appears to be bulge-dominated, but bluer and with higher surface brightness than normal bulge-dominated galaxies. The post-starburst population was found to lie predominantly in the field, and not in the cluster regions which are mostly populated by bulge-dominated (early-type) galaxies. Other studies have used cuts in the fraction of A stars and the H_α or H_β EWs to select the post-starburst population (Yan et al., 2008).

In this work, we chose the H_δ absorption line EW and examine its distribution across

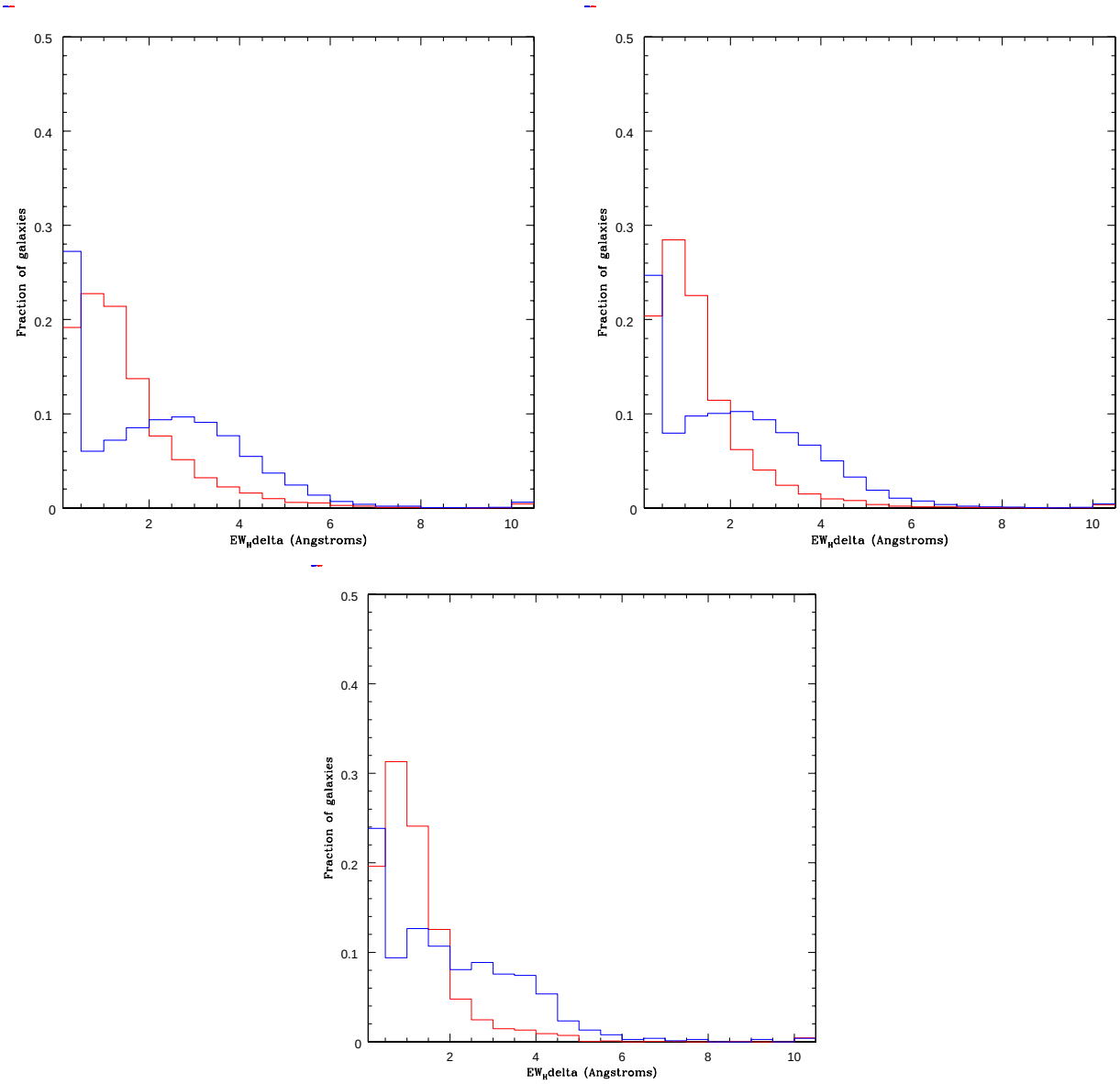

Figure 4.8: The distribution of equivalent widths for the H_δ absorption line for early-type (red) and late-type galaxies (blue) in the sample, in different environments. The three panels are for three different galaxy density intervals: Top left panel: $0.0 < \rho \leq 0.01\,(h^{-1}\,Mpc)^{-3}$. Top right: $0.01 < \rho \leq 0.04\,(h^{-1}\,Mpc)^{-3}$. Bottom panel: $0.04 < \rho \leq 0.09\,(h^{-1}\,Mpc)^{-3}$.

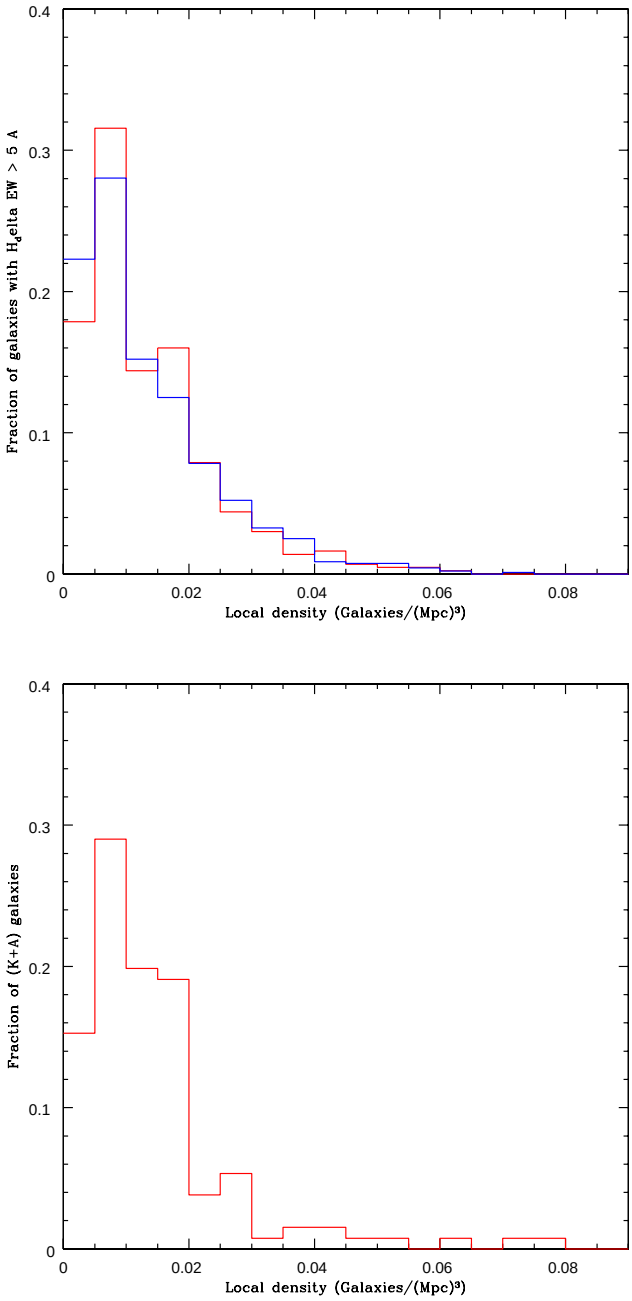

Figure 4.9: Top panel: The distribution of local galaxy densities for confirmed post-starburst galaxies (those with $H_\delta > 5A$) for early-type (red) and late-type (blue) galaxies. Bottom panel: the distribution of galaxy densities for post-starbursts (both early and late-types) from the Yan et al. catalog that are also found in this sample.

different intervals of local density for both early-type and late-type galaxies. Goto et al. (2003b) made a careful analysis, comparing different methods of measuring the H_δ absorption lines and studying the effect of stellar absorption, dust extinction and emission-filling in their measurements. In our study, we wish to see if the distribution of the H_δ EW (1) is different for early-type galaxies as it is for late-type galaxies and (2) changes with galaxy density. Figure 4.8 shows our results.

We find that the distributions of early-type galaxies and late-type galaxies are indeed very different, with the H_δ distribution for early-type galaxies peaking at low H_δ EWs, while the late-type H_δ EW distribution has a longer tail at higher EWs. For $EW > 5\mathring{A}$ though – the criteria used by Goto et al. (2003b) to select post-starburst candidates – there is a very small fraction of either type. The environment has little impact on the distributions, except that that there is a slightly higher fraction of early-type galaxies with low H_δ at high densities, while the late-type fraction with low H_δ decreases slightly.

Figure 4.9 demonstrates how the proportion of H_δ-selected post-starburst galaxies (those with strong H_δ absorption, $EW > 5\mathring{A}$) changes with environment. We see that in the case of both early-type and late-type galaxies, the post-starburst population is confirmed as being a low-density phenomenon, and not prevalent in the cluster environments. The result that the population is largely present in the field was confirmed independently with a population of ~ 150 post-starburst galaxies in the SDSS, selected based on cuts in f_A (the fraction of A stars) and the H_β EW, by Yan et al. (2008). A more detailed study of this post-starburst population in the SDSS and the spatial variation of SF within its galaxies, as well as the environmental dependence of this spatial variation, is a subject of future work.

4.6 SUMMARY

Here we divide SDSS galaxies by morphology in order to study the role of the density-morphology relation on the spatially resolved SF in galaxies. A density-morphology relation is quantified for our volume-limited galaxy sample. We find that a suppression of SF occurs in the most active and highly star-forming systems in the highest density environments for both broad galaxy morphological types. Neither "infall and quench" mechanisms nor the density-morphology relation appear to account for the observed suppression of SF in either early or late-type galaxies. The results are consistent with the picture of "downsizing" in galaxy formation, together with the idea that late-type galaxy bulges form and evolve in the same fashion as early-type galaxies, leading to a lower SFR in high-density environments.

In particular, we observe the following:

- Early and late-type galaxies in the SDSS have distinct spatial variations of SF, with early types having a SFR distribution that extends further (relative to the galaxy scale length) compared to late-type galaxies.
- A suppression of SF occurs in the most active and highly star-forming systems in the highest density environments for either galaxy type. The suppression takes place in the innermost regions of the galaxies, occurring at $0.125 < r/R_p < 0.25$ for early-type galaxies and $r/R_p < 0.125$ for late-type galaxies. No suppression of SF is detected in the outskirts of galaxies of either type.
- In early-type galaxies, only those in the top quartile of the total SFR distribution (SFR $> 0.45\,\mathrm{M}_\odot\,\mathrm{yr}^{-1}$) show any significant SF suppression in cluster environments. In late-types galaxies, there is a much larger range of total SFR in these galaxies (the top two quartiles) where a suppression of SF is observed.
- We find no significant environmental dependence when considering the full sample of early-type and late-type galaxies, indicating that the trends with environment are driven by the highly star-forming galaxies.
- The suppression of SF is seen primarily in lower-luminosity galaxies ($-21.5 < M_r < -20.5$) in our sample, while we detect no environmental dependence on the radial distribution of SF for brighter galaxies.

- By appropriately weighting the average SFR profiles of early-type and late-type galaxies in low-density regions by the proportions of these types found at high densities, we show that the density-morphology relation alone cannot account for the suppression of SF in the highest density environments.

In future work we will probe whether the "downsizing" of star formation in galaxy bulges is indeed responsible for our observed trends by exploring these trends as a function of stellar mass, together with the local density. Since "downsizing" is concerned with the mass dependence of the SFR history of galaxies, this will allow for a more detailed exploration of the origins and likely evolution of the observed variation in the spatially resolved SF in galaxies.

5.0 CONCLUSIONS

This work explores the complex relationship between galaxy properties and their environment. We focus in particular on the role of star formation in galaxies. By studying how the star formation varies with the galaxy environment, we aim to determine whether it is indeed the physical "infall and quench" processes – ram-pressure stripping, galaxy harassment, mergers etc. – that shape the properties of galaxies or whether there exists some other means by which those galaxy properties are determined. Despite some agreement between theoretical predictions for hierarchical structure formation and the observed correlations between galaxy properties (such as luminosity, color and SFR) and their environment, there exists little empirical evidence that any of the "infall and quench" processes are actually responsible for driving trends in galaxy evolution.

An alternative scenario to the "infall and quench" models is that galaxies evolve primarily because of their intrinsic properties, such as mass. These properties can still be shaped by the galaxy environment – indeed we know that more massive galaxies reside preferentially in more dense environments (Dressler, 1980; Postman and Geller, 1984)– but not through these strong physical interactions that galaxies suffer. We refer to this latter scenario as "environmentally-governed evolution". Their already exists observational evidence for such an evolution – this has been termed "downsizing" (Cowie et al., 1996). In this scenario, more massive galaxies (which form in more dense environments in the Universe) form their stars early and then undergo passive evolution, while less massive galaxies form their stars later but over a longer period of time. This would also explain the observed SFR-environment relation observed locally in galaxies.

The two scenarios should affect the spatial distribution of star formation within galaxies, in different ways. "Infall and quench" mechanisms should affect the outskirts of galaxies

before they affect the interiors. This suggests that galaxies in dense environments should show a SFR distribution that is progressively suppressed from the outside in, as the outer regions are those which will be affected first by their rapidly changing environment. The "environmentally-governed evolution" scenario makes a different prediction, suggesting instead that the suppression should either happen uniformly as a galaxy ages, or that the inner regions should be suppressed first. Thus by studying the spatial distribution of SFR in star-forming galaxies as a function of environment, we aim to distinguish clearly between these two scenarios.

We use the "pixel-z" technique to explore spatially distributed galaxy properties, including the SFR. The technique combines stellar population synthesis models with photometric redshift template-fitting on the scale of individual pixels in multi-band galaxy images. Over 2000 spectral energy distributions (SEDs) are constructed, sampling a wide range of properties of the underlying stellar populations, such as SFR, dust obscuration and metallicity. The SEDs are redshifted and convolved with the photometric filters of the detector. The SED fluxes are then compared to the observed fluxes through each pixel in each of the passbands. In this method, however, we fix the redshift of the pixel (which is known since the redshift of the host galaxy is known) and fit for the spectral type only. The best-fit SED is then returned for every pixel within the galaxy. This allows the properties of the stellar populations in that pixel to be determined. We also calculate an associated uncertainty in each of these parameters that arises from the fit. In an initial application to galaxies in the Hubble Deep Field, we showed that the technique allows us to connect features of the galaxy morphology (such as the presence of spiral arms or knots of star formation) with physical properties (such as the age of the stellar populations, the timescale of star formation decline, the dust obscuration and metallicity).

We then apply the technique to a large sample of galaxies in the SDSS, being primarily focused on the star formation within the pixels. Since the method enables a spatial resolution of the star formation distribution *within* galaxies, we can now explore how the SFR of each galaxy – both total SFR and the spatial distribution of SFR within galaxies – varies as a function of the galaxy environment. We draw several conclusions about the environmental dependence of spatially resolved galaxy star formation.

By summing the SFRs in individual pixels, a total SFR-density relation is established. The SFR-density relation measured from emission lines (Gómez et al. (2003), Lewis et al. (2002)) is confirmed based on SFRs inferred from SED template-fitting to pixel fluxes across five bands. The total SFR-density relation is found to be independent of morphological type of the galaxy. Therefore, the SFR-density relation of galaxies in the SDSS is not solely a result of having a larger fraction of early types as we go to higher densities (the morphology-density relation). So there is indeed a SFR suppression in more dense environments.

Within galaxies, star formation, averaged over all morphological types and inclinations, is highest in a region spanning $0.125 < r/R_p < 0.5$, with the specific location of the peak dependent on local density. Star formation is lower in both the innermost region $0 < r/R_p < 0.125$ and in the outskirts than in the region $0.125 < r/R_p < 0.5$. In denser environments, the low mean SFR in the innermost regions is further decreased. The higher mean SFR in the region $0.125 < r/R_p < 0.25$ is also lessened in more dense regions. The SFR beyond $r/R_p \approx 0.25$ and in the outskirts of galaxies is not affected by a changing environment. It is thus a depression of SF in the innermost annuli that accounts for the dependence of total galaxy SFR on density. This suggests that quenching mechanisms such as ram-pressure stripping are not the sole drivers of the observed SFR-density relation in galaxies. When the sample is split based on the total SFR of galaxies, it is the highly star-forming systems that are found to be responsible for the dependence of radial SFR on local density. The low star-forming galaxies show little dependence of radial SFR on environment.

Next, we explore in the detail the effect of the density-morphology relation on the spatial distribution of star formation in galaxies. We divide SDSS galaxies using the concentration index as a proxy for morphology. A density-morphology relation is quantified for our volume-limited galaxy sample. We find that a suppression of SF occurs in the most active and highly star-forming systems in the highest density environments for both broad galaxy morphological types. We find that neither "infall and quench" mechanisms nor the density-morphology relation by themselves can account for this observed suppression of SF in either early or late-type galaxies. The results are consistent with the picture of "downsizing" in galaxy formation, together with the idea that late-type galaxy bulges form and evolve in the same fashion as early-type galaxies, leading to a lower SFR in high-density environments.

In particular, we find that early and late-type galaxies in the SDSS have distinct spatial variation of SF, with early types having a SFR distribution that extends further (relative to the galaxy scale length) compared to late-type galaxies. A suppression of SF occurs in the most active and highly star-forming systems in the highest density environments for either galaxy type. The suppression takes place in the innermost regions of the galaxies, occurring at $0.125 < r/R_p < 0.25$ for early-type galaxies and $r/R_p < 0.125$ for late-type galaxies. No suppression of SF is detected in the outskirts of galaxies of either type. In early-type galaxies, only those in the top quartile of the total SFR distribution ($\mathrm{SFR} > 0.45\,\mathrm{M}_\odot\,\mathrm{yr}^{-1}$) show any significant SF suppression in cluster environments. In late-types galaxies, we find a broader range of total SFR where there is an effect of the environment. We find no significant environmental dependence when considering the full sample of early and late-type galaxies, indicating that the trends with environment are driven by these highly star-forming galaxies. The suppression of SF is also seen primarily in lower-luminosity galaxies ($-21.5 < M_r < -20.5$) in our sample, while we detect no environmental dependence on the radial distribution of SF for brighter galaxies.

It is worth noting that the lack of effect on the outskirts of galaxies suggests that "infall and quench" mechanisms are not the dominant mechanism by which star formation is suppressed in more density environments. It is important to note that we cannot rule out their contribution, however small, by this analysis alone. The lack of effect in the outskirts could alternatively be due to the fact that these processes affect only a small fraction of the population. The short timescales for the physical mechanisms of SFR quenching would also make them difficult for our method to detect as they will only be detectable for a small fraction of the sample at any given redshift, and this will be hidden by our quartile sampling statistics. There is also the possibility that some of these processes could be taking place at much lower densities than we are probing.

By appropriately weighting the average SFR profiles of early and late-type galaxies in low-density regions by the proportions of these types found in high-densities, we show that the density-morphology relation alone cannot account for the suppression of SF in the highest density environments. That would imply that both physical "infall and quench" mechanisms and the density-morphology relation are ruled out as the *dominant* means of SF suppression

in either type of galaxy, given the caveats mentioned above. We can then explain the trends observed by extending the "downsizing of SF" hypothesis laid out earlier in terms of galaxy morphology.

To interpret our results we consider a population of galaxies that is active and highly star forming at high redshift. Some of these will eventually become early-type galaxies – a proportion of these will be massive ellipticals that form within the more massive dark-matter halos in dense environments and still have some ongoing SF. As the SF, in the "downsizing" scenario, is progressively associated with less massive galaxies in lower-mass halos and less dense environments, the SF in these early-type galaxies moves from being dominant in cluster regions at high redshift to being dominant in low-density regions at low redshifts. This would result in a predominance of low star-forming early-type systems in clusters and thereby explain the density-morphology relation. To explain the radial dependence of SF with environment – the central suppression of SF in the high-SF galaxies – we consider that bulges within late-type galaxies may form and evolve similarly to early-type galaxies (Driver et al., 2007). This will result in late-type galaxies in high-density environments having bulges that formed the bulk of their stars earlier than similar late-types in lower-density environments. These will consequently show the same kind of reduced current SF (at low redshifts), purely as a consequence of their rapid early evolution, compared to late-types in lower-density environments. This is also consistent with the observed reduction in the SFR of early-types in high-density environments.

Our observations could well be driven by the downsizing of SF together with a treatment of late-type galaxy bulges in a similar fashion to early-type galaxies, resulting in the observed central suppression of SF in both types in high density environments. However, more work needs to be done on the theoretical front if the observed dependence of radial SF with environment is to be reproduced in the models.

There is a final "quench mechanism" which could influence the interpretation of the results. It could also be possible that this SFR suppression in galaxy cores may be a consequence of feedback from an active galactic nucleus (AGN). In particular, if AGN feedback in more massive systems is more efficient than in lower mass systems, and since dense environments are known to host more massive galaxies on average (Dressler, 1980; Postman and

Geller, 1984) this could perhaps lead to preferential suppression of central star formation in more dense environments. This can be probed by looking for AGN activity in the spectra of SDSS galaxies. The mechanism could be explored further by looking into the mass dependence of the SFR suppression in galaxies, although this was beyond the scope of the current analysis. The radius out to which such a feedback mechanism could suppress SF also needs to be quantified.

I summarize the main findings of this dissertation below.

- A total SFR-density relation is established. The SFR-density relation measured from emission lines is confirmed based on SFRs inferred from SED template-fitting to pixel fluxes across five bands.
- The total SFR-density relation is found to be independent of the morphological type of the galaxy.
- Within galaxies, star formation, averaged over all morphological types and inclinations, is highest in a region spanning $0.125 < r/R_p < 0.5$, with the specific location of the peak dependent on the local density.
- In denser environments, the low mean SFR in the nuclear regions appears lower still. The higher mean SFR in the circumnuclear region is also lessened in more dense regions, with the peak SFR moving towards larger radii.
- The SFR in the outskirts of galaxies is not affected by a changing environment. It is thus a depression of SF in the innermost annuli that accounts for the dependence of total galaxy SFR on density. This suggests that "infall and quench" processes are not the sole mechanism of SFR suppression in dense environments.
- It is the highly star-forming systems that are responsible for the dependence of radial SFR on environment while the low star-forming galaxies show little dependence of radial SFR on environment.
- Early and late-type galaxies in the SDSS have distinct spatial variations of SF, with early types having a SFR distribution that extends further (relative to the galaxy scale length) compared to late-type galaxies.
- A suppression of SF occurs in the most active and highly star-forming systems in the highest density environments for either galaxy type. The suppression takes place in

the innermost regions of the galaxies, occurring at $0.125 < r/R_p < 0.25$ for early-type galaxies and $r/R_p < 0.125$ for late-type galaxies. No suppression of SF is detected in the outskirts of galaxies of either type.

- We find no significant environmental dependence when considering the full sample of early and late-type galaxies, indicating that the trends with environment are driven by the highly star-forming galaxies.
- The suppression of SF is seen primarily in lower-luminosity galaxies in the sample, while we detect no environmental dependence of the radial distribution of SF for brighter galaxies.
- By appropriately weighting the average SFR profiles of early and late-type galaxies in low-density regions by the proportions of these types found in high densities, we show that the density-morphology relation alone cannot account for the suppression of SF in the highest density environments.

In future work, I would like to undertake the following:

- One of the main limitations of the technique are the SED degeneracies that arise from using a large number of template SEDs in the fitting procedure, and from correlations between the stellar population parameters. I aim to undertake a systematic study to quantify the effects of SED degeneracies and propagate their uncertainties into the results for the annular SFR. In particular, I aim to quantify the uncertainties due to correlations between the stellar population parameters.
- I aim to explore the differences that may arise from using templates from a different stellar population synthesis model, in order to determine if the statistical results obtained are in fact dependent on the model chosen and the different degeneracies that exist among the various parameters in that model. In future work, I aim to explore this issue using models such as PEGASE (Fioc and Rocca-Volmerange, 1997).
- I have used the concentration index as the primary morphological classifier in our investigation of the impact of the density-morphology relation. As there remains the possibility of misidentifying a fraction of early-types as late-types and vice-versa, I checked the robustness of the results for the radial SF variation by selecting galaxies based on their

Sersic index as well. In the future, I aim to use different morphological classifiers in order to test the robustness of the results. Recently, morphological classifications based on visual inspection of SDSS galaxies have been made available ("The Galaxy Zoo" project, Lintott et al. (2008)).

- I would like to probe whether the "downsizing" of star formation in galaxy bulges is indeed responsible for our observed trends by exploring galaxy populations as a function of stellar mass, together with the local density. Since "downsizing" is concerned with the mass dependence of the SFR history of galaxies, this will allow a more detailed exploration of the origins and likely evolution of the observed variation in the spatially resolved SF in galaxies.

- To further explore and support the "downsizing" idea, I also plan to extend this work to include an analysis on galaxies in a high redshift sample, from COSMOS (Koekemoer et al., 2007), GOODS (Giavalisco et al., 2004), or AEGIS (Davis et al., 2007). At high redshifts the high density environments are less evolved, and the relationship between SFR and density is likely to be quite different. Indeed, as discussed earlier, Elbaz et al. (2007), using GOODS data, has shown that the SFR-density relationship is inverted by $z \approx 1$, such that dense environments support enhanced, rather than suppressed, star formation. We could thus extend our study to these high redshifts in order to see if such an enhancement in the SFR occurs and if so, if this takes place in the centers of the galaxies or in their outskirts. Using DEEP2 Galaxy Redshift Survey data, Cooper et al. (2006) also suggest that bright blue galaxies in overdense regions at high redshift have their star formation quenched and evolve into members of the red sequence by $z \approx 0$. These conclusions indicate that there exists a population of massive blue galaxies that has likely undergone quenching at $z \approx 1$, which has no high-mass counterpart today, and that there is a downsizing of the characteristic mass (or luminosity) at which the quenching of a galaxy's star formation becomes efficient. They suggest that the quenching mechanism must operate efficiently in both cluster and group environments for consistency between their $z \approx 1$ and $z \approx 0$ results. Using pixel-z to explore the relationship between environment and the SFR distribution within galaxies at high redshift will aid in constraining the process by which such a mechanism might operate.

- I am currently undertaking a project with the aim of studying the effect of galaxy interactions (such as mergers) on the SFR in the galaxies, from both a theoretical and observational front. Star formation in close pairs of galaxies can be tidally triggered and numerical models have been able to match the tidal trails and streams with the occurrence of starbursts. The project aims to bridge the gap between the predictions of merger hydro-dynamic simulations and the observations by doing a statistical study with a large sample of observed close pairs in the SDSS. I aim to measure the amount of triggered SF as a result of the merger and then compare this to the predictions of a suite of merger simulations. Specifically, I wish to establish how the probability that a galaxy has a certain SFR during the merger, changes as a function of merger parameters such as the mass ratios of the merger pairs and their relative separation on the sky, over a wide dynamical scale. I wish to determine these distributions for both the observed pairs as well as the pairs in the simulations. By studying how the triggered SFR probability distribution changes as a function of both mass ratios and relative separations, I aim to put constraints on the simulations' feedback mechanisms in the ISM, which is currently not well constrained during mergers. These constraints can come from using a much larger sample of observed galaxy pairs than has previously been used. In addition, the information in the pixels should enable me to pinpoint where the triggered SF occurs within galaxies, and I aim to make a statistical comparison with the predictions of the merger simulations. The technique – once the uncertainties in the SFR measurements have been properly characterized – should provide an unprecedented ability to use observations to constrain baryonic physics on these small scales in galaxies.

BIBLIOGRAPHY

K. Abazajian, J. K. Adelman-McCarthy, M. A. Agüeros, S. S. Allam, S. F. Anderson, J. Annis, N. A. Bahcall, I. K. Baldry, S. Bastian, A. Berlind, M. Bernardi, M. R. Blanton, N. Blythe, J. J. Bochanski, Jr., W. N. Boroski, H. Brewington, J. W. Briggs, J. Brinkmann, R. J. Brunner, T. Budavári, L. N. Carey, M. A. Carr, F. J. Castander, K. Chiu, M. J. Collinge, A. J. Connolly, K. R. Covey, I. Csabai, J. J. Dalcanton, S. Dodelson, M. Doi, F. Dong, D. J. Eisenstein, M. L. Evans, X. Fan, P. D. Feldman, D. P. Finkbeiner, S. D. Friedman, J. A. Frieman, M. Fukugita, R. R. Gal, B. Gillespie, K. Glazebrook, C. F. Gonzalez, J. Gray, E. K. Grebel, L. Grodnicki, J. E. Gunn, V. K. Gurbani, P. B. Hall, L. Hao, D. Harbeck, F. H. Harris, H. C. Harris, M. Harvanek, S. L. Hawley, T. M. Heckman, J. F. Helmboldt, J. S. Hendry, G. S. Hennessy, R. B. Hindsley, D. W. Hogg, D. J. Holmgren, J. A. Holtzman, L. Homer, L. Hui, S.-i. Ichikawa, T. Ichikawa, J. P. Inkmann, Ž. Ivezić, S. Jester, D. E. Johnston, B. Jordan, W. P. Jordan, A. M. Jorgensen, M. Jurić, G. Kauffmann, S. M. Kent, S. J. Kleinman, G. R. Knapp, A. Y. Kniazev, R. G. Kron, J. Krzesiński, P. Z. Kunszt, N. Kuropatkin, D. Q. Lamb, H. Lampeitl, B. E. Laubscher, B. C. Lee, R. F. Leger, N. Li, A. Lidz, H. Lin, Y.-S. Loh, D. C. Long, J. Loveday, R. H. Lupton, T. Malik, B. Margon, P. M. McGehee, T. A. McKay, A. Meiksin, G. A. Miknaitis, B. K. Moorthy, J. A. Munn, T. Murphy, R. Nakajima, V. K. Narayanan, T. Nash, E. H. Neilsen, Jr., H. J. Newberg, P. R. Newman, R. C. Nichol, T. Nicinski, M. Nieto-Santisteban, A. Nitta, M. Odenkirchen, S. Okamura, J. P. Ostriker, R. Owen, N. Padmanabhan, J. Peoples, J. R. Pier, B. Pindor, A. C. Pope, T. R. Quinn, R. R. Rafikov, S. N. Raymond, G. T. Richards, M. W. Richmond, H.-W. Rix, C. M. Rockosi, J. Schaye, D. J. Schlegel, D. P. Schneider, J. Schroeder, R. Scranton, M. Sekiguchi, U. Seljak, G. Sergey, B. Sesar, E. Sheldon, K. Shimasaku, W. A. Siegmund, N. M. Silvestri, A. J. Sinisgalli, E. Sirko, J. A. Smith, V. Smolčić, S. A. Snedden, A. Stebbins, C. Steinhardt, G. Stinson, C. Stoughton, I. V. Strateva, M. A. Strauss, M. SubbaRao, A. S. Szalay, I. Szapudi, P. Szkody, L. Tasca, M. Tegmark, A. R. Thakar, C. Tremonti, D. L. Tucker, A. Uomoto, D. E. Vanden Berk, J. Vandenberg, M. S. Vogeley, W. Voges, N. P. Vogt, L. M. Walkowicz, D. H. Weinberg, A. A. West, S. D. M. White, B. C. Wilhite, B. Willman, Y. Xu, B. Yanny, J. Yarger, N. Yasuda, C.-W. Yip, D. R. Yocum, D. G. York, N. L. Zakamska, I. Zehavi, W. Zheng, S. Zibetti, and D. B. Zucker. The First Data Release of the Sloan Digital Sky Survey. *AJ*, 126:2081–2086, October 2003.

R. G. Abraham, R. S. Ellis, A. C. Fabian, N. R. Tanvir, and K. Glazebrook. The star formation history of the Hubble sequence: spatially resolved colour distributions of intermediate-

redshift galaxies in the Hubble Deep Field. *MNRAS*, 303:641–658, March 1999.

R. G. Abraham, S. van den Bergh, and P. Nair. A New Approach to Galaxy Morphology. I. Analysis of the Sloan Digital Sky Survey Early Data Release. *ApJ*, 588:218–229, May 2003.

J. K. Adelman-McCarthy, M. A. Agüeros, S. S. Allam, K. S. J. Anderson, S. F. Anderson, J. Annis, N. A. Bahcall, I. K. Baldry, J. C. Barentine, A. Berlind, M. Bernardi, M. R. Blanton, W. N. Boroski, H. J. Brewington, J. Brinchmann, J. Brinkmann, R. J. Brunner, T. Budavári, L. N. Carey, M. A. Carr, F. J. Castander, A. J. Connolly, I. Csabai, P. C. Czarapata, J. J. Dalcanton, M. Doi, F. Dong, D. J. Eisenstein, M. L. Evans, X. Fan, D. P. Finkbeiner, S. D. Friedman, J. A. Frieman, M. Fukugita, B. Gillespie, K. Glazebrook, J. Gray, E. K. Grebel, J. E. Gunn, V. K. Gurbani, E. de Haas, P. B. Hall, F. H. Harris, M. Harvanek, S. L. Hawley, J. Hayes, J. S. Hendry, G. S. Hennessy, R. B. Hindsley, C. M. Hirata, C. J. Hogan, D. W. Hogg, D. J. Holmgren, J. A. Holtzman, S.-i. Ichikawa, Ž. Ivezić, S. Jester, D. E. Johnston, A. M. Jorgensen, M. Jurić, S. M. Kent, S. J. Kleinman, G. R. Knapp, A. Y. Kniazev, R. G. Kron, J. Krzesinski, N. Kuropatkin, D. Q. Lamb, H. Lampeitl, B. C. Lee, R. F. Leger, H. Lin, D. C. Long, J. Loveday, R. H. Lupton, B. Margon, D. Martínez-Delgado, R. Mandelbaum, T. Matsubara, P. M. McGehee, T. A. McKay, A. Meiksin, J. A. Munn, R. Nakajima, T. Nash, E. H. Neilsen, Jr., H. J. Newberg, P. R. Newman, R. C. Nichol, T. Nicinski, M. Nieto-Santisteban, A. Nitta, W. O'Mullane, S. Okamura, R. Owen, N. Padmanabhan, G. Pauls, J. J. Peoples, J. R. Pier, A. C. Pope, D. Pourbaix, T. R. Quinn, G. T. Richards, M. W. Richmond, C. M. Rockosi, D. J. Schlegel, D. P. Schneider, J. Schroeder, R. Scranton, U. Seljak, E. Sheldon, K. Shimasaku, J. A. Smith, V. Smolčić, S. A. Snedden, C. Stoughton, M. A. Strauss, M. SubbaRao, A. S. Szalay, I. Szapudi, P. Szkody, M. Tegmark, A. R. Thakar, D. L. Tucker, A. Uomoto, D. E. Vanden Berk, J. Vandenberg, M. S. Vogeley, W. Voges, N. P. Vogt, L. M. Walkowicz, D. H. Weinberg, A. A. West, S. D. M. White, Y. Xu, B. Yanny, D. R. Yocum, D. G. York, I. Zehavi, S. Zibetti, and D. B. Zucker. The Fourth Data Release of the Sloan Digital Sky Survey. *ApJS*, 162:38–48, January 2006.

W. Baade. The Resolution of Messier 32, NGC 205, and the Central Region of the Andromeda Nebula. *ApJ*, 100:137–+, September 1944.

M. L. Balogh, S. L. Morris, H. K. C. Yee, R. G. Carlberg, and E. Ellingson. Star Formation in Cluster Galaxies at 0.2 Z 0.55. *ApJ*, 488:L75+, October 1997.

M. L. Balogh, S. L. Morris, H. K. C. Yee, R. G. Carlberg, and E. Ellingson. Differential Galaxy Evolution in Cluster and Field Galaxies at z˜0.3. *ApJ*, 527:54–79, December 1999.

M. L. Balogh, J. F. Navarro, and S. L. Morris. The Origin of Star Formation Gradients in Rich Galaxy Clusters. *ApJ*, 540:113–121, September 2000.

M. L. Balogh, I. Smail, R. G. Bower, B. L. Ziegler, G. P. Smith, R. L. Davies, A. Gaztelu, J.-P. Kneib, and H. Ebeling. Distinguishing Local and Global Influences on Galaxy Morphology:

A Hubble Space Telescope Comparison of High and Low X-Ray Luminosity Clusters. *ApJ*, 566:123–136, February 2002.

W. A. Baum. Population Inferences from Star Counts, Surface Brightness and Colors. *PASP*, 71:106–117, April 1959.

E. F. Bell, C. Wolf, K. Meisenheimer, H.-W. Rix, A. Borch, S. Dye, M. Kleinheinrich, L. Wisotzki, and D. H. McIntosh. Nearly 5000 Distant Early-Type Galaxies in COMBO-17: A Red Sequence and Its Evolution since z˜1. *ApJ*, 608:752–767, June 2004.

N. Benítez. Bayesian Photometric Redshift Estimation. *ApJ*, 536:571–583, June 2000.

A. J. Benson, C. M. Baugh, S. Cole, C. S. Frenk, and C. G. Lacey. The dependence of velocity and clustering statistics on galaxy properties. *MNRAS*, 316:107–119, July 2000.

A. J. Benson, C. S. Frenk, C. M. Baugh, S. Cole, and C. G. Lacey. The clustering evolution of the galaxy distribution. *MNRAS*, 327:1041–1056, November 2001.

J. P. Blakeslee, A. Vazdekis, and E. A. Ajhar. Stellar populations and surface brightness fluctuations: new observations and models. *MNRAS*, 320:193–216, January 2001.

M. R. Blanton, J. Brinkmann, I. Csabai, M. Doi, D. Eisenstein, M. Fukugita, J. E. Gunn, D. W. Hogg, and D. J. Schlegel. Estimating Fixed-Frame Galaxy Magnitudes in the Sloan Digital Sky Survey. *AJ*, 125:2348–2360, May 2003a.

M. R. Blanton, J. Dalcanton, D. Eisenstein, J. Loveday, M. A. Strauss, M. SubbaRao, D. H. Weinberg, J. E. Anderson, Jr., J. Annis, N. A. Bahcall, M. Bernardi, J. Brinkmann, R. J. Brunner, S. Burles, L. Carey, F. J. Castander, A. J. Connolly, I. Csabai, M. Doi, D. Finkbeiner, S. Friedman, J. A. Frieman, M. Fukugita, J. E. Gunn, G. S. Hennessy, R. B. Hindsley, D. W. Hogg, T. Ichikawa, Ž. Ivezić, S. Kent, G. R. Knapp, D. Q. Lamb, R. F. Leger, D. C. Long, R. H. Lupton, T. A. McKay, A. Meiksin, A. Merelli, J. A. Munn, V. Narayanan, M. Newcomb, R. C. Nichol, S. Okamura, R. Owen, J. R. Pier, A. Pope, M. Postman, T. Quinn, C. M. Rockosi, D. J. Schlegel, D. P. Schneider, K. Shimasaku, W. A. Siegmund, S. Smee, Y. Snir, C. Stoughton, C. Stubbs, A. S. Szalay, G. P. Szokoly, A. R. Thakar, C. Tremonti, D. L. Tucker, A. Uomoto, D. Vanden Berk, M. S. Vogeley, P. Waddell, B. Yanny, N. Yasuda, and D. G. York. The Luminosity Function of Galaxies in SDSS Commissioning Data. *AJ*, 121:2358–2380, May 2001.

M. R. Blanton, D. Eisenstein, D. W. Hogg, D. J. Schlegel, and J. Brinkmann. Relationship between Environment and the Broadband Optical Properties of Galaxies in the Sloan Digital Sky Survey. *ApJ*, 629:143–157, August 2005.

M. R. Blanton, D. W. Hogg, N. A. Bahcall, I. K. Baldry, J. Brinkmann, I. Csabai, D. Eisenstein, M. Fukugita, J. E. Gunn, Ž. Ivezić, D. Q. Lamb, R. H. Lupton, J. Loveday, J. A. Munn, R. C. Nichol, S. Okamura, D. J. Schlegel, K. Shimasaku, M. A. Strauss, M. S. Vogeley, and D. H. Weinberg. The Broadband Optical Properties of Galaxies with Redshifts 0.02z0.22. *ApJ*, 594:186–207, September 2003b.

M. R. Blanton, D. W. Hogg, N. A. Bahcall, J. Brinkmann, M. Britton, A. J. Connolly, I. Csabai, M. Fukugita, J. Loveday, A. Meiksin, J. A. Munn, R. C. Nichol, S. Okamura, T. Quinn, D. P. Schneider, K. Shimasaku, M. A. Strauss, M. Tegmark, M. S. Vogeley, and D. H. Weinberg. The Galaxy Luminosity Function and Luminosity Density at Redshift z = 0.1. *ApJ*, 592:819–838, August 2003c.

M. R. Blanton, H. Lin, R. H. Lupton, F. M. Maley, N. Young, I. Zehavi, and J. Loveday. An Efficient Targeting Strategy for Multiobject Spectrograph Surveys: the Sloan Digital Sky Survey "Tiling" Algorithm. *AJ*, 125:2276–2286, April 2003d.

G. R. Blumenthal, S. M. Faber, R. Flores, and J. R. Primack. Contraction of dark matter galactic halos due to baryonic infall. *ApJ*, 301:27–34, February 1986.

S. Boissier, A. Gil de Paz, A. Boselli, B. F. Madore, V. Buat, L. Cortese, D. Burgarella, J. C. Muñoz-Mateos, T. A. Barlow, K. Forster, P. G. Friedman, D. C. Martin, P. Morrissey, S. G. Neff, D. Schiminovich, M. Seibert, T. Small, T. K. Wyder, L. Bianchi, J. Donas, T. M. Heckman, Y.-W. Lee, B. Milliard, R. M. Rich, A. S. Szalay, B. Y. Welsh, and S. K. Yi. Radial Variation of Attenuation and Star Formation in the Largest Late-Type Disks Observed with GALEX. *ApJS*, 173:524–537, December 2007.

S. Boissier, N. Prantzos, A. Boselli, and G. Gavazzi. The star formation rate in disc galaxies: thresholds and dependence on gas amount. *MNRAS*, 346:1215–1230, December 2003.

G. D. Bothun and A. Dressler. Blue disk galaxies in the Coma Cluster - Analogs to Z = 0.5 cluster members? *ApJ*, 301:57–64, February 1986.

R. Bouwens, T. Broadhurst, and J. Silk. Cloning Hubble Deep Fields. I. A Model-independent Measurement of Galaxy Evolution. *ApJ*, 506:557–578, October 1998.

R. G. Bower, A. J. Benson, R. Malbon, J. C. Helly, C. S. Frenk, C. M. Baugh, S. Cole, and C. G. Lacey. Breaking the hierarchy of galaxy formation. *MNRAS*, 370:645–655, August 2006.

J. Brinchmann, R. Abraham, D. Schade, L. Tresse, R. S. Ellis, S. J. Lilly, O. Le Fevre, K. Glazebrook, F. Hammer, M. Colless, D. Crampton, and T. Broadhurst. HST imaging of CFRS and LDSS galaxies - I: Morphological Properties. *ArXiv Astrophysics e-prints*, December 1997.

A. M. Brooks, F. Governato, C. M. Booth, B. Willman, J. P. Gardner, J. Wadsley, G. Stinson, and T. Quinn. The Origin and Evolution of the Mass-Metallicity Relationship for Galaxies: Results from Cosmological N-Body Simulations. *ApJ*, 655:L17–L20, January 2007.

R. J. Brunner, A. J. Connolly, and A. S. Szalay. The Statistical Approach to Quantifying Galaxy Evolution. *ApJ*, 516:563–581, May 1999.

G. Bruzual and S. Charlot. Stellar population synthesis at the resolution of 2003. *MNRAS*, 344:1000–1028, October 2003.

G. Bruzual A. and S. Charlot. Spectral evolution of stellar populations using isochrone synthesis. *ApJ*, 405:538–553, March 1993.

T. Budavári, A. S. Szalay, A. J. Connolly, I. Csabai, and M. Dickinson. Creating Spectral Templates from Multicolor Redshift Surveys. *AJ*, 120:1588–1598, September 2000.

T. Budavári, A. S. Szalay, A. J. Connolly, I. Csabai, M. E. Dickinson, and The Hdf/Nicmos Team. Creating Spectral Templates from Multicolor Redshift Surveys. In R. Weymann, L. Storrie-Lombardi, M. Sawicki, and R. Brunner, editors, *Photometric Redshifts and the Detection of High Redshift Galaxies*, volume 191 of *Astronomical Society of the Pacific Conference Series*, pages 19–+, 1999.

H. Butcher and A. Oemler, Jr. The evolution of galaxies in clusters. I - ISIT photometry of C1 0024+1654 and 3C 295. *ApJ*, 219:18–30, January 1978.

G. Byrd and M. Valtonen. Tidal generation of active spirals and S0 galaxies by rich clusters. *ApJ*, 350:89–94, February 1990.

N. Caldwell, R. Kennicutt, A. C. Phillips, and R. A. Schommer. A study of star formation in the disks of SA galaxies. *ApJ*, 370:526–540, April 1991.

D. Calzetti. The Dust Opacity of Star-forming Galaxies. *PASP*, 113:1449–1485, December 2001.

D. Calzetti, L. Armus, R. C. Bohlin, A. L. Kinney, J. Koornneef, and T. Storchi-Bergmann. The Dust Content and Opacity of Actively Star-forming Galaxies. *ApJ*, 533:682–695, April 2000.

A. Cattaneo, A. Dekel, J. Devriendt, B. Guiderdoni, and J. Blaizot. Modelling the galaxy bimodality: shutdown above a critical halo mass. *MNRAS*, 370:1651–1665, August 2006.

A. Cattaneo, A. Dekel, S. M. Faber, and B. Guiderdoni. Downsizing by shutdown in red galaxies. *MNRAS*, pages 858–+, July 2008.

S. Charlot and A. G. Bruzual. Stellar population synthesis revisited. *ApJ*, 367:126–140, January 1991.

A. L. Coil, J. A. Newman, D. Croton, M. C. Cooper, M. Davis, S. M. Faber, B. F. Gerke, D. C. Koo, N. Padmanabhan, R. H. Wechsler, and B. J. Weiner. The DEEP2 Galaxy Redshift Survey: Color and Luminosity Dependence of Galaxy Clustering at z˜1. *ApJ*, 672:153–176, January 2008.

S. Cole, C. G. Lacey, C. M. Baugh, and C. S. Frenk. Hierarchical galaxy formation. *MNRAS*, 319:168–204, November 2000.

G. D. Coleman, C.-C. Wu, and D. W. Weedman. Colors and magnitudes predicted for high redshift galaxies. *ApJS*, 43:393–416, July 1980.

J. J. Condon. Radio emission from normal galaxies. *ARA&A*, 30:575–611, 1992.

A. J. Connolly, T. Budavári, A. S. Szalay, I. Csabai, and R. J. Brunner. An Orthogonal Approach to Photometric Redshifts. In R. Weymann, L. Storrie-Lombardi, M. Sawicki, and R. Brunner, editors, *Photometric Redshifts and the Detection of High Redshift Galaxies*, volume 191 of *Astronomical Society of the Pacific Conference Series*, pages 13–+, 1999.

A. J. Connolly, I. Csabai, A. S. Szalay, D. C. Koo, R. G. Kron, and J. A. Munn. Slicing Through Multicolor Space: Galaxy Redshifts from Broadband Photometry. *AJ*, 110:2655–+, December 1995.

C. J. Conselice. The fundamental properties of galaxies and a new galaxy classification system. *MNRAS*, 373:1389–1408, December 2006.

A. Conti, A. J. Connolly, A. M. Hopkins, T. Budavári, A. S. Szalay, I. Csabai, S. J. Schmidt, C. Adams, and N. Petrovic. The Star Formation History of Galaxies Measured from Individual Pixels. I. The Hubble Deep Field North. *AJ*, 126:2330–2345, November 2003.

A. Conti, J. D. Kennefick, P. Martini, and P. S. Osmer. Quasar Candidates in the Hubble Deep Field. *AJ*, 117:645–657, February 1999.

M. C. Cooper, J. A. Newman, A. L. Coil, D. J. Croton, B. F. Gerke, R. Yan, M. Davis, S. M. Faber, P. Guhathakurta, D. C. Koo, and B. J. Weiner. The DEEP2 Galaxy Redshift Survey: Evolution of the Color-Density Relation at 0.4 z 1.35. *ArXiv Astrophysics e-prints*, July 2006.

M. C. Cooper, J. A. Newman, B. J. Weiner, R. Yan, C. N. A. Willmer, K. Bundy, A. L. Coil, C. J. Conselice, M. Davis, S. M. Faber, B. F. Gerke, P. Guhathakurta, D. C. Koo, and K. G. Noeske. The DEEP2 Galaxy Redshift Survey: the role of galaxy environment in the cosmic star formation history. *MNRAS*, 383:1058–1078, January 2008.

W. J. Couch, M. L. Balogh, R. G. Bower, I. Smail, K. Glazebrook, and M. Taylor. A Low Global Star Formation Rate in the Rich Galaxy Cluster AC 114 at z=0.32. *ApJ*, 549: 820–831, March 2001.

L. L. Cowie and A. Songaila. Thermal evaporation of gas within galaxies by a hot intergalactic medium. *Nature*, 266:501–503, April 1977.

L. L. Cowie, A. Songaila, E. M. Hu, and J. G. Cohen. New Insight on Galaxy Formation and Evolution From Keck Spectroscopy of the Hawaii Deep Fields. *AJ*, 112:839–+, September 1996.

D. J. Croton, V. Springel, S. D. M. White, G. De Lucia, C. S. Frenk, L. Gao, A. Jenkins, G. Kauffmann, J. F. Navarro, and N. Yoshida. The many lives of active galactic nuclei:

cooling flows, black holes and the luminosities and colours of galaxies. *MNRAS*, 365:11–28, January 2006.

I. Csabai, T. Budavári, A. J. Connolly, A. S. Szalay, Z. Győry, N. Benítez, J. Annis, J. Brinkmann, D. Eisenstein, M. Fukugita, J. Gunn, S. Kent, R. Lupton, R. C. Nichol, and C. Stoughton. The Application of Photometric Redshifts to the SDSS Early Data Release. *AJ*, 125:580–592, February 2003.

I. Csabai, A. J. Connolly, A. S. Szalay, and T. Budavári. Reconstructing Galaxy Spectral Energy Distributions from Broadband Photometry. *AJ*, 119:69–78, January 2000.

O. Cucciati, A. Iovino, C. Marinoni, O. Ilbert, S. Bardelli, P. Franzetti, O. Le Fèvre, A. Pollo, G. Zamorani, A. Cappi, L. Guzzo, H. J. McCracken, B. Meneux, R. Scaramella, M. Scodeggio, L. Tresse, E. Zucca, D. Bottini, B. Garilli, V. Le Brun, D. Maccagni, J. P. Picat, G. Vettolani, A. Zanichelli, C. Adami, M. Arnaboldi, S. Arnouts, M. Bolzonella, S. Charlot, P. Ciliegi, T. Contini, S. Foucaud, I. Gavignaud, B. Marano, A. Mazure, R. Merighi, S. Paltani, R. Pellò, L. Pozzetti, M. Radovich, M. Bondi, A. Bongiorno, G. Busarello, S. de La Torre, L. Gregorini, F. Lamareille, G. Mathez, Y. Mellier, P. Merluzzi, V. Ripepi, D. Rizzo, S. Temporin, and D. Vergani. The VIMOS VLT Deep Survey: the build-up of the colour-density relation. *A&A*, 458:39–52, October 2006.

M. Davis, P. Guhathakurta, N. P. Konidaris, J. A. Newman, M. L. N. Ashby, A. D. Biggs, P. Barmby, K. Bundy, S. C. Chapman, A. L. Coil, C. J. Conselice, M. C. Cooper, D. J. Croton, P. R. M. Eisenhardt, R. S. Ellis, S. M. Faber, T. Fang, G. G. Fazio, A. Georgakakis, B. F. Gerke, W. M. Goss, S. Gwyn, J. Harker, A. M. Hopkins, J.-S. Huang, R. J. Ivison, S. A. Kassin, E. N. Kirby, A. M. Koekemoer, D. C. Koo, E. S. Laird, E. Le Floc'h, L. Lin, J. M. Lotz, P. J. Marshall, D. C. Martin, A. J. Metevier, L. A. Moustakas, K. Nandra, K. G. Noeske, C. Papovich, A. C. Phillips, R. M. Rich, G. H. Rieke, D. Rigopoulou, S. Salim, D. Schiminovich, L. Simard, I. Smail, T. A. Small, B. J. Weiner, C. N. A. Willmer, S. P. Willner, G. Wilson, E. L. Wright, and R. Yan. The All-Wavelength Extended Groth Strip International Survey (AEGIS) Data Sets. *ApJ*, 660:L1–L6, May 2007.

R. de Grijs, J. T. Lee, M. C. Mora Herrera, U. Fritze-v. Alvensleben, and P. Anders. Stellar populations and star cluster formation in interacting galaxies with the Advanced Camera for Surveys. *New Astronomy*, 8:155–171, February 2003.

G. De Lucia. How 'heredity' and 'environment' shape galaxy properties. *ArXiv Astrophysics e-prints*, November 2006.

G. De Lucia, V. Springel, S. D. M. White, D. Croton, and G. Kauffmann. The formation history of elliptical galaxies. *MNRAS*, 366:499–509, February 2006.

G. de Vaucouleurs, A. de Vaucouleurs, H. G. Corwin, Jr., R. J. Buta, G. Paturel, and P. Fouque. *Third Reference Catalogue of Bright Galaxies*. Volume 1-3, XII, 2069 pp. 7 figs.. Springer-Verlag Berlin Heidelberg New York, 1991.

A. Dekel and Y. Birnboim. Gravitational quenching in massive galaxies and clusters by clumpy accretion. *MNRAS*, 383:119–138, January 2008.

A. Diaferio, G. Kauffmann, M. L. Balogh, S. D. M. White, D. Schade, and E. Ellingson. The spatial and kinematic distributions of cluster galaxies in a ΛCDM universe: comparison with observations. *MNRAS*, 323:999–1015, May 2001.

M. T. Doyle and M. J. Drinkwater. The effect of local galaxy surface density on star formation for HI selected galaxies. *MNRAS*, 372:977–991, November 2006.

A. Dressler. Galaxy morphology in rich clusters - Implications for the formation and evolution of galaxies. *ApJ*, 236:351–365, March 1980.

A. Dressler, A. J. Oemler, W. J. Couch, I. Smail, R. S. Ellis, A. Barger, H. Butcher, B. M. Poggianti, and R. M. Sharples. Evolution since Z = 0.5 of the Morphology-Density Relation for Clusters of Galaxies. *ApJ*, 490:577–+, December 1997.

A. Dressler, I. B. Thompson, and S. A. Shectman. Statistics of emission-line galaxies in rich clusters. *ApJ*, 288:481–486, January 1985.

S. P. Driver, P. D. Allen, J. Liske, and A. W. Graham. The Millennium Galaxy Catalogue: The Luminosity Functions of Bulges and Disks and Their Implied Stellar Mass Densities. *ApJ*, 657:L85–L88, March 2007.

S. P. Driver, C. C. Popescu, R. J. Tuffs, A. W. Graham, J. Liske, and I. Baldry. The Energy Output of the Universe from 0.1 to 1000 μm. *ApJ*, 678:L101–L104, May 2008.

O. J. Eggen, D. Lynden-Bell, and A. R. Sandage. Evidence from the motions of old stars that the Galaxy collapsed. *ApJ*, 136:748–+, November 1962.

D. Elbaz, E. Daddi, D. Le Borgne, M. Dickinson, D. M. Alexander, R.-R. Chary, J.-L. Starck, W. N. Brandt, M. Kitzbichler, E. MacDonald, M. Nonino, P. Popesso, D. Stern, and E. Vanzella. The reversal of the star formation-density relation in the distant universe. *A&A*, 468:33–48, June 2007.

S. M. Faber and R. E. Jackson. Velocity dispersions and mass-to-light ratios for elliptical galaxies. *ApJ*, 204:668–683, March 1976.

S. M. Faber, C. N. A. Willmer, C. Wolf, D. C. Koo, B. J. Weiner, J. A. Newman, M. Im, A. L. Coil, C. Conroy, M. C. Cooper, M. Davis, D. P. Finkbeiner, B. F. Gerke, K. Gebhardt, E. J. Groth, P. Guhathakurta, J. Harker, N. Kaiser, S. Kassin, M. Kleinheinrich, N. P. Konidaris, R. G. Kron, L. Lin, G. Luppino, D. S. Madgwick, K. Meisenheimer, K. G. Noeske, A. C. Phillips, V. L. Sarajedini, R. P. Schiavon, L. Simard, A. S. Szalay, N. P. Vogt, and R. Yan. Galaxy Luminosity Functions to z˜1 from DEEP2 and COMBO-17: Implications for Red Galaxy Formation. *ApJ*, 665:265–294, August 2007.

R. Farouki and S. L. Shapiro. Computer simulations of environmental influences on galaxy evolution in dense clusters. II - Rapid tidal encounters. *ApJ*, 243:32–41, January 1981.

G. Fasano, B. M. Poggianti, W. J. Couch, D. Bettoni, P. Kjærgaard, and M. Moles. The Evolution of the Galactic Morphological Types in Clusters. *ApJ*, 542:673–683, October 2000.

A. Fernández-Soto, K. M. Lanzetta, and A. Yahil. A New Catalog of Photometric Redshifts in the Hubble Deep Field. *ApJ*, 513:34–50, March 1999.

G. Feulner, A. Gabasch, M. Salvato, N. Drory, U. Hopp, and R. Bender. Specific Star Formation Rates to Redshift 5 from the FORS Deep Field and the GOODS-S Field. *ApJ*, 633:L9–L12, November 2005.

M. Fioc and B. Rocca-Volmerange. PEGASE: a UV to NIR spectral evolution model of galaxies. Application to the calibration of bright galaxy counts. *A&A*, 326:950–962, October 1997.

A. E. Firth, R. S. Somerville, R. G. McMahon, O. Lahav, R. S. Ellis, C. N. Sabbey, P. J. McCarthy, H.-W. Chen, R. O. Marzke, J. Wilson, R. G. Abraham, M. G. Beckett, R. G. Carlberg, J. R. Lewis, C. D. Mackay, D. C. Murphy, A. E. Oemler, and S. E. Persson. The Las Campanas Infrared Survey - II. Photometric redshifts, comparison with models and clustering evolution. *MNRAS*, 332:617–646, May 2002.

Y. Fujita. Ram-Pressure Stripping of Galaxies in High-Redshift Clusters and the Influence of Intracluster Medium Heating. *ApJ*, 550:612–621, April 2001.

M. Fukugita, T. Ichikawa, J. E. Gunn, M. Doi, K. Shimasaku, and D. P. Schneider. The Sloan Digital Sky Survey Photometric System. *AJ*, 111:1748–+, April 1996.

D. Gamerman. *Markov Chain Monte Carlo : Stochastic Simulation for Bayesian Inference*. London : New York : Chapman Hall, 1997.

G. Gavazzi. 21 centimeter study of spiral galaxies in the Coma supercluster. *ApJ*, 320: 96–121, September 1987.

M. Giavalisco, H. C. Ferguson, A. M. Koekemoer, M. Dickinson, D. M. Alexander, F. E. Bauer, J. Bergeron, C. Biagetti, W. N. Brandt, S. Casertano, C. Cesarsky, E. Chatzichristou, C. Conselice, S. Cristiani, L. Da Costa, T. Dahlen, D. de Mello, P. Eisenhardt, T. Erben, S. M. Fall, C. Fassnacht, R. Fosbury, A. Fruchter, J. P. Gardner, N. Grogin, R. N. Hook, A. E. Hornschemeier, R. Idzi, S. Jogee, C. Kretchmer, V. Laidler, K. S. Lee, M. Livio, R. Lucas, P. Madau, B. Mobasher, L. A. Moustakas, M. Nonino, P. Padovani, C. Papovich, Y. Park, S. Ravindranath, A. Renzini, M. Richardson, A. Riess, P. Rosati, M. Schirmer, E. Schreier, R. S. Somerville, H. Spinrad, D. Stern, M. Stiavelli, L. Strolger, C. M. Urry, B. Vandame, R. Williams, and C. Wolf. The Great Observatories Origins Deep Survey: Initial Results from Optical and Near-Infrared Imaging. *ApJ*, 600:L93–L98, January 2004.

L. Girardi, A. Bressan, G. Bertelli, and C. Chiosi. Evolutionary tracks and isochrones for low- and intermediate-mass stars: From 0.15 to 7 $M_{sun}, and from Z = 0.0004 to 0.03. A\&AS, 141 : 371 - -383, February 2000.$

P. L. Gómez, R. C. Nichol, C. J. Miller, M. L. Balogh, T. Goto, A. I. Zabludoff, A. K. Romer, M. Bernardi, R. Sheth, A. M. Hopkins, F. J. Castander, A. J. Connolly, D. P. Schneider, J. Brinkmann, D. Q. Lamb, M. SubbaRao, and D. G. York. Galaxy Star Formation as a Function of Environment in the Early Data Release of the Sloan Digital Sky Survey. *ApJ*, 584:210–227, February 2003.

T. Goto, R. C. Nichol, S. Okamura, M. Sekiguchi, C. J. Miller, M. Bernardi, A. Hopkins, C. Tremonti, A. Connolly, F. J. Castander, J. Brinkmann, M. Fukugita, M. Harvanek, Z. Ivezic, S. J. Kleinman, J. Krzesinski, D. Long, J. Loveday, E. H. Neilsen, P. R. Newman, A. Nitta, S. A. Snedden, and M. Subbarao. Hδ-Strong Galaxies in the Sloan Digital Sky Survey: I. The Catalog. *PASJ*, 55:771–787, June 2003a.

T. Goto, C. Yamauchi, Y. Fujita, S. Okamura, M. Sekiguchi, I. Smail, M. Bernardi, and P. L. Gomez. The morphology-density relation in the Sloan Digital Sky Survey. *MNRAS*, 346:601–614, December 2003b.

J. E. Gunn, M. Carr, C. Rockosi, M. Sekiguchi, K. Berry, B. Elms, E. de Haas, Ž. Ivezić, G. Knapp, R. Lupton, G. Pauls, R. Simcoe, R. Hirsch, D. Sanford, S. Wang, D. York, F. Harris, J. Annis, L. Bartozek, W. Boroski, J. Bakken, M. Haldeman, S. Kent, S. Holm, D. Holmgren, D. Petravick, A. Prosapio, R. Rechenmacher, M. Doi, M. Fukugita, K. Shimasaku, N. Okada, C. Hull, W. Siegmund, E. Mannery, M. Blouke, D. Heidtman, D. Schneider, R. Lucinio, and J. Brinkman. The Sloan Digital Sky Survey Photometric Camera. *AJ*, 116:3040–3081, December 1998.

J. E. Gunn and J. R. I. Gott. On the Infall of Matter Into Clusters of Galaxies and Some Effects on Their Evolution. *ApJ*, 176:1–+, August 1972.

J. E. Gunn, W. A. Siegmund, E. J. Mannery, R. E. Owen, C. L. Hull, R. F. Leger, L. N. Carey, G. R. Knapp, D. G. York, W. N. Boroski, S. M. Kent, R. H. Lupton, C. M. Rockosi, M. L. Evans, P. Waddell, J. E. Anderson, J. Annis, J. C. Barentine, L. M. Bartoszek, S. Bastian, S. B. Bracker, H. J. Brewington, C. I. Briegel, J. Brinkmann, Y. J. Brown, M. A. Carr, P. C. Czarapata, C. C. Drennan, T. Dombeck, G. R. Federwitz, B. A. Gillespie, C. Gonzales, S. U. Hansen, M. Harvanek, J. Hayes, W. Jordan, E. Kinney, M. Klaene, S. J. Kleinman, R. G. Kron, J. Kresinski, G. Lee, S. Limmongkol, C. W. Lindenmeyer, D. C. Long, C. L. Loomis, P. M. McGehee, P. M. Mantsch, E. H. Neilsen, Jr., R. M. Neswold, P. R. Newman, A. Nitta, J. J. Peoples, J. R. Pier, P. S. Prieto, A. Prosapio, C. Rivetta, D. P. Schneider, S. Snedden, and S.-i. Wang. The 2.5 m Telescope of the Sloan Digital Sky Survey. *AJ*, 131:2332–2359, April 2006.

S. D. J. Gwyn and F. D. A. Hartwick. The Redshift Distribution and Luminosity Functions of Galaxies in the Hubble Deep Field. *ApJ*, 468:L77+, September 1996.

A. J. S. Hamilton. Evidence for biasing in the CfA survey. *ApJ*, 331:L59–L62, August 1988.

Y. Hashimoto and A. J. Oemler. The Concentration-Density Relation of Galaxies in the Las Campanas Redshift Survey. *ApJ*, 510:609–613, January 1999.

Y. Hashimoto, A. J. Oemler, H. Lin, and D. L. Tucker. The Influence of Environment on the Star Formation Rates of Galaxies. *ApJ*, 499:589–+, May 1998.

A. Heavens, B. Panter, R. Jimenez, and J. Dunlop. The star-formation history of the Universe from the stellar populations of nearby galaxies. *Nature*, 428:625–627, April 2004.

S. Hermit, B. X. Santiago, O. Lahav, M. A. Strauss, M. Davis, A. Dressler, and J. P. Huchra. The two-point correlation function and morphological segregation in the Optical Redshift Survey. *MNRAS*, 283:709–720, December 1996.

D. W. Hogg, M. R. Blanton, J. Brinchmann, D. J. Eisenstein, D. J. Schlegel, J. E. Gunn, T. A. McKay, H.-W. Rix, N. A. Bahcall, J. Brinkmann, and A. Meiksin. The Dependence on Environment of the Color-Magnitude Relation of Galaxies. *ApJ*, 601:L29–L32, January 2004.

D. W. Hogg, M. R. Blanton, D. J. Eisenstein, J. E. Gunn, D. J. Schlegel, I. Zehavi, N. A. Bahcall, J. Brinkmann, I. Csabai, D. P. Schneider, D. H. Weinberg, and D. G. York. The Overdensities of Galaxy Environments as a Function of Luminosity and Color. *ApJ*, 585: L5–L9, March 2003.

D. W. Hogg, J. G. Cohen, R. Blandford, S. D. J. Gwyn, F. D. A. Hartwick, B. Mobasher, P. Mazzei, M. Sawicki, H. Lin, H. K. C. Yee, A. J. Connolly, R. J. Brunner, I. Csabai, M. Dickinson, M. U. Subbarao, A. S. Szalay, A. Fernández-Soto, K. M. Lanzetta, and A. Yahil. A Blind Test of Photometric Redshift Prediction. *AJ*, 115:1418–1422, April 1998.

D. W. Hogg, D. P. Finkbeiner, D. J. Schlegel, and J. E. Gunn. A Photometricity and Extinction Monitor at the Apache Point Observatory. *AJ*, 122:2129–2138, October 2001.

D. W. Hogg, M. Masjedi, A. A. Berlind, M. R. Blanton, A. D. Quintero, and J. Brinkmann. What Triggers Galaxy Transformations? The Environments of Poststarburst Galaxies. *ApJ*, 650:763–769, October 2006.

B. P. Holden, G. D. Illingworth, M. Franx, J. P. Blakeslee, M. Postman, D. D. Kelson, A. van der Wel, R. Demarco, D. K. Magee, K.-V. Tran, A. Zirm, H. Ford, P. Rosati, and N. Homeier. Mass Selection and the Evolution of the Morphology-Density Relation from z = 0.8 to 0. *ApJ*, 670:190–205, November 2007.

A. M. Hopkins, A. J. Connolly, D. B. Haarsma, and L. E. Cram. Toward a Resolution of the Discrepancy between Different Estimators of Star Formation Rate. *AJ*, 122:288–296, July 2001.

A. M. Hopkins, C. J. Miller, R. C. Nichol, A. J. Connolly, M. Bernardi, P. L. Gómez, T. Goto, C. A. Tremonti, J. Brinkmann, Ž. Ivezić, and D. Q. Lamb. Star Formation Rate Indicators in the Sloan Digital Sky Survey. *ApJ*, 599:971–991, December 2003.

E. P. Hubble. Realm of the Nebulae. *Yale University Press*, 1936.

O. Ilbert, S. Lauger, L. Tresse, V. Buat, S. Arnouts, O. Le Fèvre, D. Burgarella, E. Zucca, S. Bardelli, G. Zamorani, D. Bottini, B. Garilli, V. Le Brun, D. Maccagni, J.-P. Picat, R. Scaramella, M. Scodeggio, G. Vettolani, A. Zanichelli, C. Adami, M. Arnaboldi, M. Bolzonella, A. Cappi, S. Charlot, T. Contini, S. Foucaud, P. Franzetti, I. Gavignaud, L. Guzzo, A. Iovino, H. J. McCracken, B. Marano, C. Marinoni, G. Mathez, A. Mazure, B. Meneux, R. Merighi, S. Paltani, R. Pello, A. Pollo, L. Pozzetti, M. Radovich, M. Bondi, A. Bongiorno, G. Busarello, P. Ciliegi, Y. Mellier, P. Merluzzi, V. Ripepi, and D. Rizzo. The VIMOS-VLT Deep Survey. Galaxy luminosity function per morphological type up to z = 1.2. *A&A*, 453:809–815, July 2006.

Ž. Ivezić, R. H. Lupton, D. Schlegel, B. Boroski, J. Adelman-McCarthy, B. Yanny, S. Kent, C. Stoughton, D. Finkbeiner, N. Padmanabhan, C. M. Rockosi, J. E. Gunn, G. R. Knapp, M. A. Strauss, G. T. Richards, D. Eisenstein, T. Nicinski, S. J. Kleinman, J. Krzesinski, P. R. Newman, S. Snedden, A. R. Thakar, A. Szalay, J. A. Munn, J. A. Smith, D. Tucker, and B. C. Lee. SDSS data management and photometric quality assessment. *Astronomische Nachrichten*, 325:583–589, October 2004.

H. M. Johnston, R. W. Hunstead, G. Cotter, and E. M. Sadler. MRC B1221-423: a compact steep-spectrum radio source in a merging galaxy. *MNRAS*, 356:515–523, January 2005.

S. Juneau, K. Glazebrook, D. Crampton, P. J. McCarthy, S. Savaglio, R. Abraham, R. G. Carlberg, H.-W. Chen, D. Le Borgne, R. O. Marzke, K. Roth, I. Jørgensen, I. Hook, and R. Murowinski. Cosmic Star Formation History and Its Dependence on Galaxy Stellar Mass. *ApJ*, 619:L135–L138, February 2005.

S. A. Kassin, J. A. Frogel, R. W. Pogge, G. P. Tiede, and K. Sellgren. Stellar Populations in NGC 4038/39 (the Antennae): Exploring a Galaxy Merger Pixel by Pixel. *AJ*, 126: 1276–1285, September 2003.

G. Kauffmann, J. M. Colberg, A. Diaferio, and S. D. M. White. Clustering of galaxies in a hierarchical universe - I. Methods and results at z=0. *MNRAS*, 303:188–206, February 1999.

G. Kauffmann, A. Nusser, and M. Steinmetz. Galaxy formation and large-scale bias. *MNRAS*, 286:795–811, April 1997.

G. Kauffmann, S. D. M. White, and B. Guiderdoni. The Formation and Evolution of Galaxies Within Merging Dark Matter Haloes. *MNRAS*, 264:201–+, September 1993.

R. C. Kennicutt, Jr. The star formation law in galactic disks. *ApJ*, 344:685–703, September 1989.

R. C. Kennicutt, Jr. Star Formation in Galaxies Along the Hubble Sequence. *ARA&A*, 36: 189–232, 1998a.

R. C. Kennicutt, Jr. The Global Schmidt Law in Star-forming Galaxies. *ApJ*, 498:541–+, May 1998b.

T. Kodama, I. Smail, F. Nakata, S. Okamura, and R. G. Bower. The Transformation of Galaxies within the Large-Scale Structure around a z=0.41 Cluster. *ApJ*, 562:L9–L13, November 2001.

A. M. Koekemoer, H. Aussel, D. Calzetti, P. Capak, M. Giavalisco, J.-P. Kneib, A. Leauthaud, O. Le Fèvre, H. J. McCracken, R. Massey, B. Mobasher, J. Rhodes, N. Scoville, and P. L. Shopbell. The COSMOS Survey: Hubble Space Telescope Advanced Camera for Surveys Observations and Data Processing. *ApJS*, 172:196–202, September 2007.

D. C. Koo. Optical multicolors - A poor person's Z machine for galaxies. *AJ*, 90:418–440, March 1985.

J. Kormendy. Brightness distributions in compact and normal galaxies. II - Structure parameters of the spheroidal component. *ApJ*, 218:333–346, December 1977.

K. Kuijken and M. R. Merrifield. Establishing the connection between peanut-shaped bulges and galactic bars. *ApJ*, 443:L13–L16, April 1995.

M. M. Lanyon-Foster, C. J. Conselice, and M. R. Merrifield. Structure through colour: a pixel approach towards understanding galaxies. *MNRAS*, 380:571–584, September 2007.

B. Lanzoni, B. Guiderdoni, G. A. Mamon, J. Devriendt, and S. Hatton. GALICS- VI. Modelling hierarchical galaxy formation in clusters. *MNRAS*, 361:369–384, August 2005.

J.-F. Le Borgne, G. Bruzual, R. Pelló, A. Lançon, B. Rocca-Volmerange, B. Sanahuja, D. Schaerer, C. Soubiran, and R. Vílchez-Gómez. STELIB: A library of stellar spectra at R ˜ 2000. *A&A*, 402:433–442, May 2003.

G. Lemson and G. Kauffmann. Environmental influences on dark matter haloes and consequences for the galaxies within them. *MNRAS*, 302:111–117, January 1999.

I. Lewis, M. Balogh, R. De Propris, W. Couch, R. Bower, A. Offer, J. Bland-Hawthorn, I. K. Baldry, C. Baugh, T. Bridges, R. Cannon, S. Cole, M. Colless, C. Collins, N. Cross, G. Dalton, S. P. Driver, G. Efstathiou, R. S. Ellis, C. S. Frenk, K. Glazebrook, E. Hawkins, C. Jackson, O. Lahav, S. Lumsden, S. Maddox, D. Madgwick, P. Norberg, J. A. Peacock, W. Percival, B. A. Peterson, W. Sutherland, and K. Taylor. The 2dF Galaxy Redshift Survey: the environmental dependence of galaxy star formation rates near clusters. *MNRAS*, 334:673–683, August 2002.

C. J. Lintott, K. Schawinski, A. Slosar, K. Land, S. Bamford, D. Thomas, M. J. Raddick, R. C. Nichol, A. Szalay, D. Andreescu, P. Murray, and J. van den Berg. Galaxy Zoo :

Morphologies derived from visual inspection of galaxies from the Sloan Digital Sky Survey. *ArXiv e-prints*, 804, April 2008.

M. C. Liu, S. Charlot, and J. R. Graham. Theoretical Predictions for Surface Brightness Fluctuations and Implications for Stellar Populations of Elliptical Galaxies. *ApJ*, 543: 644–668, November 2000.

R. Lupton, J. E. Gunn, Z. Ivezić, G. R. Knapp, and S. Kent. The SDSS Imaging Pipelines. In F. R. Harnden, Jr., F. A. Primini, and H. E. Payne, editors, *Astronomical Data Analysis Software and Systems X*, volume 238 of *Astronomical Society of the Pacific Conference Series*, pages 269–+, 2001.

R. H. Lupton, J. E. Gunn, and A. S. Szalay. A Modified Magnitude System that Produces Well-Behaved Magnitudes, Colors, and Errors Even for Low Signal-to-Noise Ratio Measurements. *AJ*, 118:1406–1410, September 1999.

H. Mathis, G. Lemson, V. Springel, G. Kauffmann, S. D. M. White, A. Eldar, and A. Dekel. Simulating the formation of the local galaxy population. *MNRAS*, 333:739–762, July 2002.

C. F. McKee and E. C. Ostriker. Theory of Star Formation. *ARA&A*, 45:565–687, September 2007.

J. C. Mihos. Interactions and Mergers of Cluster Galaxies. In J. S. Mulchaey, A. Dressler, and A. Oemler, editors, *Clusters of Galaxies: Probes of Cosmological Structure and Galaxy Evolution*, pages 277–+, 2004.

H. J. Mo and S. D. M. White. An analytic model for the spatial clustering of dark matter haloes. *MNRAS*, 282:347–361, September 1996.

B. Mobasher, T. Dahlen, A. Hopkins, N. Z. Scoville, P. Capak, R. M. Rich, D. B. Sanders, E. Schinnerer, O. Ilbert, M. Salvato, and K. Sheth. Relation Between Stellar Mass and Star Formation Activity in Galaxies. *ArXiv e-prints*, 808, August 2008.

B. Moore, N. Katz, G. Lake, A. Dressler, and A. Oemler. Galaxy harassment and the evolution of clusters of galaxies. *Nature*, 379:613–616, February 1996.

B. Moore, G. Lake, and N. Katz. Morphological Transformation from Galaxy Harassment. *ApJ*, 495:139–+, March 1998.

B. Moore, G. Lake, T. Quinn, and J. Stadel. On the survival and destruction of spiral galaxies in clusters. *MNRAS*, 304:465–474, April 1999.

K. Nagamine, M. Fukugita, R. Cen, and J. P. Ostriker. Evolution of the luminosity function and colours of galaxies in a Λ cold dark matter universe. *MNRAS*, 327:L10–L14, October 2001.

J. F. Navarro and M. Steinmetz. The Effects of a Photoionizing Ultraviolet Background on the Formation of Disk Galaxies. *ApJ*, 478:13–+, March 1997.

E. Neistein, F. C. van den Bosch, and A. Dekel. Natural downsizing in hierarchical galaxy formation. *MNRAS*, 372:933–948, October 2006.

C. A. Norman, J. A. Sellwood, and H. Hasan. Bar Dissolution and Bulge Formation: an Example of Secular Dynamical Evolution in Galaxies. *ApJ*, 462:114–+, May 1996.

P. E. J. Nulsen. Transport processes and the stripping of cluster galaxies. *MNRAS*, 198: 1007–1016, March 1982.

A. J. Oemler. The Systematic Properties of Clusters of Galaxies. Photometry of 15 Clusters. *ApJ*, 194:1–20, November 1974.

J. P. Ostriker and S. D. Tremaine. Another evolutionary correction to the luminosity of giant galaxies. *ApJ*, 202:L113–L117, December 1975.

N. Padmanabhan, D. J. Schlegel, D. P. Finkbeiner, J. C. Barentine, M. R. Blanton, H. J. Brewington, J. E. Gunn, M. Harvanek, D. W. Hogg, Ž. Ivezić, D. Johnston, S. M. Kent, S. J. Kleinman, G. R. Knapp, J. Krzesinski, D. Long, E. H. Neilsen, Jr., A. Nitta, C. Loomis, R. H. Lupton, S. Roweis, S. A. Snedden, M. A. Strauss, and D. L. Tucker. An Improved Photometric Calibration of the Sloan Digital Sky Survey Imaging Data. *ApJ*, 674:1217–1233, February 2008.

B. Panter. MOPED Analysis of the SDSS DR1-Stellar Mass Function, Star Formation Rates and Downsizing from the Fossil Record. In V. Le Brun, A. Mazure, S. Arnouts, and D. Burgarella, editors, *The Fabulous Destiny of Galaxies: Bridging Past and Present*, pages 65–+, January 2006.

B. Panter, A. F. Heavens, and R. Jimenez. The mass function of the stellar component of galaxies in the Sloan Digital Sky Survey. *MNRAS*, 355:764–768, December 2004.

C. Park and Y.-Y. Choi. Morphology Segregation of Galaxies in Color-Color Gradient Space. *ApJ*, 635:L29–L32, December 2005.

C. Park, Y.-Y. Choi, M. S. Vogeley, J. R. I. Gott, and M. R. Blanton. Environmental Dependence of Properties of Galaxies in the Sloan Digital Sky Survey. *ApJ*, 658:898–916, April 2007.

P. G. Pérez-González, R. C. Kennicutt, Jr., K. D. Gordon, K. A. Misselt, A. Gil de Paz, C. W. Engelbracht, G. H. Rieke, G. J. Bendo, L. Bianchi, S. Boissier, D. Calzetti, D. A. Dale, B. T. Draine, T. H. Jarrett, D. Hollenbach, and M. K. M. Prescott. Ultraviolet through Far-Infrared Spatially Resolved Analysis of the Recent Star Formation in M81 (NGC 3031). *ApJ*, 648:987–1006, September 2006.

V. Petrosian. Surface Brightness and Evolution of Galaxies. *ApJ*, 210:L53+, December 1976.

J. R. Pier, J. A. Munn, R. B. Hindsley, G. S. Hennessy, S. M. Kent, R. H. Lupton, and Ž. Ivezić. Astrometric Calibration of the Sloan Digital Sky Survey. *AJ*, 125:1559–1579, March 2003.

B. M. Poggianti, I. Smail, A. Dressler, W. J. Couch, A. J. Barger, H. Butcher, R. S. Ellis, and A. J. Oemler. The Star Formation Histories of Galaxies in Distant Clusters. *ApJ*, 518: 576–593, June 1999.

B. M. Poggianti, A. von der Linden, G. De Lucia, V. Desai, L. Simard, C. Halliday, A. Aragón-Salamanca, R. Bower, J. Varela, P. Best, D. I. Clowe, J. Dalcanton, P. Jablonka, B. Milvang-Jensen, R. Pello, G. Rudnick, R. Saglia, S. D. M. White, and D. Zaritsky. The Evolution of the Star Formation Activity in Galaxies and Its Dependence on Environment. *ApJ*, 642:188–215, May 2006.

M. Postman and M. J. Geller. The morphology-density relation - The group connection. *ApJ*, 281:95–99, June 1984.

M. Postman, L. M. Lubin, and J. B. Oke. A Study of Nine High-Redshift Clusters of Galaxies. IV. Photometry and Spectra of Clusters 1324+3011 and 1604+4321. *AJ*, 122: 1125–1150, September 2001.

W. H. Press and P. Schechter. Formation of Galaxies and Clusters of Galaxies by Self-Similar Gravitational Condensation. *ApJ*, 187:425–438, February 1974.

N. Purger, I. Csabai, T. Budavári, and Z. Győry. Photometric Redshifts For The SDSS Data Release 5. *The Virtual Observatory in Action: New Science, New Technology, and Next Generation Facilities, 26th meeting of the IAU, Special Session 3, 17-18, 21-22 August, 2006 in Prague, Czech Republic, SPS3, #40*, 3, August 2006.

V. Quilis, B. Moore, and R. Bower. Gone with the Wind: The Origin of S0 Galaxies in Clusters. *Science*, 288:1617–1620, June 2000.

A. D. Quintero, D. W. Hogg, M. R. Blanton, D. J. Schlegel, D. J. Eisenstein, J. E. Gunn, J. Brinkmann, M. Fukugita, K. Glazebrook, and T. Goto. Selection and Photometric Properties of K+A Galaxies. *ApJ*, 602:190–199, February 2004.

J. Reunanen, L. E. Tacconi-Garman, and V. D. Ivanov. VLT/SINFONI integral field spectroscopy of the Super-antennae. *MNRAS*, 382:951–959, December 2007.

D. O. Richstone. Collisions of galaxies in dense clusters. II - Dynamical evolution of cluster galaxies. *ApJ*, 204:642–648, March 1976.

M. S. Roberts and M. P. Haynes. Physical Parameters along the Hubble Sequence. *ARA&A*, 32:115–152, 1994.

B. E. Robertson and A. V. Kravtsov. Molecular Hydrogen and Global Star Formation Relations in Galaxies. *ApJ*, 680:1083–1111, June 2008.

E. E. Salpeter. The Luminosity Function and Stellar Evolution. *ApJ*, 121:161–+, January 1955.

A. Sandage. *The Hubble atlas of galaxies*. Washington: Carnegie Institution, 1961, 1961.

M. J. Sawicki, H. Lin, and H. K. C. Yee. Evolution of the Galaxy Population Based on Photometric Redshifts in the Hubble Deep Field. *AJ*, 113:1–12, January 1997.

D. J. Schlegel, D. P. Finkbeiner, and M. Davis. Maps of Dust Infrared Emission for Use in Estimation of Reddening and Cosmic Microwave Background Radiation Foregrounds. *ApJ*, 500:525–+, June 1998.

M. Schmidt. The Rate of Star Formation. *ApJ*, 129:243–+, March 1959.

L. Searle and R. Zinn. Compositions of halo clusters and the formation of the galactic halo. *ApJ*, 225:357–379, October 1978.

N. Seymour, T. Dwelly, D. Moss, I. McHardy, A. Zoghbi, G. Rieke, M. Page, A. Hopkins, and N. Loaring. The star formation history of the Universe as revealed by deep radio observations. *MNRAS*, 386:1695–1708, May 2008.

R. K. Sheth and G. Tormen. Large-scale bias and the peak background split. *MNRAS*, 308: 119–126, September 1999.

D. Sijacki, V. Springel, T. di Matteo, and L. Hernquist. A unified model for AGN feedback in cosmological simulations of structure formation. *MNRAS*, 380:877–900, September 2007.

R. S. Somerville, P. F. Hopkins, T. J. Cox, B. E. Robertson, and L. Hernquist. A Semi-Analytic Model for the Co-evolution of Galaxies, Black Holes, and Active Galactic Nuclei. *ArXiv e-prints*, 808, August 2008.

R. S. Somerville, G. Lemson, Y. Sigad, A. Dekel, G. Kauffmann, and S. D. M. White. Non-linear stochastic galaxy biasing in cosmological simulations. *MNRAS*, 320:289–306, January 2001.

R. S. Somerville and J. R. Primack. Semi-analytic modelling of galaxy formation: the local Universe. *MNRAS*, 310:1087–1110, December 1999.

M. Steinmetz and J. F. Navarro. The hierarchical origin of galaxy morphologies. *New Astronomy*, 7:155–160, June 2002.

C. Stoughton, R. H. Lupton, M. Bernardi, M. R. Blanton, S. Burles, F. J. Castander, A. J. Connolly, D. J. Eisenstein, J. A. Frieman, G. S. Hennessy, R. B. Hindsley, Ž. Ivezić, S. Kent, P. Z. Kunszt, B. C. Lee, A. Meiksin, J. A. Munn, H. J. Newberg, R. C. Nichol, T. Nicinski, J. R. Pier, G. T. Richards, M. W. Richmond, D. J. Schlegel, J. A. Smith, M. A. Strauss, M. SubbaRao, A. S. Szalay, A. R. Thakar, D. L. Tucker, D. E. Vanden Berk, B. Yanny, J. K. Adelman, J. E. Anderson, Jr., S. F. Anderson, J. Annis, N. A. Bahcall, J. A. Bakken, M. Bartelmann, S. Bastian, A. Bauer, E. Berman, H. Böhringer, W. N. Boroski, S. Bracker, C. Briegel, J. W. Briggs, J. Brinkmann, R. Brunner, L. Carey, M. A. Carr, B. Chen, D. Christian, P. L. Colestock, J. H. Crocker, I. Csabai, P. C. Czarapata, J. Dalcanton, A. F. Davidsen, J. E. Davis, W. Dehnen, S. Dodelson, M. Doi, T. Dombeck, M. Donahue, N. Ellman, B. R. Elms, M. L. Evans, L. Eyer, X. Fan, G. R.

Federwitz, S. Friedman, M. Fukugita, R. Gal, B. Gillespie, K. Glazebrook, J. Gray, E. K. Grebel, B. Greenawalt, G. Greene, J. E. Gunn, E. de Haas, Z. Haiman, M. Haldeman, P. B. Hall, M. Hamabe, B. Hansen, F. H. Harris, H. Harris, M. Harvanek, S. L. Hawley, J. J. E. Hayes, T. M. Heckman, A. Helmi, A. Henden, C. J. Hogan, D. W. Hogg, D. J. Holmgren, J. Holtzman, C.-H. Huang, C. Hull, S.-I. Ichikawa, T. Ichikawa, D. E. Johnston, G. Kauffmann, R. S. J. Kim, T. Kimball, E. Kinney, M. Klaene, S. J. Kleinman, A. Klypin, G. R. Knapp, J. Korienek, J. Krolik, R. G. Kron, J. Krzesiński, D. Q. Lamb, R. F. Leger, S. Limmongkol, C. Lindenmeyer, D. C. Long, C. Loomis, J. Loveday, B. MacKinnon, E. J. Mannery, P. M. Mantsch, B. Margon, P. McGehee, T. A. McKay, B. McLean, K. Menou, A. Merelli, H. J. Mo, D. G. Monet, O. Nakamura, V. K. Narayanan, T. Nash, E. H. Neilsen, Jr., P. R. Newman, A. Nitta, M. Odenkirchen, N. Okada, S. Okamura, J. P. Ostriker, R. Owen, A. G. Pauls, J. Peoples, R. S. Peterson, D. Petravick, A. Pope, R. Pordes, M. Postman, A. Prosapio, T. R. Quinn, R. Rechenmacher, C. H. Rivetta, H.-W. Rix, C. M. Rockosi, R. Rosner, K. Ruthmansdorfer, D. Sandford, D. P. Schneider, R. Scranton, M. Sekiguchi, G. Sergey, R. Sheth, K. Shimasaku, S. Smee, S. A. Snedden, A. Stebbins, C. Stubbs, I. Szapudi, P. Szkody, G. P. Szokoly, S. Tabachnik, Z. Tsvetanov, A. Uomoto, M. S. Vogeley, W. Voges, P. Waddell, R. Walterbos, S.-i. Wang, M. Watanabe, D. H. Weinberg, R. L. White, S. D. M. White, B. Wilhite, D. Wolfe, N. Yasuda, D. G. York, I. Zehavi, and W. Zheng. Sloan Digital Sky Survey: Early Data Release. *AJ*, 123: 485–548, January 2002.

I. Strateva, Ž. Ivezić, G. R. Knapp, V. K. Narayanan, M. A. Strauss, J. E. Gunn, R. H. Lupton, D. Schlegel, N. A. Bahcall, J. Brinkmann, R. J. Brunner, T. Budavári, I. Csabai, F. J. Castander, M. Doi, M. Fukugita, Z. Győry, M. Hamabe, G. Hennessy, T. Ichikawa, P. Z. Kunszt, D. Q. Lamb, T. A. McKay, S. Okamura, J. Racusin, M. Sekiguchi, D. P. Schneider, K. Shimasaku, and D. York. Color Separation of Galaxy Types in the Sloan Digital Sky Survey Imaging Data. *AJ*, 122:1861–1874, October 2001.

M. A. Strauss, D. H. Weinberg, R. H. Lupton, V. K. Narayanan, J. Annis, M. Bernardi, M. Blanton, S. Burles, A. J. Connolly, J. Dalcanton, M. Doi, D. Eisenstein, J. A. Frieman, M. Fukugita, J. E. Gunn, Ž. Ivezić, S. Kent, R. S. J. Kim, G. R. Knapp, R. G. Kron, J. A. Munn, H. J. Newberg, R. C. Nichol, S. Okamura, T. R. Quinn, M. W. Richmond, D. J. Schlegel, K. Shimasaku, M. SubbaRao, A. S. Szalay, D. Vanden Berk, M. S. Vogeley, B. Yanny, N. Yasuda, D. G. York, and I. Zehavi. Spectroscopic Target Selection in the Sloan Digital Sky Survey: The Main Galaxy Sample. *AJ*, 124:1810–1824, September 2002.

M. U. Subbarao, A. J. Connolly, A. S. Szalay, and D. C. Koo. Luminosity Functions From Photometric Redshifts. I. Techniques. *AJ*, 112:929–+, September 1996.

K. Tassis, A. V. Kravtsov, and N. Y. Gnedin. Scaling Relations of Dwarf Galaxies without Supernova-driven Winds. *ApJ*, 672:888–903, January 2008.

D. Thomas, C. Maraston, R. Bender, and C. Mendes de Oliveira. The Epochs of Early-Type Galaxy Formation as a Function of Environment. *ApJ*, 621:673–694, March 2005.

B. M. Tinsley. Evolution of the Stars and Gas in Galaxies. *Fundamentals of Cosmic Physics*, 5:287–388, 1980.

K.-V. H. Tran, L. Simard, A. I. Zabludoff, and J. S. Mulchaey. The Galaxy Populations of X-Ray-detected, Poor Groups. *ApJ*, 549:172–191, March 2001.

D. L. Tucker, S. Kent, M. W. Richmond, J. Annis, J. A. Smith, S. S. Allam, C. T. Rodgers, J. L. Stute, J. K. Adelman-McCarthy, J. Brinkmann, M. Doi, D. Finkbeiner, M. Fukugita, J. Goldston, B. Greenway, J. E. Gunn, J. S. Hendry, D. W. Hogg, S.-I. Ichikawa, Ž. Ivezić, G. R. Knapp, H. Lampeitl, B. C. Lee, H. Lin, T. A. McKay, A. Merrelli, J. A. Munn, E. H. Neilsen, Jr., H. J. Newberg, G. T. Richards, D. J. Schlegel, C. Stoughton, A. Uomoto, and B. Yanny. The Sloan Digital Sky Survey monitor telescope pipeline. *Astronomische Nachrichten*, 327:821–+, 2006.

R. B. Tully and J. R. Fisher. A new method of determining distances to galaxies. *A&A*, 54: 661–673, February 1977.

A. van der Wel, B. P. Holden, M. Franx, G. D. Illingworth, M. P. Postman, D. D. Kelson, I. Labbé, S. Wuyts, J. P. Blakeslee, and H. C. Ford. The Evolution of the Field and Cluster Morphology-Density Relation for Mass-Selected Samples of Galaxies. *ApJ*, 670:206–220, November 2007.

P. G. van Dokkum. The Recent and Continuing Assembly of Field Elliptical Galaxies by Red Mergers. *AJ*, 130:2647–2665, December 2005.

Y. Wang, N. Bahcall, and E. L. Turner. A Catalog of Color-based Redshift Estimates for Z ˜ 4 Galaxies in the Hubble Deep Field. *AJ*, 116:2081–2085, November 1998.

N. Welikala, A. J. Connolly, A. M. Hopkins, and R. Scranton. Spatially Resolved Galaxy Star Formation and Its Environmental Dependence. II. Effect of the Morphology-Density Relation. Submitted. *ApJ*, 2008a.

N. Welikala, A. J. Connolly, A. M. Hopkins, R. Scranton, and A. Conti. Spatially Resolved Galaxy Star Formation and Its Environmental Dependence. I. *ApJ*, 677:970–984, April 2008b.

S. D. M. White. Dynamical friction in spherical clusters. *MNRAS*, 174:19–28, January 1976.

S. D. M. White and C. S. Frenk. Galaxy formation through hierarchical clustering. *ApJ*, 379:52–79, September 1991.

S. D. M. White and M. J. Rees. Core condensation in heavy halos - A two-stage theory for galaxy formation and clustering. *MNRAS*, 183:341–358, May 1978.

B. C. Whitmore. What Determines the Morphological Fractions in Groups and Clusters? In O.-G. Richter and K. Borne, editors, *Groups of Galaxies*, volume 70 of *Astronomical Society of the Pacific Conference Series*, pages 41–+, 1995.

R. E. Williams, S. Baum, L. E. Bergeron, N. Bernstein, B. S. Blacker, B. J. Boyle, T. M. Brown, C. M. Carollo, S. Casertano, R. Covarrubias, D. F. de Mello, M. E. Dickinson, B. R. Espey, H. C. Ferguson, A. Fruchter, J. P. Gardner, A. Gonnella, J. Hayes, P. C. Hewett, I. Heyer, R. Hook, M. Irwin, D. Jones, M. E. Kaiser, Z. Levay, A. Lubenow, R. A. Lucas, J. Mack, J. W. MacKenty, P. Madau, R. B. Makidon, C. L. Martin, L. Mazzuca, M. Mutchler, R. P. Norris, B. Perriello, M. M. Phillips, M. Postman, P. Royle, K. Sahu, S. Savaglio, A. Sherwin, T. E. Smith, M. Stiavelli, N. B. Suntzeff, H. I. Teplitz, R. P. van der Marel, A. R. Walker, R. J. Weymann, M. S. Wiggs, G. M. Williger, J. Wilson, N. Zacharias, and D. R. Zurek. The Hubble Deep Field South: Formulation of the Observing Campaign. *AJ*, 120:2735–2746, December 2000.

R. E. Williams, B. Blacker, M. Dickinson, W. V. D. Dixon, H. C. Ferguson, A. S. Fruchter, M. Giavalisco, R. L. Gilliland, I. Heyer, R. Katsanis, Z. Levay, R. A. Lucas, D. B. McElroy, L. Petro, M. Postman, H.-M. Adorf, and R. Hook. The Hubble Deep Field: Observations, Data Reduction, and Galaxy Photometry. *AJ*, 112:1335–+, October 1996.

T. Wong and L. Blitz. The Relationship between Gas Content and Star Formation in Molecule-rich Spiral Galaxies. *ApJ*, 569:157–183, April 2002.

G. Worthey. Comprehensive stellar population models and the disentanglement of age and metallicity effects. *ApJS*, 95:107–149, November 1994.

R. Yan, J. A. Newman, S. M. Faber, A. L. Coil, M. C. Cooper, M. Davis, B. J. Weiner, B. F. Gerke, and D. C. Koo. The DEEP2 Galaxy Redshift Survey: Environment of Poststarburst Galaxies at z˜0.1 and z˜0.8. *ArXiv e-prints*, 805, April 2008.

H. K. C. Yee, E. Ellingson, and R. G. Carlberg. The CNOC Cluster Redshift Survey Catalogs. I. Observational Strategy and Data Reduction Techniques. *ApJS*, 102:269–+, February 1996.

D. G. York, J. Adelman, J. E. Anderson, Jr., S. F. Anderson, J. Annis, N. A. Bahcall, J. A. Bakken, R. Barkhouser, S. Bastian, E. Berman, W. N. Boroski, S. Bracker, C. Briegel, J. W. Briggs, J. Brinkmann, R. Brunner, S. Burles, L. Carey, M. A. Carr, F. J. Castander, B. Chen, P. L. Colestock, A. J. Connolly, J. H. Crocker, I. Csabai, P. C. Czarapata, J. E. Davis, M. Doi, T. Dombeck, D. Eisenstein, N. Ellman, B. R. Elms, M. L. Evans, X. Fan, G. R. Federwitz, L. Fiscelli, S. Friedman, J. A. Frieman, M. Fukugita, B. Gillespie, J. E. Gunn, V. K. Gurbani, E. de Haas, M. Haldeman, F. H. Harris, J. Hayes, T. M. Heckman, G. S. Hennessy, R. B. Hindsley, S. Holm, D. J. Holmgren, C.-h. Huang, C. Hull, D. Husby, S.-I. Ichikawa, T. Ichikawa, Ž. Ivezić, S. Kent, R. S. J. Kim, E. Kinney, M. Klaene, A. N. Kleinman, S. Kleinman, G. R. Knapp, J. Korienek, R. G. Kron, P. Z. Kunszt, D. Q. Lamb, B. Lee, R. F. Leger, S. Limmongkol, C. Lindenmeyer, D. C. Long, C. Loomis, J. Loveday, R. Lucinio, R. H. Lupton, B. MacKinnon, E. J. Mannery, P. M. Mantsch, B. Margon, P. McGehee, T. A. McKay, A. Meiksin, A. Merelli, D. G. Monet, J. A. Munn, V. K. Narayanan, T. Nash, E. Neilsen, R. Neswold, H. J. Newberg, R. C. Nichol, T. Nicinski, M. Nonino, N. Okada, S. Okamura, J. P. Ostriker, R. Owen, A. G. Pauls, J. Peoples,

R. L. Peterson, D. Petravick, J. R. Pier, A. Pope, R. Pordes, A. Prosapio, R. Rechenmacher, T. R. Quinn, G. T. Richards, M. W. Richmond, C. H. Rivetta, C. M. Rockosi, K. Ruthmansdorfer, D. Sandford, D. J. Schlegel, D. P. Schneider, M. Sekiguchi, G. Sergey, K. Shimasaku, W. A. Siegmund, S. Smee, J. A. Smith, S. Snedden, R. Stone, C. Stoughton, M. A. Strauss, C. Stubbs, M. SubbaRao, A. S. Szalay, I. Szapudi, G. P. Szokoly, A. R. Thakar, C. Tremonti, D. L. Tucker, A. Uomoto, D. Vanden Berk, M. S. Vogeley, P. Waddell, S.-i. Wang, M. Watanabe, D. H. Weinberg, B. Yanny, and N. Yasuda. The Sloan Digital Sky Survey: Technical Summary. *AJ*, 120:1579–1587, September 2000.

I. Zehavi, M. R. Blanton, J. A. Frieman, D. H. Weinberg, H. J. Mo, M. A. Strauss, S. F. Anderson, J. Annis, N. A. Bahcall, M. Bernardi, J. W. Briggs, J. Brinkmann, S. Burles, L. Carey, F. J. Castander, A. J. Connolly, I. Csabai, J. J. Dalcanton, S. Dodelson, M. Doi, D. Eisenstein, M. L. Evans, D. P. Finkbeiner, S. Friedman, M. Fukugita, J. E. Gunn, G. S. Hennessy, R. B. Hindsley, Ž. Ivezić, S. Kent, G. R. Knapp, R. Kron, P. Kunszt, D. Q. Lamb, R. F. Leger, D. C. Long, J. Loveday, R. H. Lupton, T. McKay, A. Meiksin, A. Merrelli, J. A. Munn, V. Narayanan, M. Newcomb, R. C. Nichol, R. Owen, J. Peoples, A. Pope, C. M. Rockosi, D. Schlegel, D. P. Schneider, R. Scoccimarro, R. K. Sheth, W. Siegmund, S. Smee, Y. Snir, A. Stebbins, C. Stoughton, M. SubbaRao, A. S. Szalay, I. Szapudi, M. Tegmark, D. L. Tucker, A. Uomoto, D. Vanden Berk, M. S. Vogeley, P. Waddell, B. Yanny, and D. G. York. Galaxy Clustering in Early Sloan Digital Sky Survey Redshift Data. *ApJ*, 571:172–190, May 2002.